APPLICATION OF TISSUE ENGINEERING TECHNIQUES FOR TREATING CARTILAGE INJURY AND DIAGNOSING CANCER METASTASIS

by

Amirhossein Hakamivala

Presented to the Faculty of the Graduate School of

The University of Texas at Arlington in Partial Fulfillment

of the Requirements

for the Degree of

DOCTOR OF PHILOSOPHY IN BIOMEDICAL ENGINEERING

The University of Texas at Arlington

August 2019

ABSTRACT

APPLICATION OF TISSUE ENGINEERING TECHNIQUES FOR TREATING CARTILAGE INJURY AND DIAGNOSING CANCER METASTASIS

Amirhossein Hakamivala, PhD

The University of Texas at Arlington, 2019

Supervising Professor: Liping Tang, Ph.D.

This study focuses on the application of tissue engineering techniques for the diagnosis of cancer metastasis, cartilage regeneration, and modeling of lymph node metastasis.

Chapter 1 is an overview of tissue engineering strategies, and it describes how each chapter relates to the central theme.

Chapter 2 describes the development of 3D lymph node (LN) mimetic for studying prostate cancer metastasis. The overall objective of this chapter was to develop a biosystem with the ability to mimic metastatic LN condition. Studies were first designed to uncover the critical cells types and chemokines responsible for cancer metastasis to the LNs. An LN cell-seeded (also called as LN mimetic) device was developed and tested on its ability to mimic real metastatic lymph node. The results show that it can simulate the metastatic LN microenvironment. The device can be used to distinguish the highly metastatic cancer cells from low metastatic ones and can also provide a powerful tool to investigate the processes governing LN metastasis.

Chapter 3 illustrates our work on the establishment of a metastatic LN construct. While LN mimetic was designed for *in vitro* studies, it cannot be used for studying LN metastasis *in vivo*.

LN construct was fabricated for *in vivo* study by encapsulating combination T cells and cancer cells in alginate microbeads. The physical, chemical and biological properties of the microbeads were determined. The ability of these microbeads to induce PCa metastasis was first evaluated *in vitro*. Finally, the ability of metastatic LN construct to promote tumor cell recruitment and to reduce LN metastasis was assessed *in vivo*. Our results confirmed that the LN construct could create microenvironment resembling metastatic LNs. Such a device can be used as a unique tool to investigate how cancer:LN cells interaction lead to cancer LN metastasis.

Chapter 4 depicts the establishment of a new treatment for cartilage injury by applying an *in situ* tissue engineering approach. The goal was to develop a platform technology for regenerating injured cartilage by restoring its intrinsic chondrogenic capacity via directed endogenous progenitor cells responses following simple intra-articular injection. Using a rabbit model of full-thickness cartilage-defect, we found that erythropoietin (Epo)-loaded-hyaluronic acid (HA) microscaffolds were able to trigger endogenous progenitor cells recruitment, reduce inflammatory responses in the synovial space and facilitate cartilage defect repair.

In conclusion, these studies explore the potential of using various tissue engineering techniques on the development of various diagnosis and treatment devices for different life-treating pathological events.

ACKNOWLEDGEMENTS

Many people helped contribute to the work contained in this dissertation. I would first like to acknowledge my supervisor, Dr. Liping Tang, for all his supports, guidances and teaching me the importance of persistent and devout hard work towards my work.

I would also like to acknowledge my collaborators, Jer-Tsong Hsieh at Texas Southwestern Medical Center, Dr. Zui Pan, Dr. Kytai Nguyen and Dr. Baohong Yuan at the University of Texas at Arlington and Dr. Joseph Borrelli at Morton Plant North Bay Hospital Florida, for their useful feedbacks and supports.

Also, I Would like to thank all my lab colleagues and friends especially Dr. Ashwin Nair, Dr. Jun Zhou, Dr. Nikhil Pandey, Yihui Huang, Shuxin li, Carlose Cantu, Joyita Roy, Tanmayee Chikate, Kayti Robinson and Serkan Yaman for sharing their bright minds and beautiful friendship.

I want to express my deepest appreciation to my committee, Dr. Joseph Borrelli, Dr. Zui Pan, Dr. Kytai Nguyen, and Dr. Ashwin Nair for playing an important role in shaping the structure and content of this dissertation.

Finally, and foremost, I would like to dedicate this thesis to my family, my mom, and dad, and my sisters Mariam and Marjan who supported me spiritually throughout my life and constantly encouraged me when the tasks seemed arduous and insurmountable.

This work is supported by a grant from Wilson Charitable Foundation Trust, Congressionally Directed Medical Research Programs, 2013 Peer Reviewed Orthopaedic Research Program and the Translational Research Awards No. W81XWH-14-1-0289 and W81XWH-14-1-0459 from Department of Defense.

Amirhossein Hakamivala

August 2019

Table of Contents

List of Figures

List of Tables

LIST OF ABBREVIATIONS

Abbreviations	Term
B-cells	B lymphocytes
BVF	Bone volume fraction
CM	Conditioned media
DAB2IP-KD cells	DAB2IP gene knockdown cells PC3
DAB2IP-KD-LN CM	Conditioned media from LNs exposed to DAB2IP-KD cells
DMEM	Dulbecco's Modified Eagle's medium
DVS	Divinyl sulfone
EPO	Erythropoietin
FBS	Fetal bovine serum
GAG	Glycosaminoglycan
H&E	Hematoxylin and Eosin
HA	Hyaluronic acid
HA+EPO	Erythropoietin-loaded-hyaluronic acid microscaffolds
HAase	Hyaluronidase
HEVs	High endothelial venules
HGF	Hepatocyte growth factor
LN	Lymph node
m-LN	Metastatic Lymph node
MSCs	Mesenchymal stem cells
NHS	N-Hydroxysuccinimide
N-LN CM	Conditioned media from LNs exposed to Saline
OPN	Osteopontin
PC3-LN CM	Conditioned media from LNs exposed to PC3 cells
PCa	Prostate cancer
PTOA	Post-traumatic osteoarthritis
SDF-1α	Stromal cell-derived factor 1α
T-cells	T lymphocytes

Chapter 1

1.1.Introduction

The human body is comprised of many cells, each with its specific role and function. Whether it is their ability to proliferate and differentiate, phagocytose as macrophages, or even migrate and metastasize as cancer cells, with years of research, many facets of diverse cell populations are still being uncovered. One of the very interesting abilities of cells is their propensity to migrate in response to various stimuli. Cell migration is usually induced by an extracellular signal, which can be a result of a biochemical or mechanical process [1]. Even during embryonic development, tissue formation is solely due to cell migration processes, which allow cells to localize at specific areas and develop into specialized tissues and organs. Cell migration also plays a critical role in wound healing and immune response. For example, whenever there is an injury in the body, the lymphocytes are targeted towards the damage as a counter-response, and the migration of fibroblasts helps in healing the wound and reducing inflammation. Stem cells, that have the ability to proliferate and differentiate to mature cells of a specific organ [2], participate in the healing and regenerative process. Unfortunately, often, this process does not progress normally or in some cases never commences. Such circumstances warrant interventions which have traditionally been in the form of tissue and organ transplant. However, due to the disadvantages like the limited availability of stem cell sources, technical complexity with high medical costs, and the ethical and safety concerns of clinical translation, tissue engineering has emerged as a panacea.

Tissue engineering has presented new approaches to the reconstruction and regeneration of damaged or lost tissue. The design, manufacture or repair of tissue involves utilization of natural or synthetic materials. Recent advances have sought to address the challenges posed by the limitations of classical methods, such as the lack of resources, invasiveness of the host tissue harvesting procedure, risk of disease transmission, stimulation of the immune system, and the possibility of rejection of transplanted tissue [3]. Tissue engineering strategies can be classified

into three categories: (i) injection of bolus cells into tissue of interest, (ii) implantation of cell-seeded construct often precultured in a bioreactor and (iii) delivery of signaling factor often in the form of cytokines via cytokine/growth factor-loaded scaffolds to stimulate cell migration, growth, and differentiation [3, 4].

Cytokines are vital modulators for cell migration. Cytokines are small secreted proteins produced by cells and have a specific effect on the interactions and communications between cells [5]. Many cytokines are involved in different cell migration processes [6]. For example, various cytokines such as erythropoietin (EPO) and stromal cell-derived factor 1 (SDF-1α) upregulate the migration of stem cells at the site of injury and speed up the process of wound healing [7]. Furthermore, under the influence of SDF-1α, CXCR4 positive macrophages have been seen to migrate to the damaged sites following a spinal cord injury [8].

Interestingly, cytokines play a role not only in tissue regenerating processes but also in case of cancer cell metastasis, which involves colonizing at sites far away from the primary tumor. As tumor cells obtain the ability to infiltrate to the surrounding tissues, the process of invasion is initiated. The tumor cells migrate through the basement membrane and extracellular matrix. Eventually, they penetrate into the lymphatic or vascular circulation and metastasize to distant organs [9]. Lymph nodes are often the first sites to which the cancer cells metastasize. Hence, understanding the factors that contribute to this phenomenon could unravel the process of cancer metastasis. Understanding this could hold the key to developing better diagnostic and therapeutic strategies for a wide range of cancers.

Cell migration is now being widely used as a powerful tool for the diagnosis of metastasis in many different cancers. Certain markers, which have been seen to promote metastatic cancer migration, have recently been discovered [10]. In metastatic colorectal cancer, for example, the tumor cells

produce CD44v6, which further promotes migration of the cancer cells and induces metastasis [11]. Detection of different chemotaxis, such as hepatocyte growth factor (HGF), osteopontin (OPN), and SDF-1α, that play a major role in cancer cell migration, can be critical in determining the stage of the malignant tumors [12]. Furthermore, in an attempt to treat triple-negative breast cancer, a combination of Interleukin-6 and Interleukin-8 helped in blocking the migration of breast cancer cells [12]. Many such attempts have shown positive outcomes in the treatment of various diseases. Using a combination of these cytokines and biomaterials one can use tissue engineering principles to create a system that can mimic the process of metastasis.

In this study, tissue engineering techniques have been used for cancer diagnosis, and cartilage injury repair, while its principles have been explored in an underexplored area of modeling cancer metastasis to lymph nodes.

1.2.Overview of the Chapters

Chapter 1 is an overview of tissue engineering techniques and the importance of cell migration. It describes how cell migration plays major roles in homeostasis and life-threatening pathological conditions.

Chapter 2 is devoted to the development of a 3D lymph node (LN) mimetic for studying prostate cancer metastasis. The overall objective of this chapter is to develop a LN mimetic biosystem to improve our understanding of prostate cancer (PCa) metastasis to LNs. We first identify the critical cell types and cellular products that are responsible for PCa cell metastasis. We then explore the possibility of engineering a 3D cell culture biosystem to mimic metastatic PCa responses in LNs. Finally, the 3D culture biosystem is used to determine the lymphatic cellular responses to high and low-metastatic cancer cells.

Chapter 3 is describing cell encapsulated alginate beads for simulating metastatic lymph node. Alginate is used to encapsulate the combination of T cells and PCa cells to mimic a metastatic lymph node (m-LN) condition. The physical, chemical and biological properties of the beads are determined. Also, the effect of the encapsulation on T cell behavior and ability to induce PCa metastasis is assessed. Subsequently, the ability of the encapsulated cells to recruit PCa cells is studied *in vivo*.

Chapter 4 focuses on the recruitment of endogenous progenitor cells by EPO loaded particles for in situ cartilage regeneration. EPO loaded hyaluronic acid (HA) microscaffolds are developed with the ability to target and reduce the inflammatory response as well as recruit endogenous progenitor cells for cartilage defect regeneration. HA microscaffolds are fabricated and characterized in term of size, EPO loading capacity, cell compatibility, and targeting ability. The ability of HA+EPO microscaffolds to slowly release EPO is also assessed. Finally, the ability of HA+EPO microscaffolds to repair cartilage defects is evaluated using a rabbit model of full-thickness cartilage defect.

Each chapter is formatted and structured according to their respective target journals. Chapter 2 was accepted for publication in *Advanced Biosystem*. Chapter 3 will be submitted to a peer-reviewed journal. A target journal will be determined at a later time. Chapter 4 has been submitted to *Advanced Healthcare materials.*

Chapter 2

2.1.DEVELOPMENT of 3D LYMPH NODE MIMETIC FOR STUDYING PROSTATE CANCER METASTASIS

Keywords: Prostate cancer, metastases, lymph nodes, T lymphocytes, chemokines, Lymph node bioreactor

This article has been accepted to be published in the Journal of Advanced Biosystems.

2.2.Abstract

Lymph node (LN) metastasis contributes to poor prognosis for patients with prostate cancer (PCa). While there is abundant evidence to support the pivotal role of LN cells and cellular responses in cancer metastasis, the interplay between LN cells and PCa cells is mostly undetermined due to the extremely small size and wide-spread distribution of LNs. To identify factors responsible for cancer LN metastasis, a 3D cell culture biosystem was fabricated to simulate LN responses during cancer metastasis. We first determined that LN explants previously exposed to high metastatic PCa release substantially more chemotactic factors to promote metastatic PCa migration than those exposed to low-metastatic PCa. Further studies revealed that T lymphocytes (T-cells) were the key cells responsible for the production of chemotactic factors in LNs. Among all chemotactic factors released by LNs, CXCL12, CCL21, and IL-10 were identified to be the most potent chemokines for PCa cell migration. To mimic LN microenvironment, Cytodex® microcarrier beads were seeded with T-cells to produce LN-mimetic biosystem in both static and flow conditions. As expected, such biosystems permitted prolonged cellular responses in flow condition than in a static environment. Interestingly, the biosystems could distinguish between PCa cells with different metastatic potentials by producing PCa-specific chemokines only when highly metastatic PCa cells were introduced into the system. Such differential responses may have been caused by the strong cell:cell interactions between highly metastatic PCa cells and T-cells. Coincidentally, the LN mimetic biosystem could also trigger strong chemotactic responses to highly metastatic esophageal cancer cells as compared with control cells. These results support that the LN mimetic biosystem may serve as a unique tool for studying the processes underlying cancer metastasized LNs and for testing various treatments to reduce cancer LN metastasis.

2.3.Introduction

Prostate cancer (PCa) will account for 1 in 5 new cancer diagnoses in 2018 [13]. The metastatic disease with castration-resistant phenotypes of PCa contributes to the major mortality of PCa patients [14], which appears in both lymph nodes (LNs) and bone [15, 16]. Among these two organs, LNs are often the first metastatic site [17] before spreading to other organs [18]. Therefore, histological examination of PCa metastasis in the LNs around tumors is often used to determine disease progress, prognosis and choice of the therapy. In fact, increasing evidence supports that reduction of LN metastasis may extend the survival of patients [19]. Despite of increasing research efforts, the investigation of LN metastasis faces serious technical challenges due to the fact that there are almost 400 bean-shaped LNs throughout the human body [20] In addition, their extremely small size (1-4 mm diameter in mice; up to 1 cm in humans) [21], makes it difficult to decipher the cellular responses inside them. Consequently, there is limited knowledge on the interaction of cancer cells with LN cells and on the reduction of cancer metastasis to LN.

Many recent studies have uncovered the pivotal role of LNs in cancer metastasis. It is well established that LNs are the initial sites for metastasis of many solid tumors [22, 23]. Mounting evidence supports the active role of lymphatic vessels in tumor metastasis through lymphangiogenesis and lymphatic cellular products [24]. In addition, lymphangiogenic responses [25, 26], high endothelial venules (HEVs) [27], and the production of immunosuppressive products [28] make LN a favorable ground for tumor cells then facilitate distant metastasis. The overall cascade of responses can be summarized as follows: First, tissue fluid around tumors (along with tumor cells and cytokines) drain into the permeable lymphatic collector vessels that are connected to the extracellular membrane around a tumor through anchoring filaments [29]. Shortly after LN infiltration, a few tumor cells induce changes in the LN architecture, which favor the proliferation

of cancer cells [24]. Finally, some cancer cells are then disseminated from the lymphatic circulation to distant organs through the venous circulation [30]. Among all LN cells, T lymphocytes (T-cells) are likely to play an important role in PCa LN metastasis based on the following evidence. For example, blocking cytotoxic T-cell-associated antigen 4 was found to reduce LN metastasis in spontaneous transgenic models of PCa [31]. A recent study has shown that infiltrated CD4+ T-cells could promote PCa metastasis [32]. Furthermore, IL-4-expressing CD4+ T-cells regulate tumor-associated macrophages facilitating the invasion and subsequent metastasis of mammary adenocarcinomas [33]. Despite the fact that T-cells, one of the main cell types in LNs, play an important role in cancer metastasis, the potential role of T-cells in PCa LN metastasis is not totally understood.

Significant research efforts thus far have been placed on uncovering the "machinery" inside the LNs. Histology studies have revealed that naïve LNs are characterized by the presence of B lymphocytes (B-cells) zones or follicles in the outer cortex, T-cells zones in the middle paracortex, and macrophages distributed along the medulla along with afferent and efferent lymphatic vessels (Figure 2-1) [34]. Several *in vitro* and *in vivo* models have been established to produce LN mimetic for studying LN-associated secondary immune responses [35-38]. Progress on tissue-engineered LN systems has been limited to understanding the effect of 3D culture on cell networks [39]. Despite significant progress made on LNs fabrication to simulate immune reactions, to the best of our knowledge, there is no system which has been developed to mimic cancer LN metastasis. Studying this system could provide a better understanding of the complexities of LN and its impact on PCa metastasis.

Our group recently established the functional role of DAB2IP gene in rendering aggressiveness to PCa cells. It is known that PCa cells acquire invasive abilities by undergoing phenotypical changes like epithelial to mesenchymal transition (EMT)[40].

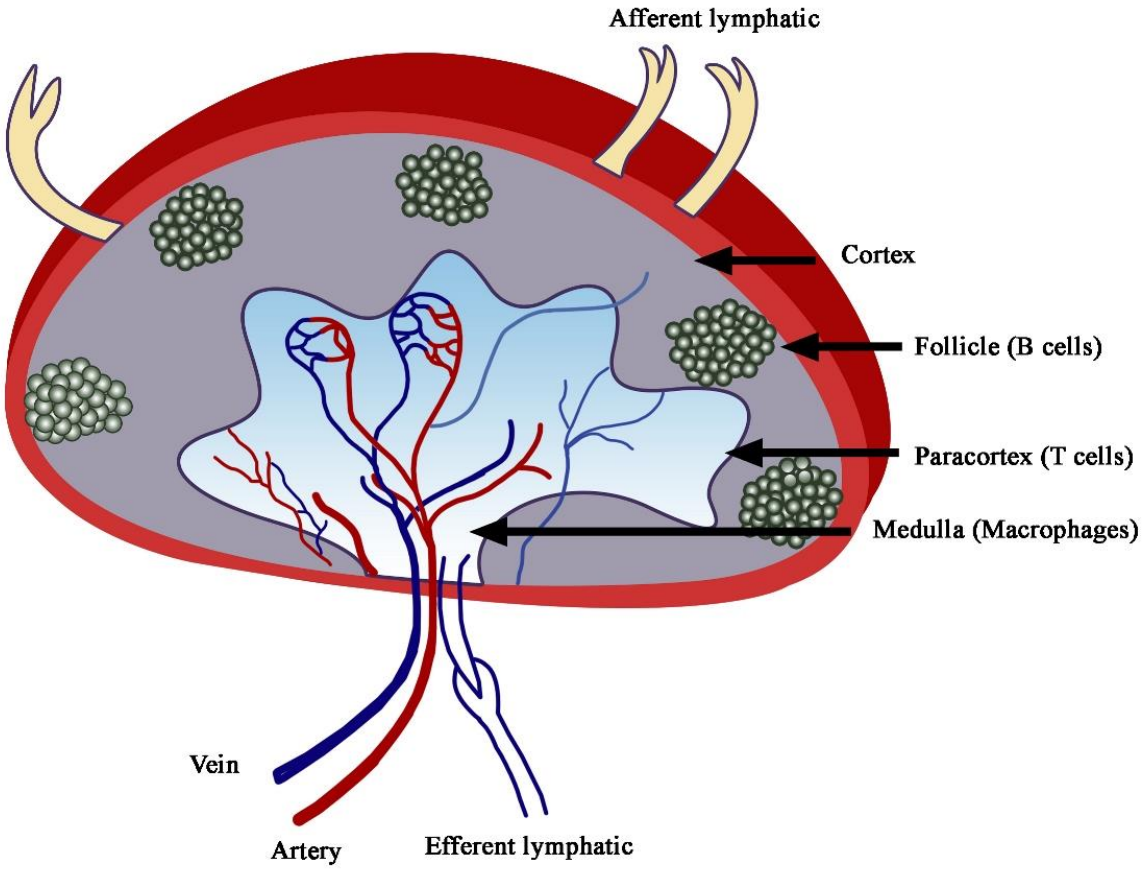

Figure 2-1 structure of a lymph node. B lymphocytes are in follicles in the cortex where they interact with follicular dendritic cells. T lymphocytes home to the paracortex where they interact with dendritic cells. The medulla contains mostly macrophages.

The overall objective of this work was to develop an LN mimetic biosystem to improve our understanding of PCa metastasis to LNs. For that, using *in vitro* and *in vivo* models, we first identified the critical cell types and cellular products which are responsible for PCa cell metastasis. We then explored the possibility of engineering a 3D cell culture biosystem which can be

fabricated to mimic metastatic PCa responses in LNs. Finally, the 3D culture biosystem was used to determine the cellular responses governing lymphatic cellular responses to high and low-metastatic cancer cells *in vitro*.

2.4.Results & Discussion

Increasing evidence supports that LNs play an important role in cancer metastasis. In fact, they are often the first step in cancer metastasis. However, the processes governing this phenomenon are not totally understood due to the small sizes and random distribution of LNs throughout the body. To overcome this limitation, it is critical to develop an *in vitro* model which can simulate the interaction between cancer cells and LNs. Several *in vitro* models have been established over the last few years to mimic the human immune system [35, 36, 38, 41, 42]. For example, LN mimetic responses were achieved by the transplantation of stromal cells in collagen sponge in renal subcapsular space in mice. This organoid construction was found to facilitate the development of the adaptive immune response and as a treatment of immune deficiency [35, 43]. In addition, to mimic T-cell activation in LN *in vitro*, a human LN was fabricated by seeding dendritic cells incubated peripheral blood mononuclear cells and lymphocytes on polyamide fiber scaffolds [37]. More recently, using an RGD-Dextran hydrogel (Cellendes) co-culture system, studies have shown that co-culture of stimulated multipotent stem cells with immune cells in hydrogel may promote antigen-specific antibody responses in immunodeficient mice [38]. In addition, tissue-engineered LN systems composed of immortalized follicular reticular cells were fabricated to demonstrate the effect of 3D culture and flow rate on 3D cell network morphology and cellular product (chemokine) productions [39]. However, these models cannot be used to evaluate the role of immune cell in cancer metastasis[38] which is the major focus of this investigation.

2.4.1. Exposure to metastatic PCa changes LN morphology

To simulate LN responses *in vitro*, the LN responses to PCa *in vivo* were investigated. The morphologies of LNs from animals implanted with PC3 and DAB2IP-KD cells for two weeks were compared. Histological results indicated that the size of mesenteric LNs exposed to highly metastatic PCa (DAB2IP-KD cells) cells is significantly larger (~2X) than those exposed to low metastatic PC3 cells and naïve LNs (**Figure 2-2 a**). The lymphadenopathy was mostly found in the Mesenteric LNs of DAB2IP-KD injected animal (**Figure 2-2 b**). It is in agreement with an earlier observation that the aggressive lymphatic metastasis and mesenteric nodes enlargement was observed in the orthotopic metastatic prostate cancer model [44]. The evaluation of LN tissue histology suggests that brief exposure to DAB2IP-KD cells was sufficient to induce the hypertrophic responses of LNs that resembled lymphadenopathy typically found in cancer metastasized LNs and antigen-stimulated LNs as compared with LNs exposed to PC3 cells and naïve LNs (**Figure 2-2 c**). In fact, LN enlargement, or tumor-reactive lymphadenopathy, is often associated with LN cell activation and cytokine production/release, which are critical for lymph-angiogenesis, invasion and metastasis [45, 46]. These signs of morphological changes support that LN cells may undergo active cell responses upon interactions with implanted DAB2IP-KD cells. However, it was still unknown about the cause of this phenomenon. Was there a downstream response to LNs' exposure to the highly metastatic DAB2IP-KD cells?

2.4.2. Chemotactic agents are released by LNs exposed to DAB2IP-KD cells

Since DAB2IP-KD cells have been shown to have a high tendency for LN spreading, we hypothesized that the cancer cells' ability to trigger the release of chemotactic agents from LNs is an indicator of their metastatic potential [47, 48]. To test this hypothesis, the CM of LNs isolated from animals implanted with either DAB2IP-KD cells or PC3 cells were tested for their ability to

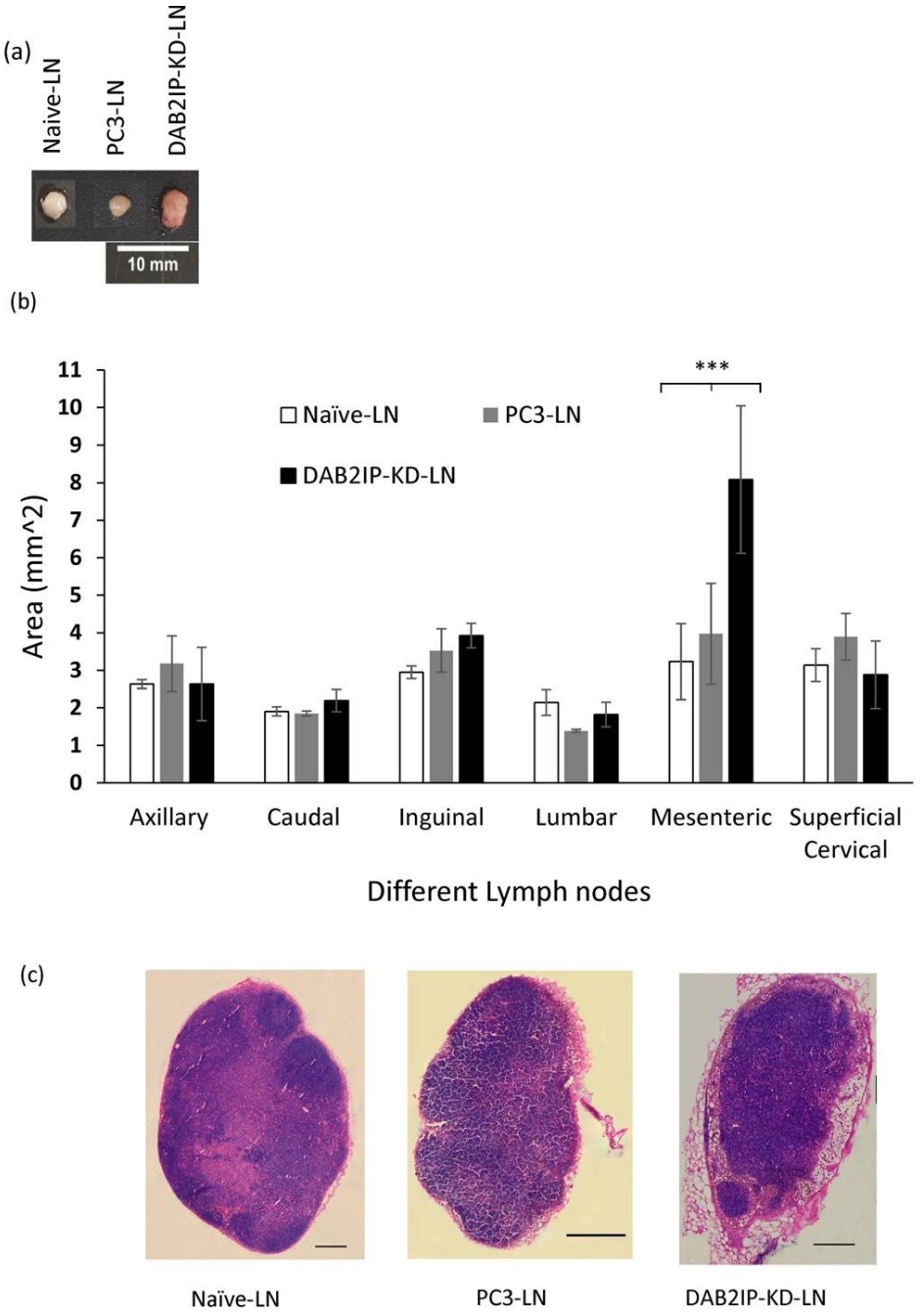

Figure 2-2 LN responses following 2-week implantation of different PCa cells (PC3 (non-metastatic) and DAB2IP-KD (metastatic)) or saline (as control). All the LNs were evaluated for (A) morphology (mesenteric LNs) (B) different LNs size, and (C) histological changes (Scale bar indicates 100 μm) (*** P-value<0.001).

promote the migration of either DAB2IP-KD cells or PC3 cells using a Transwell system. As expected, data showed that CM from naïve LNs prompted little chemotactic activities to either DAB2IP-KD cells or PC3 cells (**Figure 2-3 a**). The representative images of the migrated cells on Transwell membranes can be found in **Figure 2-4**). Similarly, CM from LNs exposed to PC3 cells (abbreviated as PC3-LNs) prompted low chemotactic activities to either DAB2IP-KD cells or PC3 cells. Interestingly, data showed that CM from LNs exposed to DAB2IP-KD cells (abbreviated as DAB2IP-KD-LN) have significantly high chemotactic activities to DAB2IP-KD cells, but not PC3 cells. The DAB2IP-KD cell chemotactic activity of DAB2IP-KD-LNs CM is ~5X higher than those of PC3-LN and naïve LN CMs (**Figure 2-3 a**). The higher *in vitro* migration of DAB2IP-KD cells toward the DAB2IP-KD-LN CM compared to PC3-LN CM and Naïve-LN (N-LN) CM, confirmed higher chemokine production in DAB2IP-KD-LN than those in PC3-LN. To further unveil this phenomenon, the gene profiles of tumor metastasis in variously treated LN tissue were compared using mouse tumor metastasis RT² Profiler™ PCR Array (see **Table 2-1** and **Table 2-2**). It is worth noting that some of the upregulated genes such as CXCL12 and VEGF-A have been implicated in tumor metastasis. Recent studies have also suggested that CXCL12, CCL21, IL-10, CCL20, CLL19 and IL-8 participate in cancer cell metastasis and migration [49-53]. In fact, CXCL12 and CCL21 are expressed highly in LNs [54-56] and their importance in migration and invasion of PCa has been

(a)

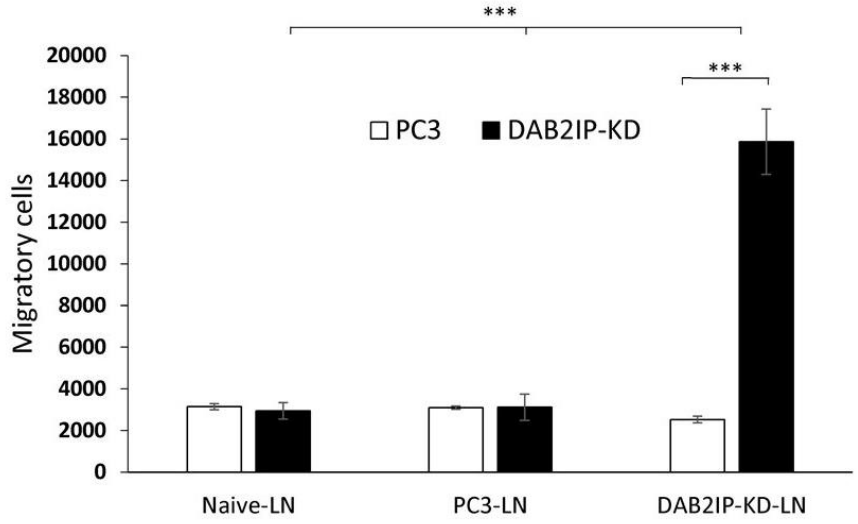

(b)

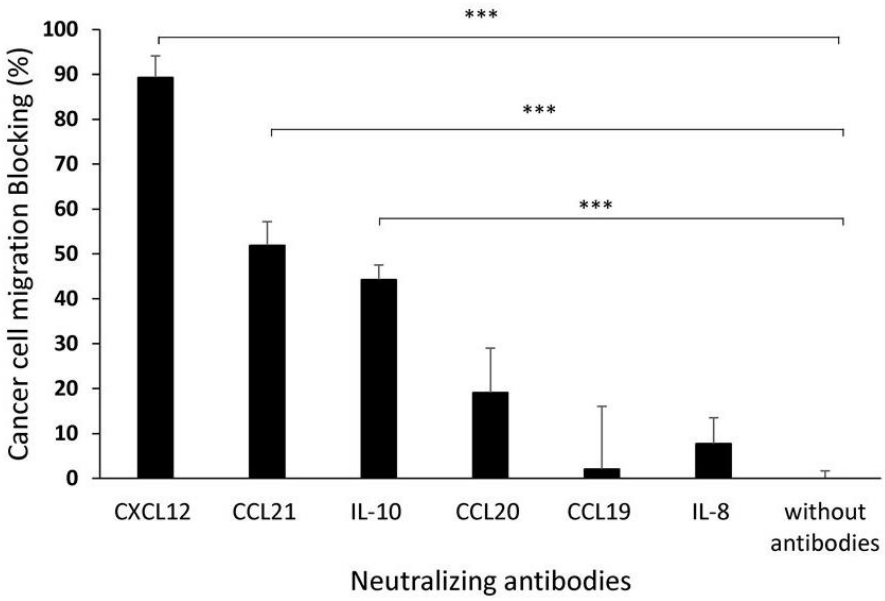

Figure 2-3 Migration of PCa cells in responding to LN CM or various chemokines was determined using Transwell cell migration assay *in vitro*. (a) The ability of various LNs' CM to promote PC3 and DAB2IP-KD cells in- vitro migration was determined. (b) The ability of various neutralizing antibodies to reduce the chemotactic ability of DAB2IP-KD-LN CM was assessed. Data are mean ± standard deviation (Std), (*** P-value<0.001).

established previously [56-58]. It has been shown that the upregulation of IL-10, an immunosuppressive cytokine, may promote tumor growth and turn on an angiogenic switch that leads to directly promoting tumorigenesis in PCa [59]. However, to determine the most important cytokines/chemokines for DAB2IP-KD cell migration in LNs relevant to our LN mimicking biosystem, we evaluated the chemotactic potential of DAB2IP-KD-LN CM neutralized with different and specific cytokines/chemokines using a Transwell migration assay. Our studies have demonstrated a significant reduction of chemotaxis such as CXCL12 (>89% blocking) in DAB2IP-KD cells compared with no treatment control (**Figure 2-3 b -** The representative images of the cells on Transwell membranes can be found in **Figure 2-5**). The concentration of CXCL12 was estimated to be 55 ng/ml based on the standard curve (**Figure 2-6**). In addition, we found that neutralizing antibodies against CCL21 and IL-10 produced 52% and 44% reduction in cancer cell migration with the estimated concentrations of 783 and 2 ng/ml, respectively. CCL20 antibody treatment only yielded ~19% blocking on cell migration. On the other hand, neutralizing antibodies against CCL19 and IL-8 exerted minimal or no effect on the reduction of DAB2IP-KD cells migration. These results suggest that CXCL12, CCL21, and IL-10 play important roles in LN metastasis of PCa. This finding is supported by previous observations. For example, it has been shown that several PCa cells lines express CXCL12 [60] and its autocrine effect may facilitate PCa invasion [61]. In addition, the critical role of the CCL21 and IL-10in recruiting DAB2IP-KD cells to the metastatic LN has been reported in previous studies [62-64].

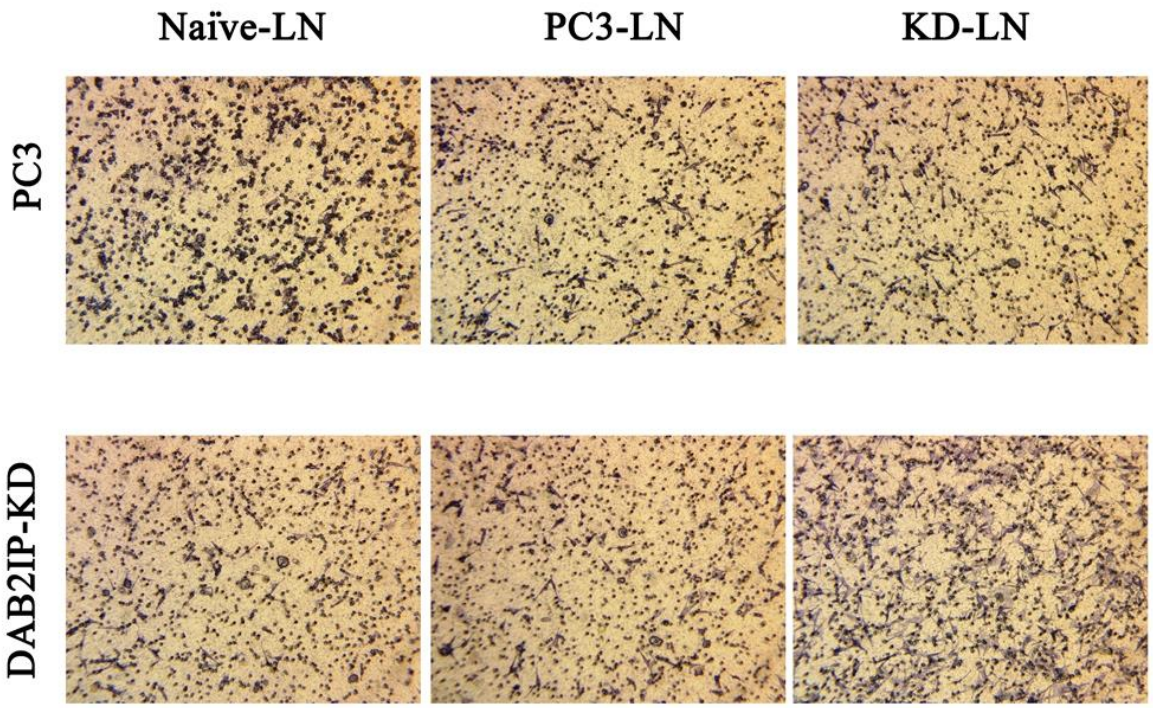

Figure 2-4 Representative images of migrated PC3 cells and DAB2IP-KD cells on membranes with conditioned media of Naïve LN (Naïve-LN), PC3 cells exposed LN (PC3-LN), or DAB2IP-KD cells exposed LN (KD-LN) in the outer reservoir chamber.

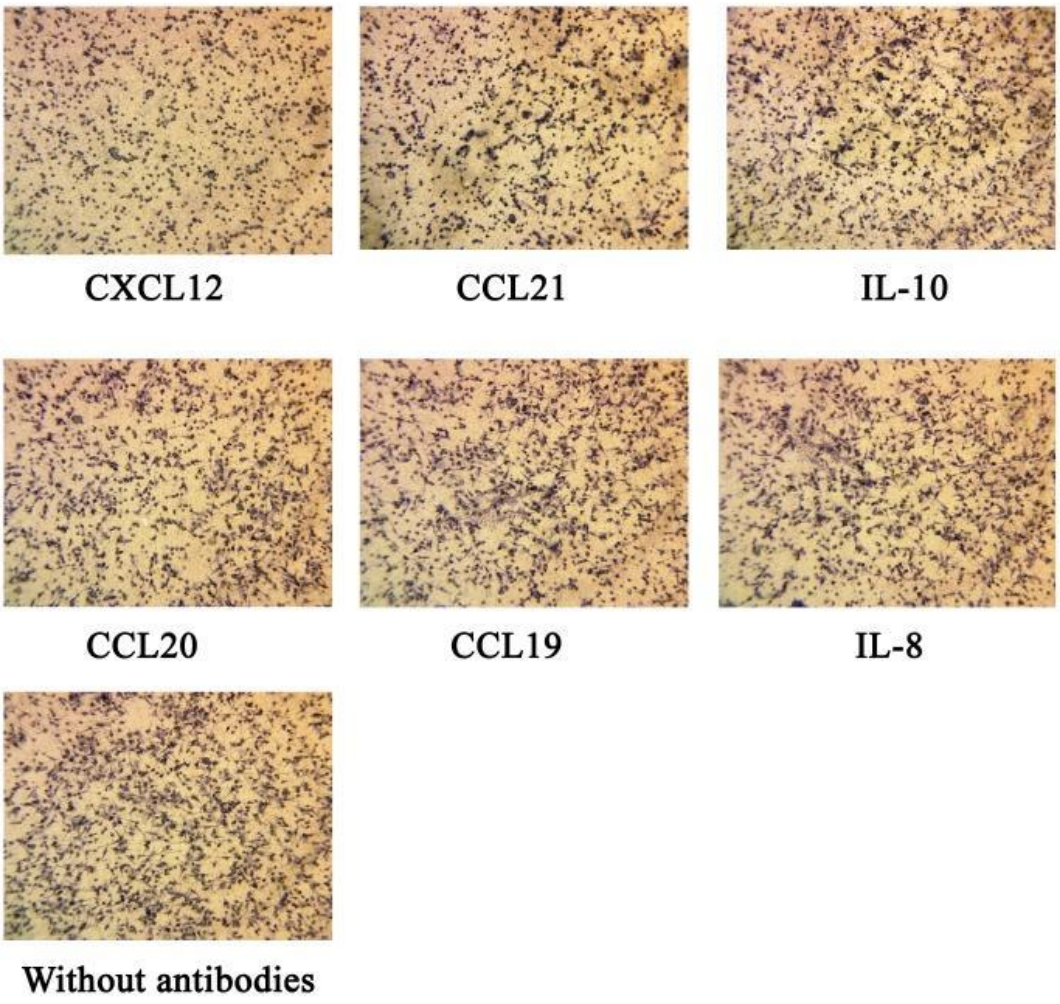

Figure 2-5 Representative images of migrated PC3 cells and DAB2IP-KD cells on membranes with conditioned media of DAB2IP-KD cells exposed LN (KD-LN) in the outer reservoir chamber with the presence of neutralizing antibodies against CXCL12, CCL21, IL-10, CCL20, CCL19, IL-8 or control media.

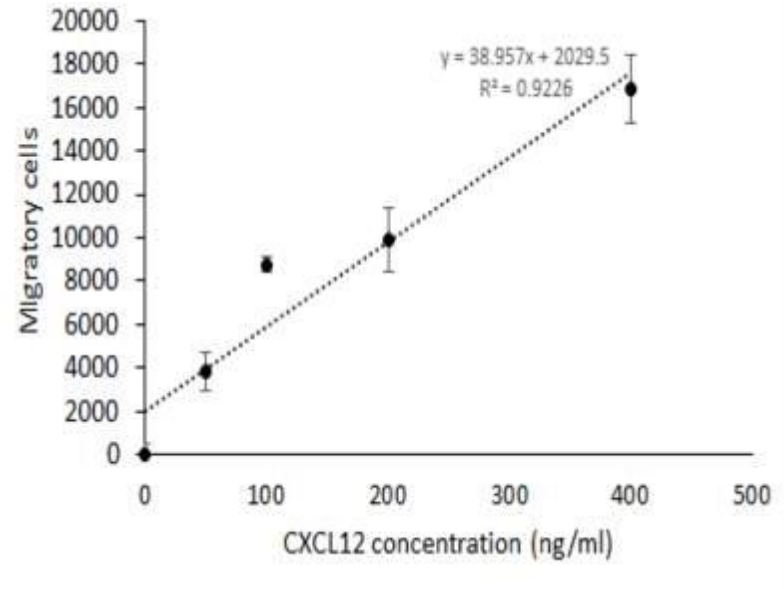

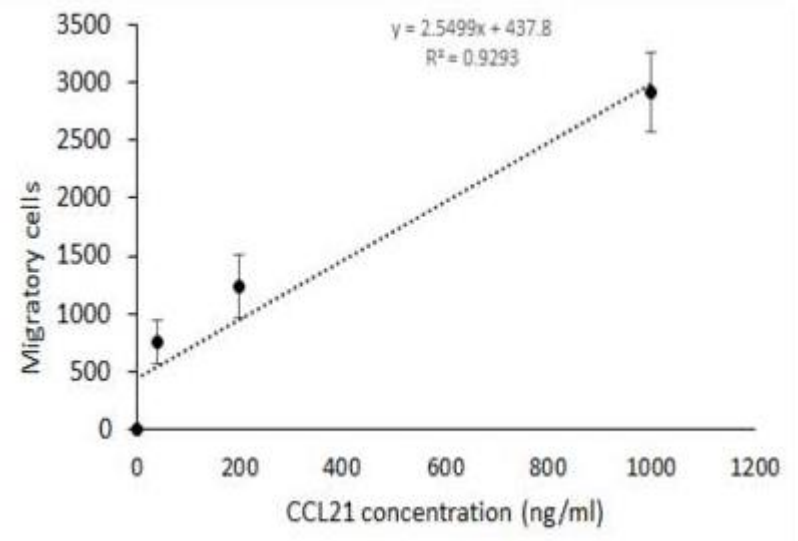

Figure 2-6 The linear relationship between the numbers of migrated cells and the concentrations of (a) CXCL12 and (b) CCL21.

Table 2-1 The list of elevated expression of genes with associated functional group in DAB2IP-KD cells compared to PC3 cells from LN mimetic

Functional Gene Grouping	Gene	Fold change	Function
Cell Adhesion Genes	Cdh11	+4.28	Cell to Cell Adhesion
	Ctnna1	+1.90	
	Itgb3	+2.88	Transmembrane Receptors
	Rpsa	+2.72	
	CD44	+1.52	
	Itga7	+2.31	
	Mtss1	+2.26	Genes Related to Adhesion
	Apc (Negative Regulation of the Cell Cycle)	+2.06	
Extracellular Matrix Proteins	Col4a2	+1.76	ECM Protein
Cell Cycle Genes	Pten (Induction of Apoptosis)	+2.47	Negative Regulation of the Cell Cycle
	Brms1 (Negative Regulation of the Cell Cycle)	+1.52	
Cell Growth and Proliferation Genes	Nf2 (Negative Regulation of the Cell Cycle)(Cell to Cell Adhesion)	+2.03	Regulation of Cell Proliferation
	Tgfb1 (Regulation of the Cell Cycle)(Growth Factors and Hormones)	+1.92	
	Csf1	+2.14	Growth Factors and Hormones
	Vegfa (Regulation of the Cell Cycle)	+10.62	
	Cxcl12	+2.04	Cytokines and Chemokines
	Cxcr2	+2.29	Receptors
	Flt4	+1.79	
	Nr4a3 (Transcription Factors)	+13.94	
	Lpar6	+2.06	
	Kras(Regulation of the Cell Cycle)	+2.1	Genes Related to Growth
	Mdm2(Cell Cycle Arrest and Checkpoint)	+2.46	
	Src	+1.83	
Transcription Factors and Regulators	Mycl1(Other Genes Related to Growth:))	+1.51	Transcription Factors
	Smad4	+2.31	
	Smad2	+1.80	Regulators
Other Genes Involved in Metastasis	Ctsk	+3.48	
	Sykb	+1.57	
	Flnc	+6.85	
	Mcam	+3.48	

Table 2-2 The list of reduced expression of genes with associated functional group in DAB2IP-KD cells compared to PC3 cells from LN mimetic.

Functional Gene Grouping	Gene	Fold change	Function
Cell Adhesion Genes	Cdh8	-7.39	Cell to Cell Adhesion
	Cdh6	-28.8	
	Fn1	-3.45	Genes Related to Adhesion
Extracellular Matrix Proteins	Timp4	-3.40	MMP Inhibitors
Cell Cycle Genes	Cdkn2a (Transcription factors)	-6.27	Negative Regulation of the Cell Cycle
	Rb1 (Transcription Regulators)	-12.57	
Cell Growth and Proliferation Genes	Il18(Cytokines and Chemokines)(Induction of Apoptosis)	-4.35	Regulation of Cell Proliferation
	Hgf	-6.50	Growth Factors and Hormones
	Ccl7	-3.27	Cytokines and Chemokines
	Cxcr4	-2.67	Receptors
	Met	-3.00	
	Sstr2	-2.42	
	Tshr	-59.32	
	Denr	-3.13	Genes Related to Growth
Apoptosis genes	Tnfsf10(Cytokines and Chemokines)	-3.46	Genes Related to Apoptosis
	Ewsr1	-2.43	
Other Genes Involved in Metastasis	Nme1	-2.08	
	Ctsl	-3.88	
	Fxyd5	-3.76	
	Hpse	-2.66	
	Cd82	-21.74	

2.4.3. T cells are critical to LN metastasis of PCa

There is plenty of evidence supporting the role played by T lymphocytes in promoting PCa metastasis to the LNs upon activation by different cytokines [65-67]. To investigate the effect of T-cells on LN metastasis of DAB2IP-KD cells, we isolated T lymphocytes and non-T lymphocytes from the DAB2IP-KD LNs. The isolated cells were then cultured to produce the CM for chemotaxis assays. Our result showed that T-cells CM induce more DAB2IP-KD cell migration than non-T cells conditioned media (**Figure 2-7 a** and **b**) (The representative images of migrated cells on Transwell membranes can be found in **Figure 2-8**).

A subsequent study was carried out to determine whether T-cells respond differently to PC3 and DAB2IP-KD cells. For that, isolated T-cells were incubated with PCa CM or PCa cells for 48 hours. They were then incubated for 2 more days in serum-free RPMI to produce the CM for chemotaxis measurement. Our studies have revealed that the culture of T-cells with DAB2IP-KD CM and DAB2IP-KD cells induced significantly more DAB2IP-KD cells migration than those incubated with PC3 CM and PC3 cells. Interestingly, we also found that the T-cells released more chemotactic factors when co-cultured with DAB2IP-KD cells than those cultured with DAB2IP-KD CM (**Figure 2-9 a**) (The representative images of migrated cells on Transwell membranes can be found in **Figure 2-10**). Studies were carried out to determine the types of chemokines/cytokines released by DAB2IP-KD cells-incubated T-cells using various neutralizing antibodies. In agreement with our previous observation, blocking of CXCL12, CCL21 or IL-10 significantly reduced 63.9±9.0, 52.8±3.1 and 64.4±3.0% of the DAB2IP-KD migration, respectively (**Figure 2-9 b**) (The representative images of migrated cells on Transwell membranes can be found in **Figure 2-11)**. Based on the standard curve of their individual chemotactic potentials, the concentration of CXCL12, CCL21 or IL-10 were calculated to be 25 ng/ml, 799 ng/ml and 3 ng/ml

(a)

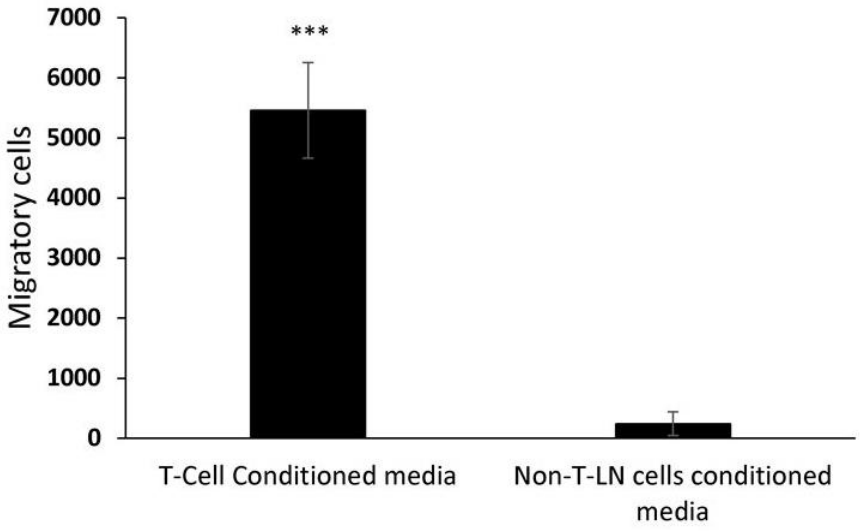

(b)

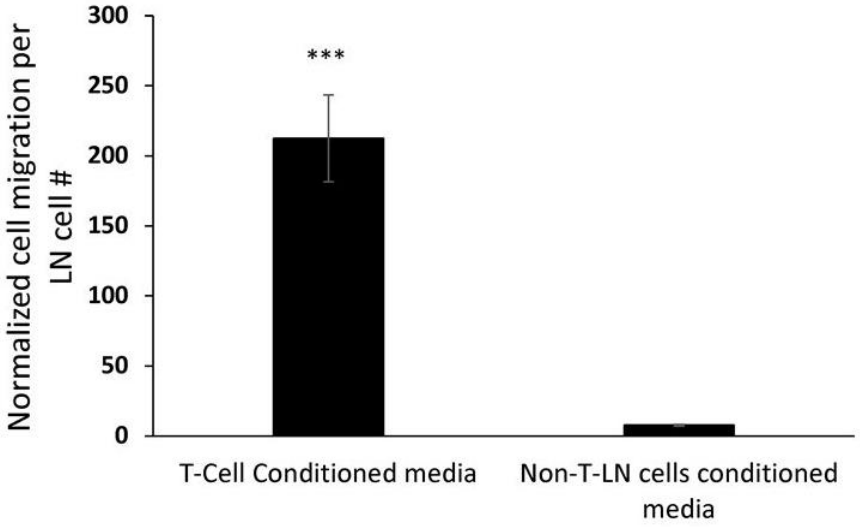

Figure 2-7 Effect of various activated LN cells (T-cells vs. non-T cells) on the migration of DAB2IP-KD was evaluated using CM of cells isolated from DAB2IP-KD-LN *in vitro*. (a) The ability of T lymphocyte CM and non-T cells CM to promote the migration of DAB2IP-KD cells was quantified. (b) The extent of DAB2IP-KD cancer cell migration was performed based on the same cell number (10^6 cells/CM). Data are mean ± Std, (*** P-value<0.001).

, respectively. These results indicate that CXCL12, CCL21 and IL-10 participate in T-cells mediated LN metastasis of DAB2IP-KD cells. These observations are supported by many recent investigations in which T-cells are found to participate in cancer cell proliferation, migration and metastasis [31-33, 68]. Specifically, T regulatory cells promote tumor growth by blocking the anti-tumor activity of cytotoxic T cells [69] Furthermore, it has been shown that T helper cells may promote tumor progression by the production of IL-17 that can induce IL-6 [70-72].

Although we garnered evidence of T-cells involvement in metastasis, it was important to simulate the LN environment as a step towards developing the LN mimetic. Many recent studies have shown that 3D culture provides better microenvironment and induces better cellular responses than 2D culture [73, 74]. For example, it has been shown that seeding cells on beads results in a homogeneous culture system and allow cells to grow at high densities in three dimensions which not only stabilizes the cells and improves the longevity of the culture but also decreases the need for external growth factors [75, 76].

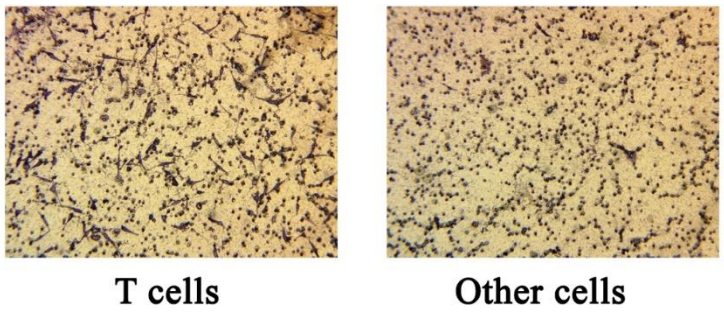

Figure 2-8 Representative images of migrated DAB2IP-KD cells on membranes with conditioned media of T-cells and non-T-cells isolated from cancer metastasized LN.

(a)

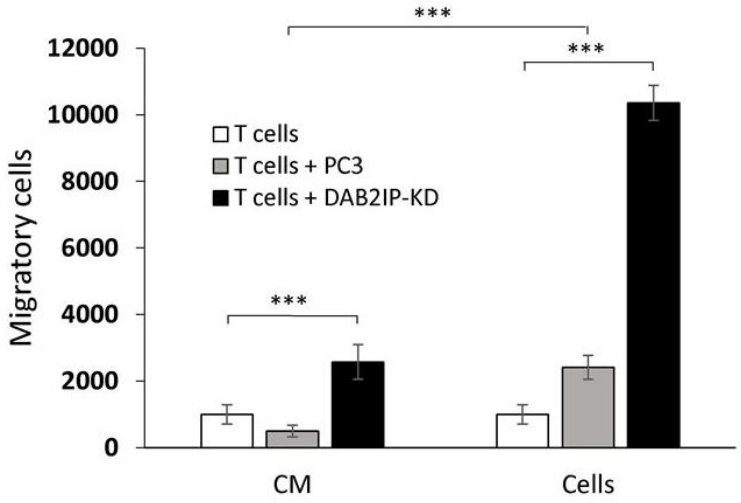

(b)

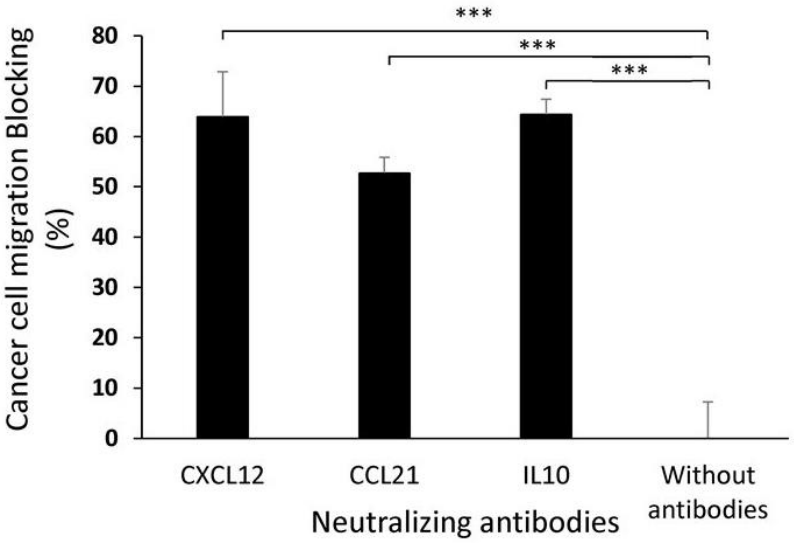

Figure 2-9 Activation of naïve T-cells after incubation with PCa cells or their CM was quantified using cell migration assay and DAB2IP-KD cells *in vitro*. (a) The extent of chemokine release by variously treated T-cells was assessed. (b) The effect of neutralizing antibodies on the reduction of chemotactic activities of T-cells co-cultured with DAB2IP-KD cells was determined. Data are mean ± Std, (*** P-value<0.001).

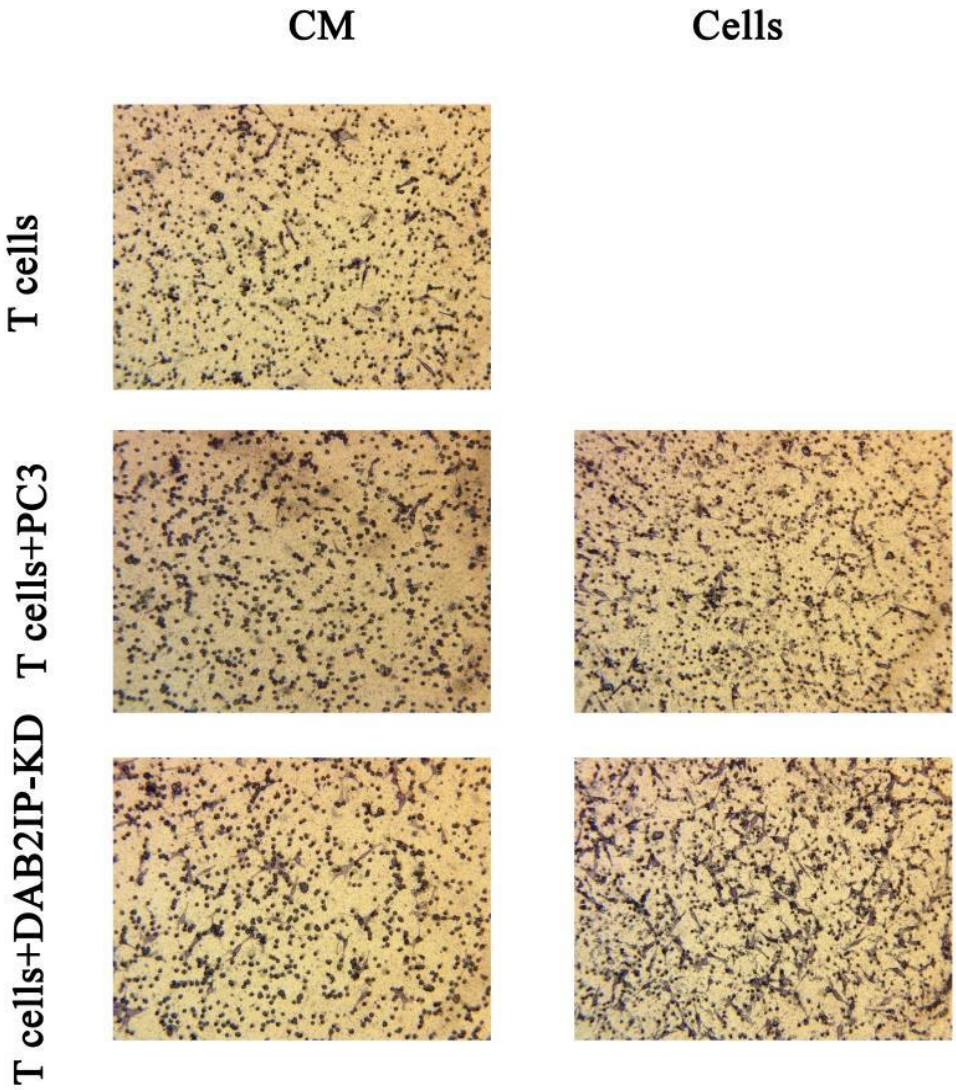

Figure 2-10 Representative images of migrated DAB2IP-KD cells on membranes with conditioned media of T-cells incubated with either cancer cells or cell condition media in the outer reservoir chamber.

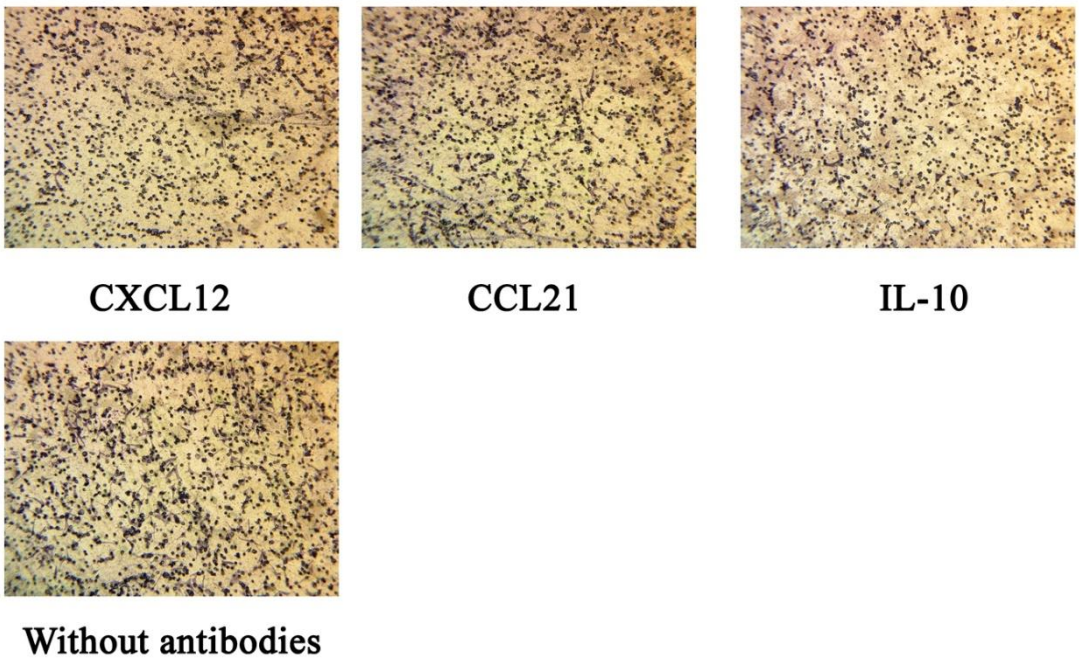

Figure 2-11 Representative images of migrated DAB2IP-KD cells on membranes with conditioned media of T-cells incubated with DAB2IP-KD cells in the presence of neutralizing antibodies against CXCL12, CCL21, or IL-10.

2.4.4. A 3D culture system for studying cancer LN metastasis

To establish a 3D LN biosystem, model T-cells (Jurkat cells) were seeded on Cytodex® I beads which have been used as T-cells carriers in the past. It has been reported that while Cytodex® beads alone have no mitogenic effect on lymphocytes, it increases stimulation in the presence of immunogens [77, 78]. Additionally, because of their large surface area to volume ratio (e.g. 5 mg of Cytodex® in 1 ml media provides 30 cm^2), the beads have been used as microcarriers to enhance cell growth and nutrient/waste exchange [79-81].

Remodeling of this cellular interaction in a dynamic tissue like LN needs controlled perfusion and mixing mobile and matrix-bound immobile cells [82]. To mimic LN environment and also to

provide optimal growth condition for the T-cells seeded on Cytodex® beads, a bioreactor system was engineered to apply flow rate similar to the LNs.

We found that T-cells could easily adhere and grow onto beads (**Figure 2-12 a**) and maintain its biomarker (CD3) (**Figure 2-13**). By quantifying the number of T-cells on Cytodex® beads at different times, we found that both initial cell seeding density of 100 and 500 cells/bead were suitable with similar cell attachment (167 ± 20 and 178 ± 24 Cells/bead) on Day 1 (**Figure 2-12 b**). With an initial cell density of 500 cells/bead, we found that the number of adherent cells on beads increased with time and reached a maximal number of 560 ± 40 cells/bead on Day 3. However, the number of adherent cells decreased sharply (~47%) on Day 4. On the beads seeded with initial 100 cells/bead, the number of adherent cells plateaued at 498 ± 17 and 443 ± 36 cells/bead on Day 3 and 4, respectively. Finally, on the beads seeded with an initial cell density of 20 cells/bead, the numbers of adherent cells increased with time and plateaued on Day 3 and 4 at ~400±28 and 425±52 cells/bead, respectively.

We then compared the cellular responses of T cells seeded on 3D (Cytodex® beads) and 2D (cell culture plates) culture. For that, both 3D and 2D T cells were incubated with DAB2IP-KD cells CM for 48 hours and then placed in regular media for 2 days to collect the CM for chemotaxis measurements. As expected, we found that T cells on Cytodex® beads (3D culture) triggered 3X more DAB2IP-KD cell migration than those on culture plates (2D culture) (**Figure 2-12 c**) (The representative images of migrated cells on Transwell membranes can be found in **Figure 2-14)**. These results support better mimicking of T cells by 3D cultures compared to 2D cultures.

Subsequent studies were carried out to assess the direct interactions between PCa cells and adherent T-cells on Cytodex® beads. For this investigation, T cells-seeded Cytodex® beads were

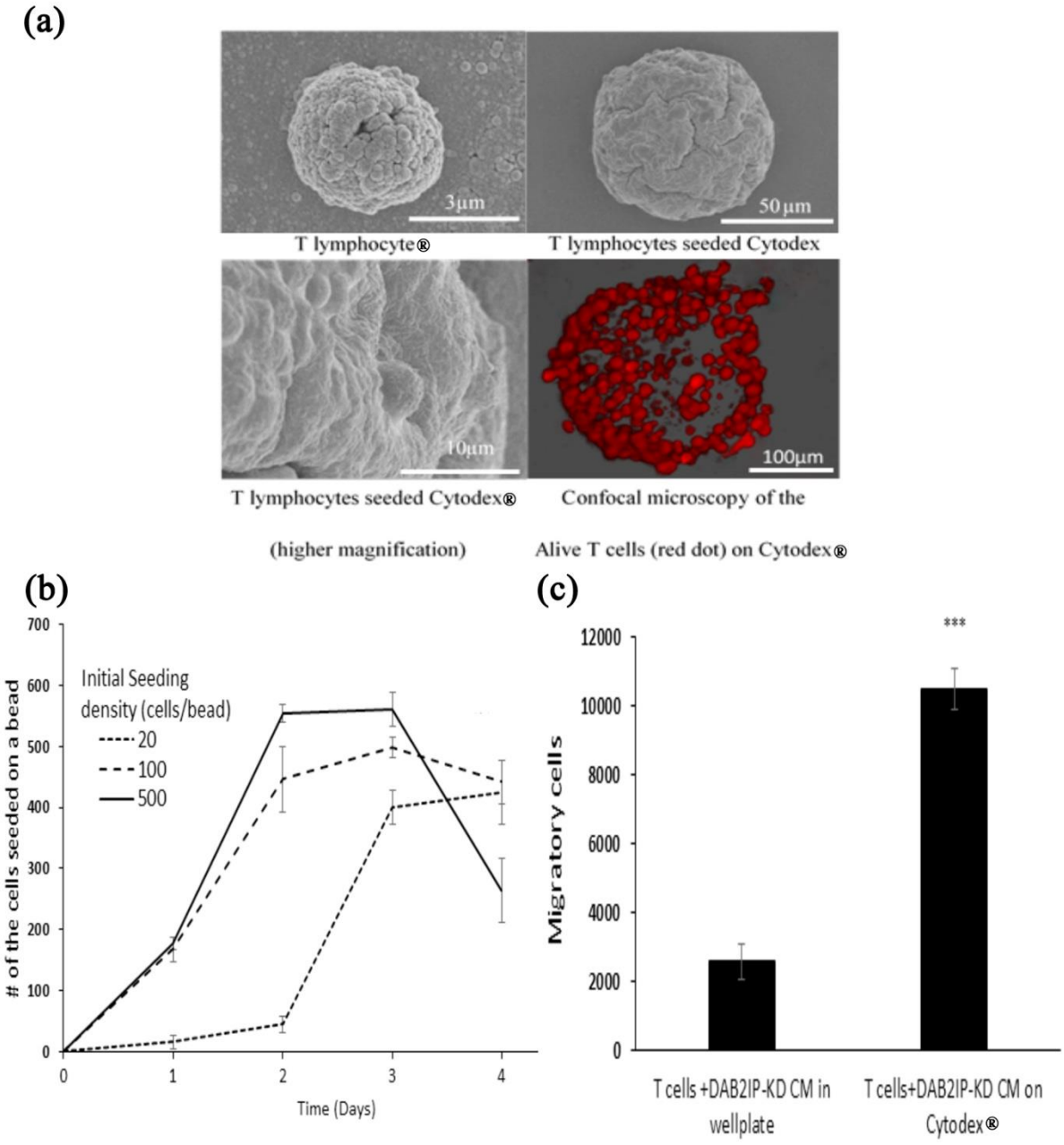

Figure 2-12 Characterization of the responses of T cells seeded on Cytodex® beads. (A) The morphology of T cells seeded on the beads was examined using SEM and confocal microscopy. (B) The influence T-cell seeding densities on cell growth at different time points was determined. (C) The pro-chemotactic responses of 2D vs 3D cultured T-cells with DAB2IP-KD CM were compared. Data are mean ± Std, (*** P-value<0.001).

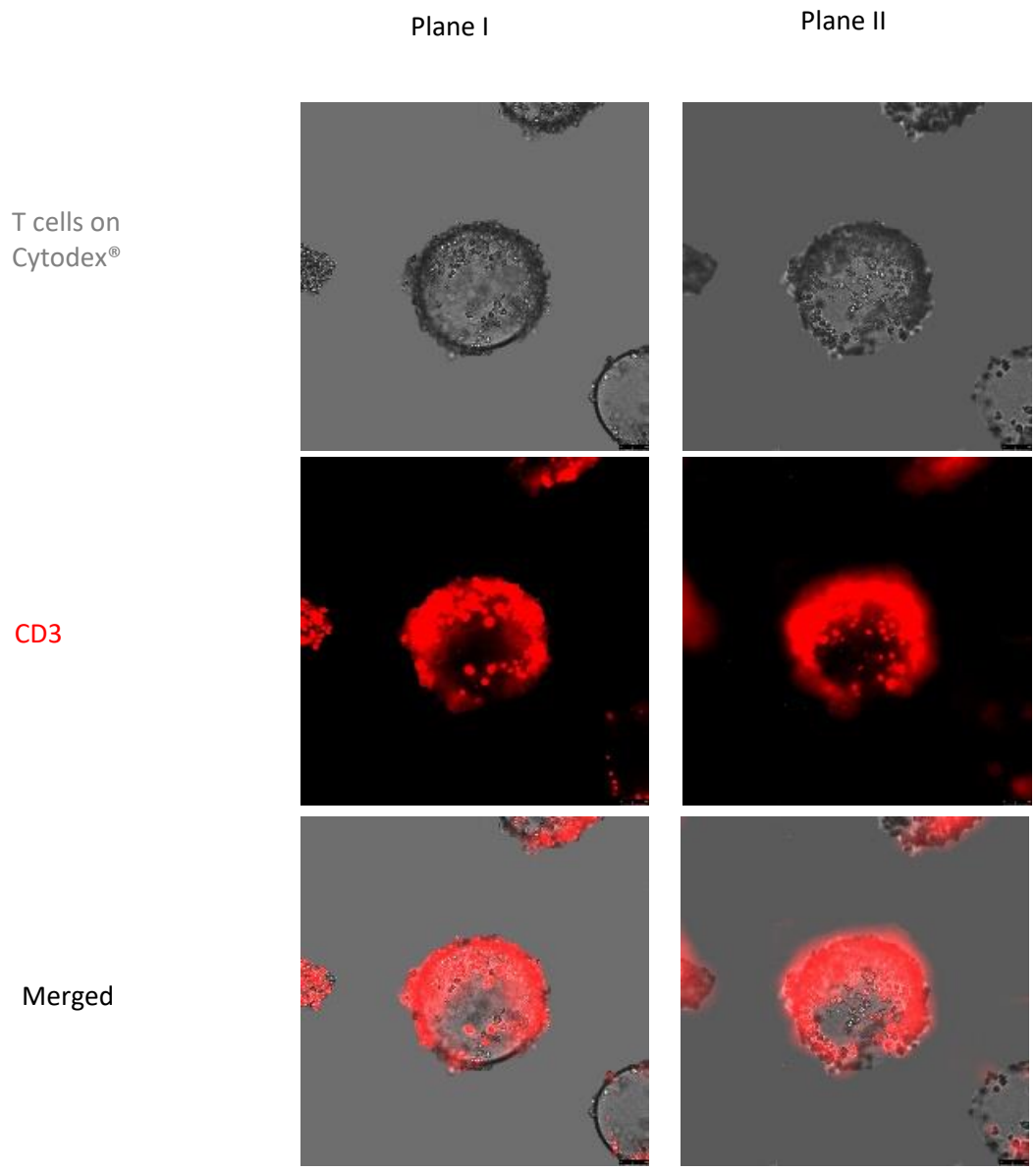

Figure 2-13 Fluorescence microscopy images of T-cells on Cytodex® bead and their corresponding CD3 expression at different Planes.

incubated with PC3 cells and DAB2IP-KD cells with 5:1 ratio of T lymphocyte to PCa cell. The CM was collected every 24 hours for 4 days for chemotactic potential measurements and some of the Cytodex® beads were recovered for confocal imaging. Confocal images reveal that there were a few PC3 cells (pink colored) on the T-cells (green colored) seeded Cytodex® beads (**Figure 2-15**

a) (The fluorescent microscopy images of T-cells on Cytodex® bead and their corresponding CD3 expression at different Planes can be found in **Figure 2-13)**. On the other hand, significantly more DAB2IP-KD cells than PC3 cells were found to accumulate on T cell-seeded Cytodex® beads (estimated 75 DAB2IP-KD/Bead vs 7 PC3/Bead).

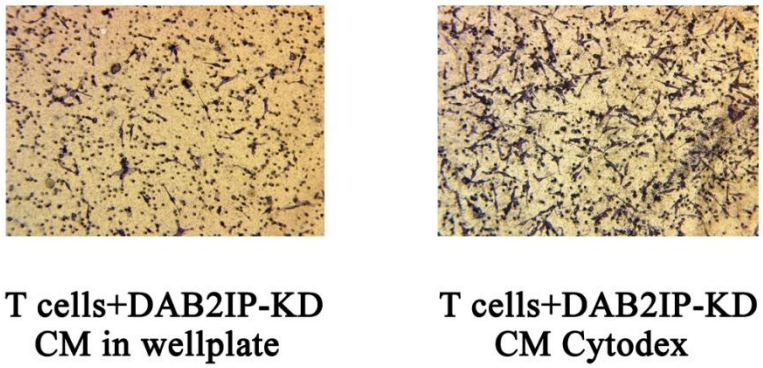

Figure 2-14 Representative images of migrated DAB2IP-KD cells on membranes with conditioned media from T-cells incubated with DAB2IP-KD CM either (1) in a well plate or (2) seeded on Cytodex® beads.

Our early results showed that LNs trigger stronger chemokine/cytokines production to DAB2IP-KD cells than PC3 cells. To assess whether 3D cultured T-cells would prompt similar responses, we measured the chemotactic potential of CM isolated from T cell-seeded Cytodex® beads incubated with either PC3 or DAB2IP-KD cells for 4 days (**Figure 2-15 b**) (The images of migrated cells on Transwell membranes can be found in **Figure 2-16)**. Our results show T-cells seeded Cytodex® beads exposed to DAB2IP-KD cells released more chemotactic factors (~3X) than those exposed to PC3 cells. However, such differential responses only last for 3 days. The short life of the differential responses could be attributed to the high consumption of media

nutrients and accumulation of toxic waste. The results suggest that a flow system is required to prolong the life span of the biosystem.

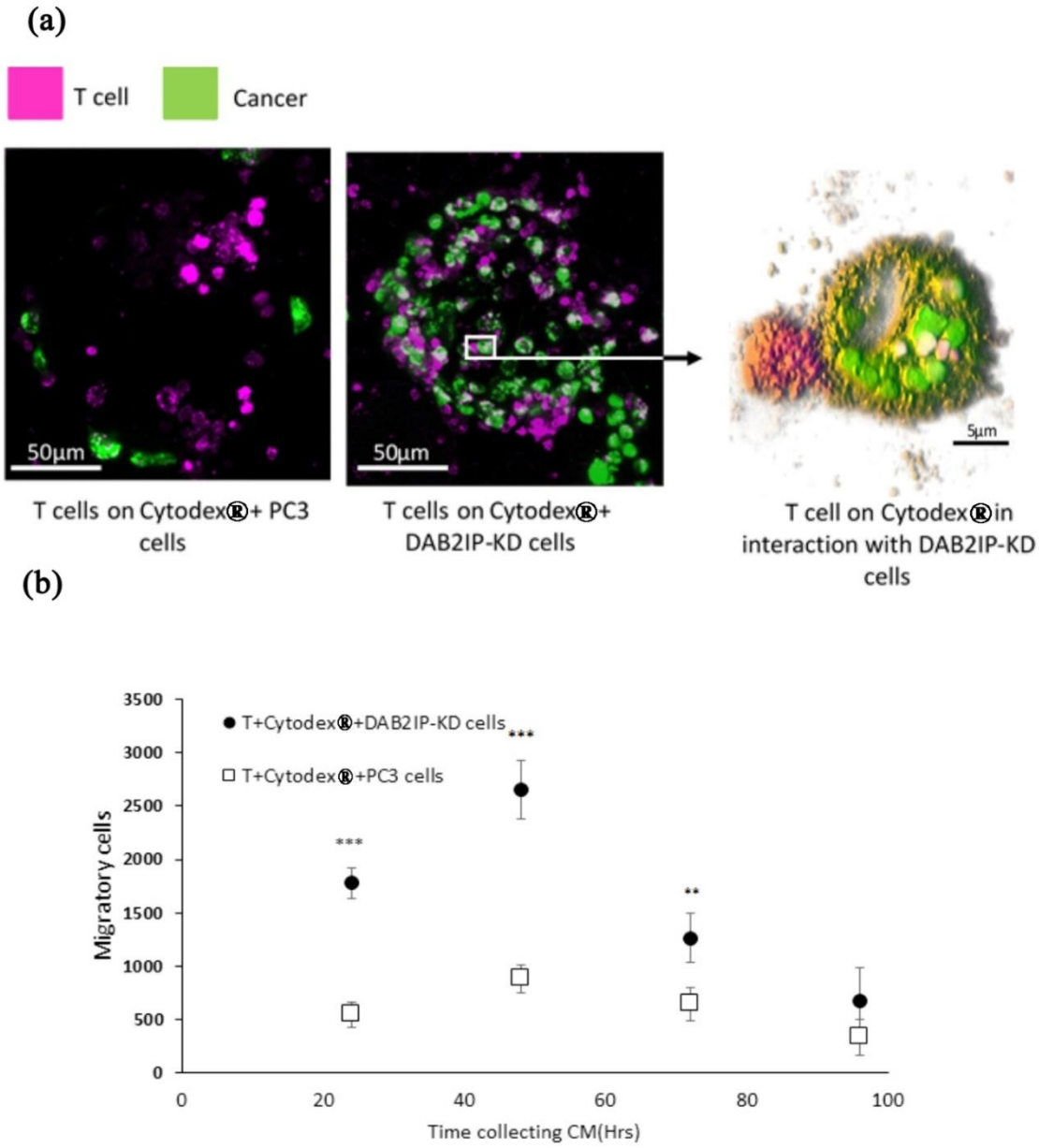

Figure 2-15 Interactions between PCa cells and T-cells seeded on Cytodex® beads were characterized using (a) confocal microscopy and (b) in vitro chemotaxis assay of CM collected at different time points. (** P-value<0.01, *** P-value<0.001).

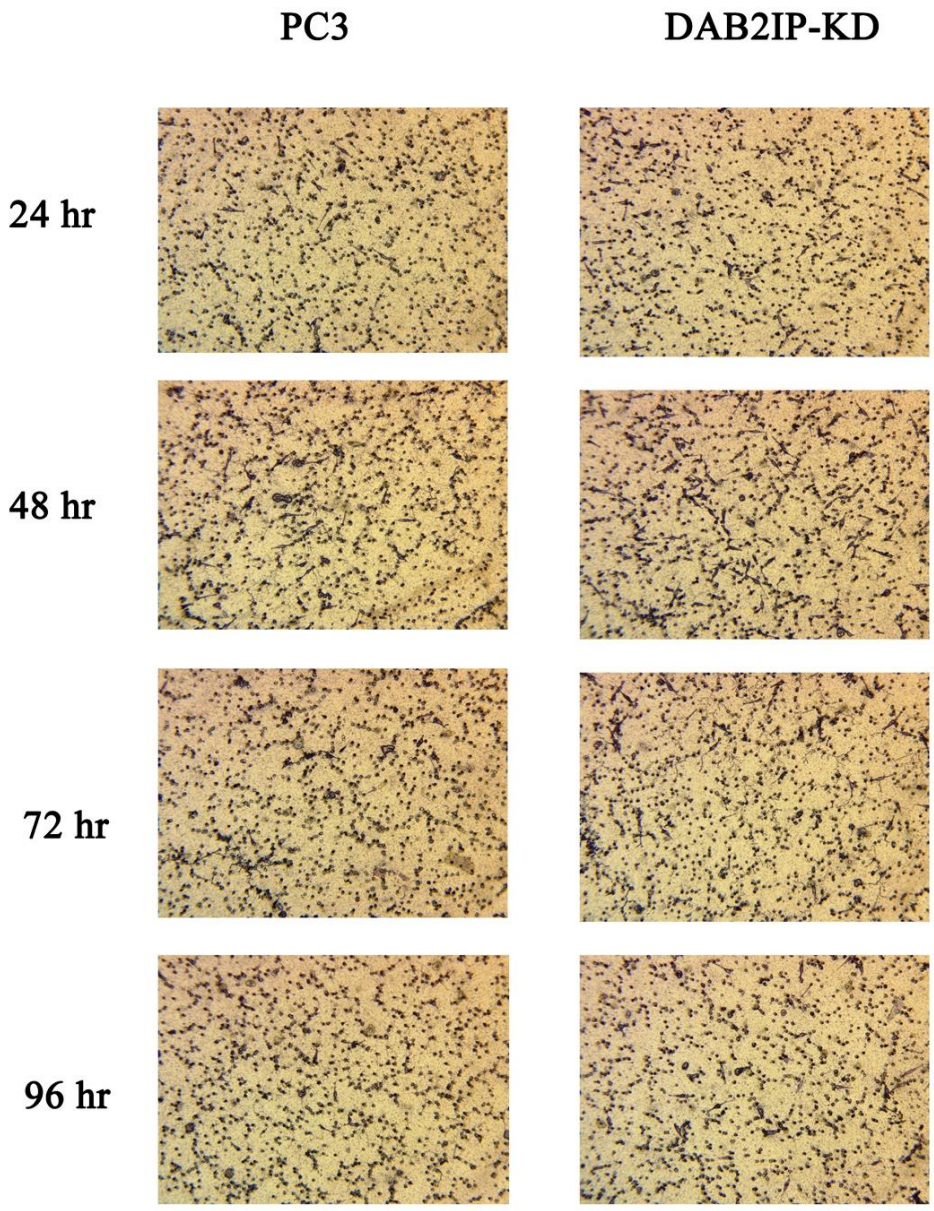

Figure 2-16 Representative images of migrated DAB2IP-KD cells on Transwell membranes with media collected from the static culture of T-cells seeded Cytodex® beads in interaction with PCa cells (PC3 and DAB2IP-KD cells) at different time points (24, 48 and 72 hours)

2.4.5. LN mimetic flow biosystem

LN responses are complex processes with many biomolecules and cells participating in the reactions at different times. In an attempt to decipher such responses and reduce the effect of high consumption of media nutrients and accumulation of toxic waste, we built an LN mimetic flow

system (**Figure 2-17 a**). This system was designed to mimic the dynamic condition of the real LN. To engineer such device, T-cells were seeded on Cytodex® beads, for two days. The seeding process was performed in modified Transwell to mimic the fibrosis capsule around the LN and keeps the beads in the bioreactor. Then the modified Transwell contains T-cells seeded Cytodex® were placed in the bioreactor where the media flow with the rate of 100 µl/hour was applied to that. The cell viability result showed that after 5 days 78.34±0.71 % of the T-cells were alive in the bioreactor (**Figure 2-17 b**). To evaluate the biological activities of the LN mimetic system, different PCa cells were added on top of the flow chambers containing T cell-seeded Cytodex®. CM was collected from the bottom of the flow chambers at different time points and analyzed for their chemotactic activities. Our results show that the introduction of DAB2IP-KD cells to T-cells seeded Cytodex® significantly increase the cancer cell chemotactic factors by compared to PC3 incubation with T cell-seeded Cytodex® beads (**Figure 2-17 c**)(The representative images of the migrated cells on Transwell membranes are shown in **Figure 2-18)**. In addition, the ability of LN mimetic system to simulate metastatic esophageal cancer LN responses was investigated. As expected, our results show that, LN mimetic biosystem induces more cancer cell chemotaxis factors with the introduction of highly metastatic esophageal cancer cells (KYSE-30 cells) than with the introduction of esophageal epithelial cells (Het-1A cells) (**Figure 2-17 d**) (The representative images of migrated cells on Transwell membranes are shown in **Figure 2-19)**. The results demonstrate that LN mimetic biosystem can simulate LN responses to cancer cells.

These results show that the LN mimetic biosystem release more chemotactic factors in the presence of metastatic PCa cells (DAB2IP-KD cells) and esophageal cancer cells (KYSE-30 cells) than those of low metastatic PCa cells (PC3 cells) and esophageal epithelial cells (Het-1A cells),

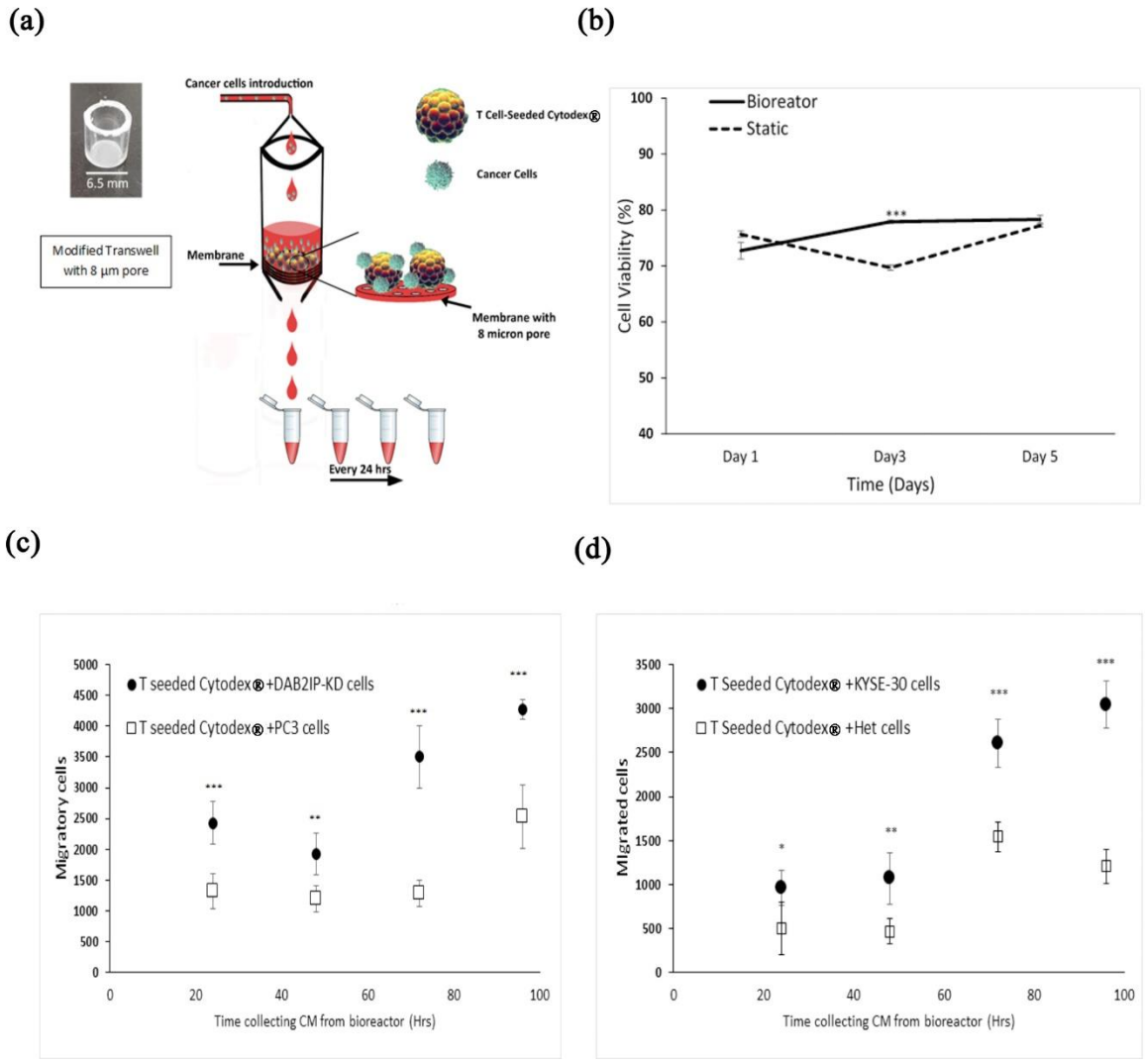

Figure 2-17 LN mimetic flow biosystem was built and functional characterized *in vitro*. (a) Schematic of LN flow biosystem design show various component of the system. (b) The influence of flow biosystem on the viability of the T-cells seeded on Cytodex® beads was assessed at different time points. (c) The ability of different CM collected at different time points from T-cells seeded Cytodex® beads in interaction with PCa cells (PC3 and DAB2IP-KD cells) to promote the migration of DAB2IP-KD. (d) The ability of different CMs collected at different time points from T-cells seeded Cytodex® beads in interaction with esophageal cancer cells (Het-1a and KYSE-30 cells) to promote the migration of KYSE-30 (* P-value<0.05, ** P-value<0.01, *** P-value<0.001).

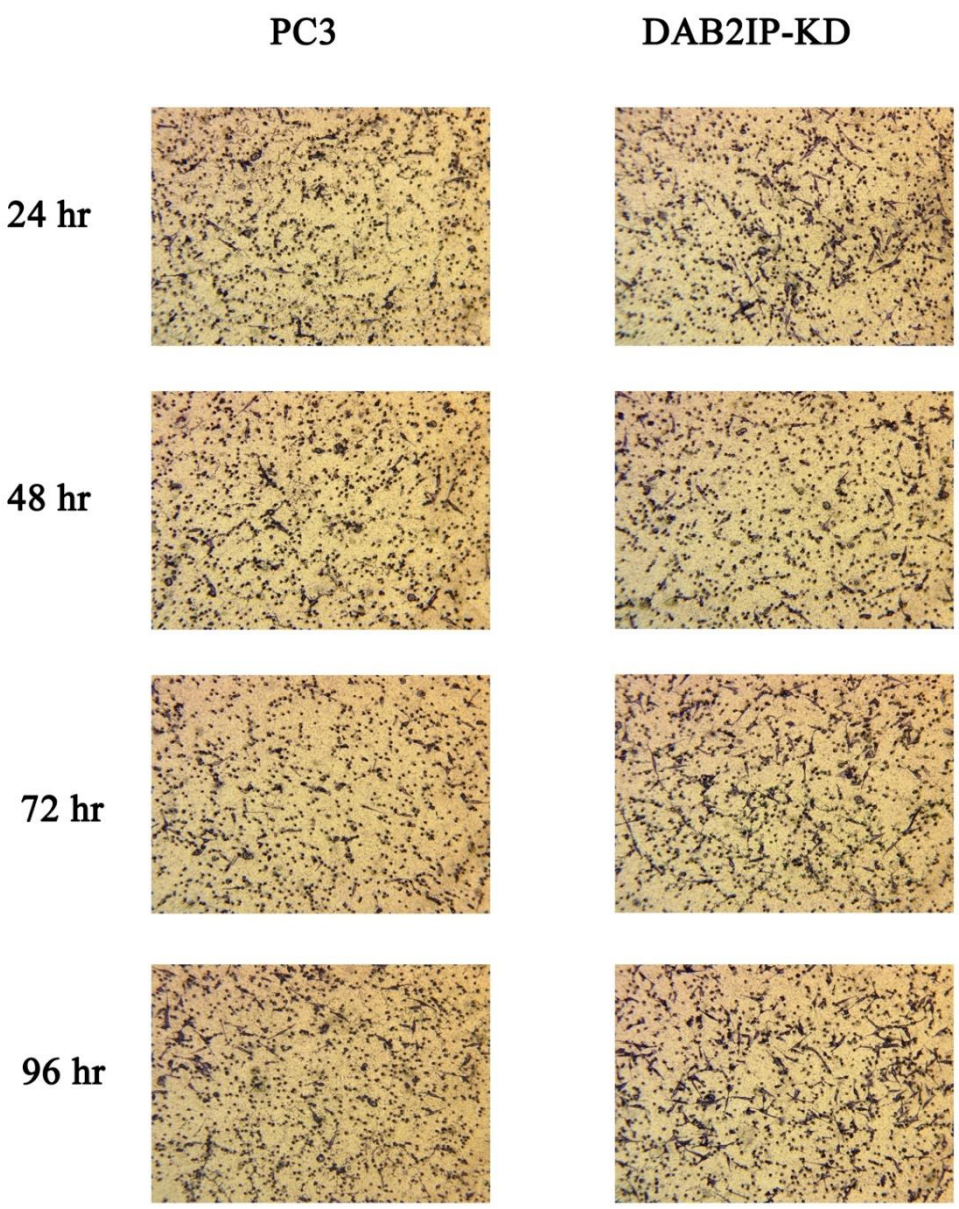

Figure 2-18 Representative images of migrated DAB2IP-KD cells on Transwell membranes with media collected from the T-cells seeded Cytodex® beads bioreactor after the introduction of either PC3 cells or DAB2IP-KD cells at different time points (24, 48, 72, and 96 hours).

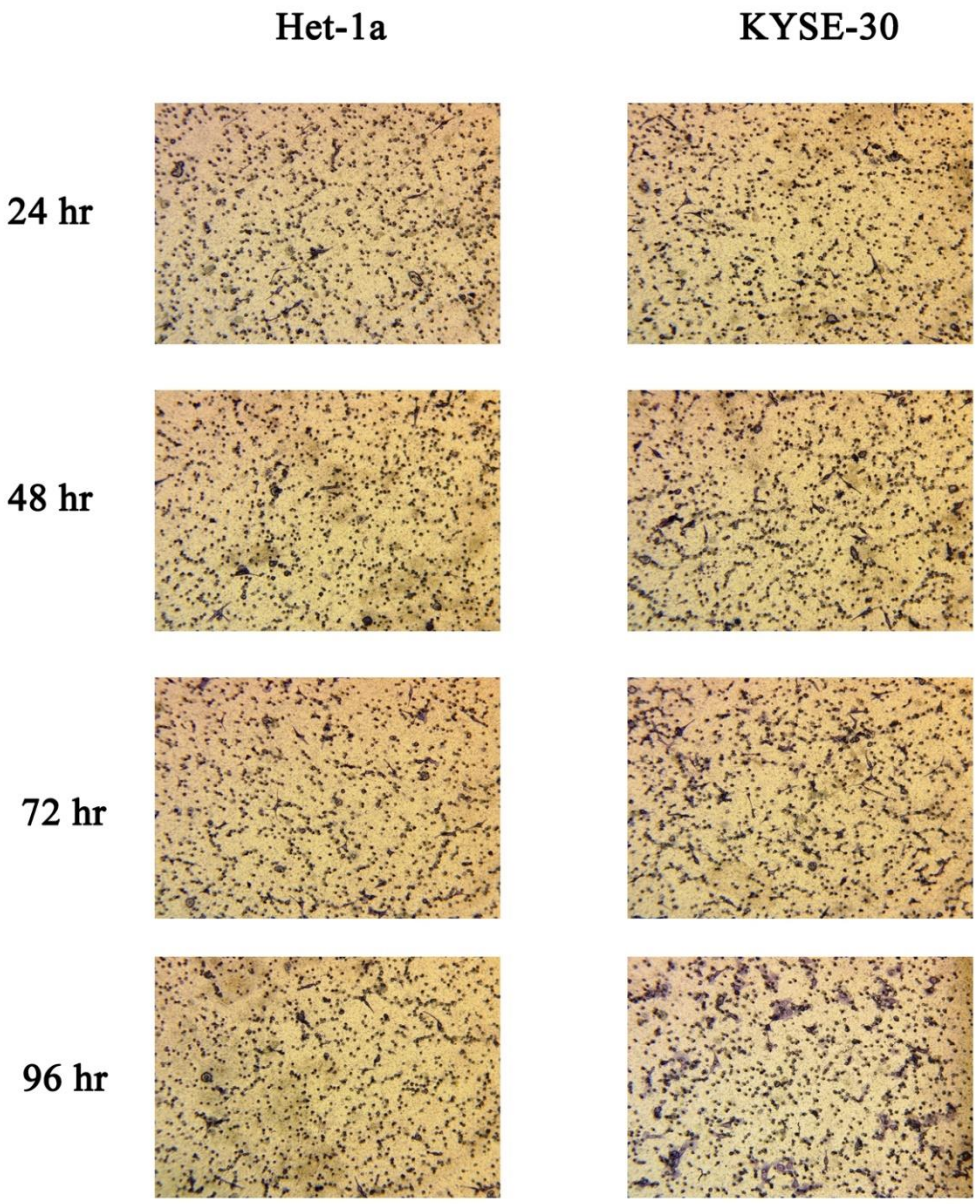

Figure 2-19 Representative images of migrated KYSE-30 cells on Transwell membranes with media collected from the T-cells seeded Cytodex® beads Bioreactor after the introduction of esophageal cancer cell (Het-1a and KYSE-30) at different time points (24, 48, 72, and 96 hours).

respectively. This supports the possibility of using this new LN mimetic biosystem for studying the mechanism governing LN cancer metastasis as well as to distinguish between high and low metastatic cancer cells. In addition, by analyzing T-cell responses to the cancer cells isolated from cancer/tumor biopsy, this new system can be used for assessing the metastatic potential of isolated cells.

2.5. Conclusion

In conclusion, our work has led to the creation of a LN-mimetic biosystem to simulate LN microenvironment. Our results have demonstrated that this new LN flow biosystem provides an excellent tool to investigate the interaction between PCa cells and LN microenvironment during the metastatic process. It is our belief that this new LN mimetic biosystem can be used not only to study the LN responses to cancers but also to explore various cancer treatments for reducing LN metastasis.

2.6. Experimental Section

2.6.1. Materials

Cytodex® I beads with average dry size of 190 μm (GE Healthcare Life Sciences, Pittsburgh, PA); Transwell cell migration insert with pore size of 8.0 μm (Corning Inc, Tewksbury, MA); 70 μm SmartStrainer (Miltenyi Biotec Inc. Auburn, CA) and MagniSort™ mouse CD3 Positive Selection Kit (Thermo Fisher Scientific, Waltham, MA) were purchased. Cell culture supplies were purchased from different vendors, including Ham's F12, DMEM, RPMI (all from Sigma-Aldrich, St. Louis, MO), fetal bovine serum (FBS) (Atlanta Biologicals, Atlanta, GA), penicillin/streptomycin, Geneticin G418, Puromycin were purchased from Gibco (Waltham, MA), and GT-T551 media from Takara (Japan). (ATCC, Manassas, VA). Dispase, DNAse and Collagenase P were purchased from Roche (Indianapolis, IN). Qiagen RNeasy Mini kit (Qiagen

Inc. Valencia, CA), Cell Counting Kit-8 (Dojindo Molecular Technologies, Inc. Rockville, MD), and LIVE/DEAD Viability/Cytotoxicity Kit for mammalian cells. (Molecular Probes, Inc., Eugene, OR) were also purchased.

2.6.2. Cell lines, isolation, and culture

Human prostate cancer cell lines, PC3 and DAB2IP gene knockdown PC3 (abbreviated as DAB2IP-KD) cells, were used as PCa cells with low and high metastatic potential, respectively [83]. PCa cells were cultured in RPMI supplemented with 10% heat-inactivated FBS and 1% penicillin/streptomycin. In addition, PC3 cells were supplemented with G418 (200 µg/mL), and DAB2IP-KD cells were supplemented with G418 (800 µg/mL) and Puromycin (500 ng/ml). Metastatic (KYSE-30) human esophageal cancer cells and non-tumorigenic esophageal epithelial cells (Het-1A) were cultured in 50:50 Ham's F-12/RPMI-1640 medium supplemented with 5% heat-inactivated FBS, 1% penicillin/streptomycin. Jurkat T cells (Clone E6-1, ATCC® TIB-152™) were obtained from the American Type Culture Collection and cultured in GT-T551 media supplemented with 10% heat-inactivated fetal bovine serum. Cultured cells were kept at 37 °C in a humidified incubator in the presence of 5% CO_2. LN cell isolation was carried out using MagniSort™ mouse CD3 Positive Selection Kit by following the manufacturer's instructions. Briefly, LNs minced into 1 mm pieces with sterile scalpels or scissors were digested with RPMI containing enzymes 0.8 mg/ml Dispase, 0.1 mg/ml DNase I and 0.2 mg/ml Collagenase P. The digested solution was then passed through 70 µm Smart Strainer to generate LN cells suspension. The isolation of T lymphocytes and non-T lymphocytes was carried out using MagniSort™ mouse CD3 Positive magnetic beads. Isolated LN cells were cultured in RPMI supplemented with 10% heat-inactivated FBS.

2.6.3. Characterization of lymph nodes in cancer implanted animals

To investigate cancer metastasized LN responses, the intraperitoneal implantation mouse model was used [84]. The animal protocols were approved by the University of Texas at Arlington's Animal Care and Use Committee. Immunocompetent mice were used in this study since immune-deficient animals do not have normal LN cells and structure. Briefly, Balb/c mice (both genders and 6 to 8 weeks old) were purchased from Jackson Laboratory (Bar Harbor, ME). The animals were implanted intraperitoneally with either PC3 or DAB2IP-KD (5×10^6 cells/500 µl per animals, N=6). After implantation for two weeks, the animals were sacrificed. The LN tissue was isolated for a series of analyses. Some of the tissues were used for histological evaluation [85].

2.6.4. Gene profile analyses of LNs:

The gene expression of various LNs was determined using the mouse tumor metastasis RT² Profiler™ PCR Array, which contains 84 genes known to be involved in metastasis. Briefly, RNAs were isolated from different LNs using Qiagen RNeasy Mini kit and were then converted to cDNA and assessed using a real-time PCR machine.

2.6.5. Measurement of cancer metastasis potential:

The ability of LN cells and cellular products was assessed using a Transwell system, as described earlier [86]. Briefly, LN tissue, LN cells or LN cell-seeded Cytodex® beads were incubated with RPMI media with 1% FBS for different durations to generate conditioned media (CM). The CM was then used in the Transwell cell migration assay as described earlier [87, 88]. To determine the type of cytokines responsible for cancer cell migration, a limited study was carried out in which CM was incubated with neutralizing antibodies against CXCL12, CCL21, IL-10, CCL20, CLL19 and IL-8 (all from R&D Systems, Minneapolis, MN) for 2 hours. Then, the ability of variously treated CM to promote the migration of DAB2IP-KD cells was quantified using Transwell

migration assay as described above. Based on their chemotactic potential, The concentration of CXCL12, CCL21 or IL-10 were calculated using standard curves of chemotactic potential established by the manufacture and earlier publication[89, 90].

2.6.6. Fabrication of 3D LN mimetic

For simulating LN microenvironment in 3D and providing an ECM that act like the reticular cells in real LNs, Cytodex® 1 beads were used as microcarriers. T cell-seeded Cytodex® beads with different cell seeding densities (20, 100, or 500 cells/ bead) were fabricated. After culturing for different periods (1, 2, 3 and 4 days), the number of cells on the beads were counted using Cell Counting Kit-8 by following the manufacturer's instructions. In addition, the morphology of seeded cells on beads was observed using SEM (FE-SEM, S-4800 Hitachi, operating at 5 kV) and laser scanning confocal microscope (A1R, Nikon). To study the interactions between PCa cells and T-cells, cells-seeded beads were co-cultured with PCa cells or PCa CM for 24 hours. The chemotactic effect was assessed using a Transwell migration assay.

2.6.7. Development of 3D lymphatic system:

To simulate the lymphatic system and preventing high consumption of media nutrients and accumulation of toxic waste, a flow perfusion bioreactor system was fabricated using a perfusion pump (Harvard Apparatus, Holliston, MA), polyurethane tubing (3 mm diameter) and polypropylene cascade (7 mm diameter) under sterile condition at 37 °C in a humidified incubator in the presence of 5% CO_2. Briefly, T cells were seeded on Cytodex® inside modified Transwell (**Figure 2-17 a**) (6.5 mm diameter, 8-micrometer porosity) for 2 days. Then the modified Transwell containing T-seeded Cytodex® beads were placed inside the polypropylene cascade. The system was placed under a static flow (100 microliters/hour) of media (RPMI + 1% heat-inactivated FBS). T-cell viability in the bioreactor was assessed after 1, 3 and 5 days using

LIVE/DEAD Viability/Cytotoxicity Kit for mammalian cells as follows. T-cells were seeded on Cytodex® (in bioreactor and static culture) with identical cell numbers and media volume. After culturing the cells for different periods of time, their viability was determined using LIVE/DEAD assay. For that, the beads were incubated with calcein AM and EthD-1 for 45 mins. After washing with PBS 3X, fluorescence intensities associated with the beads were measured using a microplate reader (Tecan, San Jose, CA). The viability was then determined by dividing this fluorescence intensity with that from cells alone.

To simulate cancer metastasis, cancer cells (PC3/DAB2IP cells or Het-1a/KYSE-30 cells) were added on top of the T-cells seeded beads. The media flowing through the bead system was collected every 24 hours for 4 days. The cancer chemotactic activities of the media were then assessed using a Transwell cell migration assay.

2.6.8. Statistical analysis:

All the data are shown as means $\pm$ standard deviation. The normality of the samples was evaluated using the Shapiro-Wilk test and normal probability plot. ANOVA and independent student t-test were performed in order to evaluate the difference between group averages. F test was used to test the equality of the variance. The level of significance of experimental groups with respect to controls was determined at a P-value of less than 0.05 ($P < 0.05$). All statistical analyses were performed using SPSS 16 and XLSTAT.

Chapter 3

3.1.CELL ENCAPSULATED ALGINATE BEADS FOR SIMULATING LYMPH NODE RESPONSES OF METASTATIC CANCERS

Keywords: Prostate cancer, metastatic lymph nodes, Alginate beads, metastatic Lymph node mimetic, in vivo model

3.2. Abstract

Lymph node (LN) metastasis is a well-known prognostic factor in many solid cancers. However, the mechanism(s) governing LN metastasis is not totally understood due to the lack of LN culture system mimicking metastatic LN (mLN). To overcome this challenge, an mLN mimetic 3D culture system was fabricated by encapsulating T-cells and cancer cells inside alginate beads. Such a system was then tested both *in vitro* and *in vivo*. First, co-culture of T-cells and metastatic prostate cancer cells are able to produce abundant cancer chemotactic agents resemble metastatic LNs. Second, the alginate bead encapsulation process was optimized to retain the viability and function of T cells and cancer cells. Third, beads with encapsulated co-cultured cells were confirmed to release biomolecules capable triggering the migration and invasion of metastatic cancer cells. Finally, the ability of this system to promote cancer metastasis was assessed *in vivo*. Overall, our results support the creation of mLN system, which can be used as a powerful 3D culture system for studying the processes governing LN metastasis.

3.3. Introduction

Cancer metastasis, the spread of malignant cells to new areas of the body to initiate the growth of a secondary tumor at a distant site, is responsible for the majority of death in cancer-specific mortality [91, 92]. Among all the organs, lymph nodes (LNs) are often the first ones to which cancer cells metastasize [17, 93]. In fact, there is abundant evidence to support that LN metastasis is an early event of many solid tumor metastases [94, 95]. Furthermore, regional LNs metastasis is often associated with higher rates of tumor recurrence and cause of death in cancer patients [96-98].

Cancer LN metastasis is governed by complex processes starting with the escape of tumor cells from the primary tumor site and permeate the surrounding lymphatics [99]. Coincidentally, it has been shown that cancer metastasized LNs may turn into tumor-draining lymph node (TDLN) and TDLN may release biomolecules to have a profound influence on the rest of the immune system [18, 100, 101]. Furthermore, cancer metastasized lymphatic vessels are found to produce chemokine and cytokines that promote cancer cell metastasis [99, 102] and LN lymphangiogenesis – a growth of new lymphatic vessels [103-105]. On the other hand, recent studies have shown that lymphatic endothelial cells produce vascular endothelial growth factors (VEGF), such as VEGF-C and VEGF-D, and that the latter stimulates the integrin $\alpha 4\beta 1$ expression, lymphangiogenesis, and, thus, tumor metastasis [25, 106-109]. VEGF-A is also known to stimulate lymphangiogenesis, although it is not as potent as VEGF-C and VEGF-D [110]. In addition, several cytokines like CXCL12, CCL21 and CCL19 in the LNs also affect cancer cells metastasis [54, 111-113]. Despite these exciting findings, the critical cell types and cellular products in metastasized LN responses are not totally understood.

While cancer cell LN metastasis often leads to devastating clinical outcome, very few treatment options have been found to be effective in eradicating cancer LN metastasis [114, 115]. To overcome this drawback, there is a critical need for the development of treatment to reduce cancer LN metastasis. Our laboratory has previously shown that an implantable "cancer trap" implants can be fabricated to actively recruit metastatic cancer cells by releasing specific biomolecule [87]. Interestingly, the cancer trap implants were found to be able to capture circulating metastatic cancer cells and to prolong the lifespan of cancer-bearing animals [87]. In a separate study, we have uncovered that cancer cell metastasized LNs release abundant biomolecules to promote cancer cell metastasis [116]. Furthermore, after incubated with cancer cells, T cells seeded on Cytodex beads were able to produce cancer cell chemokines similar to metastatic LN [116]. The above observations support that a cancer cells-T cells co-culture device may be fabricated to simulate metastatic LNs.

Cell encapsulation was originally introduced to assist in xenogenic or allogenic cell transplantation to permit the release of a biomolecule from transplanted cells while avoiding immune rejection by the host [117]. For that, one or multiple types of cells are encapsulated in a biocompatible, semipermeable physical membrane [118]. To protect immune reactions, the porosity of membranes is selected to exclude immune cells and antibodies. At the same time, the membrane permits the free passage of nutrients, oxygen, and small molecules. Alginate, a natural and anionic oligosaccharide, is one of the most commonly used materials for cell encapsulation. It has high biocompatibility, long-term stability and viability of the encapsulated cells both *in vitro* and *in vivo* [119]. Therefore, alginate is chosen to fabricate the cell co-culture device.

To test the hypothesis, our study was focused on prostate cancer (PCa), since PCa is considered as the second most common type of cancer in men [120]. PCa usually remains undetected until

becoming metastatic [121] and LN metastasis is commonly found in patients with late-stage PCa [122]. To fabricate metastasized LN mimetic, we first determine the optimal ratio of the cancer cells and T lymphocyte for triggering maximal cancer chemotactic agents. We then optimize the procedure for generating cell co-culture encapsulated beads using alginate. The physical, chemical and biological properties of the beads were then determined. The ability of metastasized LN mimetic devices to induce PCa metastasis was then assessed and the types of chemokines most important to cell migration were also determined. Finally, a preliminary *in vivo* study was carried out to assess the ability of metastasized LN mimetic devices to trigger cancer cell migration.

3.4. Materials and methods

3.4.1. Materials

Transwell cell migration insert with pore size of 8.0 μm were purchased Corning Inc, (Tewksbury, MA); Sodium Alginate (A0682, Mw 12–80 kDa), Calcium Chloride, RPMI media 1640 were purchased Sigma-Aldrich (St. Louis, MO); fetal bovine serum (FBS) was purchased from Atlanta Biologicals (Atlanta, GA); penicillin/streptomycin, Geneticin G418 and Puromycin were purchased from Gibco (Waltham, MA); GT-T551 media from Takara (Japan). Jurkat T cells (Clone E6-1, ATCC® TIB-152™) were obtained from the American Type Culture Collection (ATCC, Manassas, VA). LIVE/DEAD Viability/Cytotoxicity Kit for mammalian cells were purchased from Molecular Probes Inc. (Eugene, OR).

3.4.2. Cell lines and culture

Our recent study has uncovered that the interaction between T cells and cancer cells are essential to simulate metastasized LN responses [116]. Therefore, both T cells and PCa cells were used in this study. Specifically, human prostate cancer cells (PC3) with and without DAB2IP gene knockdown (abbreviated as DAB2IP-KD) were used as low and high metastatic PCa, respectively

[83]. Both cell lines were a kind gift from Dr. Jer-Tsong Hsieh (Department of Urology, University of Texas Southwestern Medical Center at Dallas). Both the cells were cultured in RPMI-1640 supplemented with 10% heat-inactivated fetal bovine serum and 1% penicillin/streptomycin (Gibco). 200 and 800 µg/ml G418 (Gibco) were used in PC3 and KD media, respectively. 500 ng/ml Puromycin (Gibco) also has been used in KD media. Jurkat T cells were cultured in GT-T551 media supplemented with 10% heat-inactivated fetal bovine serum. All the cells and conditioned media (CM) were kept at 37 °C in a humidified incubator in the presence of 5% CO2. To study the effect of the interaction of the T cells and PCa on recruiting metastatic cancer cells, T-cell has been co-cultured with KD cells in the different ratio in serum-free media. The CMs collected after 48 hrs to evaluate for chemokine production using Transwell migration assay as shown earlier [116].

3.4.3. Cell encapsulation optimization

To optimize the encapsulation condition based on cell viability, 3-level factorial response surface methodology (RSM) (design expert 11, Stat-Ease Inc. Minneapolis, MN) has been used. A total of 9 experimental runs suggested by the software (**Table** 3-1). T cells were encapsulated in alginate beads based on the published methods [123]. Briefly, T cells were suspended in different concentrations of alginate (1%, 1.5% or 2%) in cell culture media with the final concentration of 10^6 cells/ml. The cell suspension solution extruded through a 27 g needle under constant injection using a perfusion pump (Harvard Apparatus, Holliston, MA), into 20 ml of CaCl2 (1%, 3% or 5% w/v) solution under constant stirring at room temperature. After ten days of incubation at 37 °C in a humidified atmosphere, the encapsulated T cells viability was assessed using LIVE/DEAD Viability/Cytotoxicity Kit for mammalian cells (Molecular Probes Inc. Eugene, OR) by following manufacturer's instructions [124]. Furthermore, to determine the stability of the beads in

physiological condition, the exact number of intact capsules were monitored in a light microscope while the media was changed every three days [125].

Table 3-1 9 experimental runs suggested by RSM for optimization of the cell encapsulation process. A 3-level factorial has been utilized to evaluate the effect of the independent variables on Viability of the encapsulated cells, including the Alginate concentration (1, 1.5 and 2 w/v%) and Calcium Chloride concentration (1,3 and 5 w/v%). (Design expert 11, Stat-Ease Inc. Minneapolis, MN)

Run	Alginate concentration (w/v%)	$CaCl_2$ Concentration (w/v%)
1	1.5	3
2	2	3
3	1.5	1
4	2	1
5	1	5
6	2	5
7	1	1
8	1	3
9	1.5	5

3.4.4. Alginate beads characterization

The optimized alginate beads were prepared using 1% w/v sodium alginate in RPMI under constant injection using into 20 ml of 1% w/v $CaCl_2$ solution under constant stirring at room temperature. The beads formed immediately and were left in crosslinker solution for 30 min to ensure internal gelation. The beads were then filtered with a stainless steel strainer and washed in

fresh media. The beads' images were taken using an inverted microscope and analyzed for size distribution using ImageJ [126]. Permeability of the beads was assessed using FITC dextran polymers (different MW: 10, 70, 150, 500 kDa) encapsulated in the beads. The release of FITC dextran into the environment was measured at different time points as established earlier [127]. Finally, T cells were encapsulated in alginate beads under the optimized condition and incubated for 3, 5, 7 or 10 days following cell viability assessment.

3.4.5. Cancer chemotactic property of cells encapsulated alginate beads in vitro

To study the ability of encapsulated cells to recruit PCa, alginate beads encapsulated with different ratio of the T cells and PCa were produced (3:1, 1:1, 1:3). Various conditioned media (CMs) were generated by incubating different groups of alginate beads in serum-free media. After culture for four days, the CMs were collected for cell migration study using Transwell system as described earlier [86].

3.4.6. Cancer recruitment property of cells encapsulated alginate beads in vivo

Metastasized LNs have been shown to promote cancer cell migration [116, 128, 129]. To assess its ability for simulating metastasized LN, cell encapsulated alginate beads were implanted on the back of animals as described earlier [87]. Three groups of alginate beads (T cells, T cells+KD cells, and beads only as a control) were implanted. The Luc-expressed KD cells (1 to 5 x 10^6 cells per animals) was Intravenously implanted in animal and monitored using live animal imaging system for three days as described earlier [130].

3.4.7. Statistical analysis:

Experimental design and statistical analysis were performed using Design Expert 11 (Stat-Ease Inc. Minneapolis, MN). The small difference between the adjusted and predicted R-squared

indicates the validity of the model [131]. The migration of cells in response to various CMs was analyzed using two-way ANOVA (level of significance at $p<0.05$).

3.5. Results and Discussion

3.5.1. T cells and cancer cells co-culturing can induce cancer cell migration

It has been shown that in metastatic condition, malignant cells may interact with LN component to induce a conductive microenvironment for their survival [132]. In fact, our recent study demonstrated that the interaction of cancer cells and LN T cells in 3D culture lead to the production of biomolecules similar to metastasized LNs. To fabricate a device to simulate metastasized LNs, we first determine the optimal co-culture condition of T cells and metastatic PCa cells. For that, various CMs were prepared by co-culturing T cells and KD cells with different cell ratio to determine the optimal cell compositions. For that, different cell compositions (3:1, 1:1, 1:3) of T cells and PCa cells were cultured for 4 days. The cell-free CMs were extracted and then assessed on their ability to promote PCa cell migration. Interestingly, we find that the CM of 50:50 T:KD cells had the highest cell migration potential among all test groups (**Figure** 3-1). Such results support that the interactions between T cells and PCa cells are essential to the production of chemotactic biomolecules. This observation is supported by an early finding that direct interaction with tumor cells or their extract is essential to the activation of lymphocytes at least *in vitro* [133].

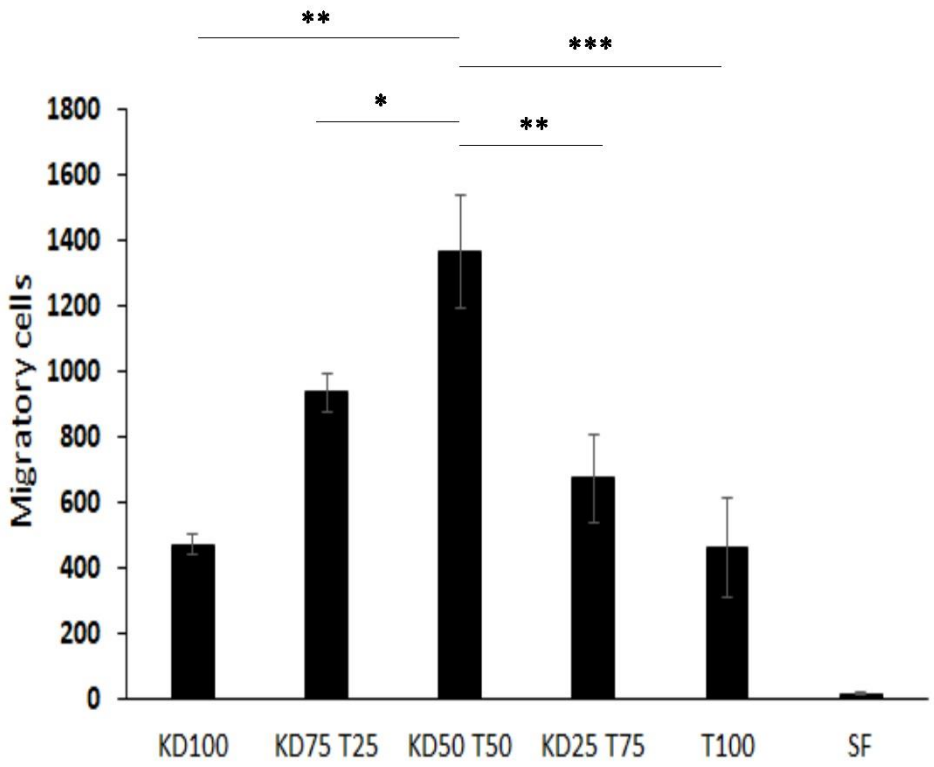

Figure 3-1 T cells and PCa KD cells coculture was carried out in different compositions – 100% KD cells (labeled as KD100), 75% KD with 25% T (labeled as KD75 T25), 50% KD with 50% T (labeled as KD50 T50), 25% KD with 75% T (labeled as KD25 T75) and 100% T cells (labeled as T100)- Serum-free media (labeled as SF) as a control. After cultured for 2 days, the cell-free conditioned media was isolated to assess their ability to trigger KD cell migration using a Transwell system. Data are mean ± Std, (*P-value<0.05, ** P-value<0.01, *** P-value<0.001

3.5.2. Alginate bead optimization

Subsequent studies were carried out to fabricate metastasized LN mimicking device by producing alginate beads encapsulated T cell:KD cell co-culture. It is well established that alginate beads can

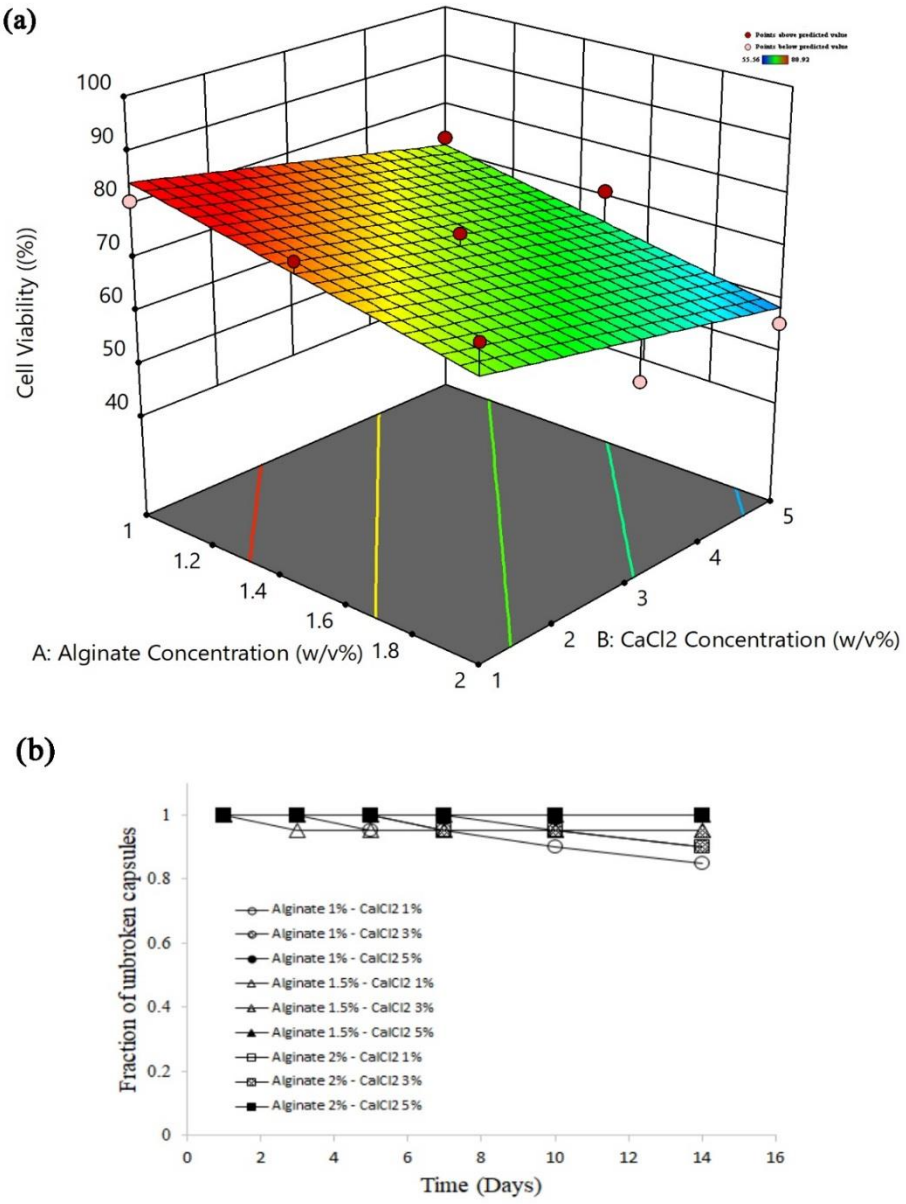

Figure 3-2 Optimization of cell encapsulate alginate bead fabrication condition. (a) 3-level factorial RSM analysis on the viability of cells inside alginate microbeads fabricated in different conditions. (b) Stability of the alginate beads fabricated in different conditions was assessed using the explosion assay in cell culture media.

be used as an isolated chamber for cell growth inside the chamber while permitting the exchanges of gas/nutrients and the diffusion of small molecule protein [134]. Several parameters in the encapsulation process, such as alginate and $CaCl_2$ concentration, have been shown to affect cell viability [135, 136]. To optimize the encapsulation processes, a 3-level factorial RSM, was employed to evaluate the effect of Alginate and $CaCl_2$ concentration on cell viability as described earlier [135]. The results revealed that cells enclosed in alginate microcapsules fabricated by sodium alginate of low concentration (1% w/v) had higher cell viability while increasing alginate concentration decreased it (**Figure** 3-2 **a**). In addition, it demonstrated crosslinking of alginate using a high concentration of $CaCl_2$ may have a detrimental effect on cells viability. Indeed, the study has shown that high calcium ions could inhibit cell proliferation [137]. Furthermore, using the explosion assay [125], the influence of encapsulation condition on alginate bead integrity was determined (**Figure** 3-2 **b**). As expected, all beads remain intact, at least, for the duration of this study (14 days). In the subsequent experiments, cell encapsulation beads were fabricated with the optimized condition (1% alginate, 1% $CaCl_2$).

3.5.3. Characterization of cell encapsulated alginate beads

The morphology of cell encapsulated alginate beads was examined under a fluorescent microscope. First, we find that >60% of the beads are in the range of 500 to 600 micrometer (**Figure** 3-3 **a**). It is estimated that there were 65±7 cells per bead. The pore size of alginate beads was determined using FITC dextran diffusion method [127]. By comparing the release profile of FITC-labeled dextran polymers with different molecular weights (MW: 10, 70, 150, 500 kDa) during 24 hours, our results show that the alginate beads can retain near 80% and 90% of the dextran polymer with the molecular weight of 70 kDa and 150 kDa, respectively **(Figure** 3-3 **b)**. It is likely that the alginate beads permit protein biomolecules (<70 kDa) to transfer in and out of

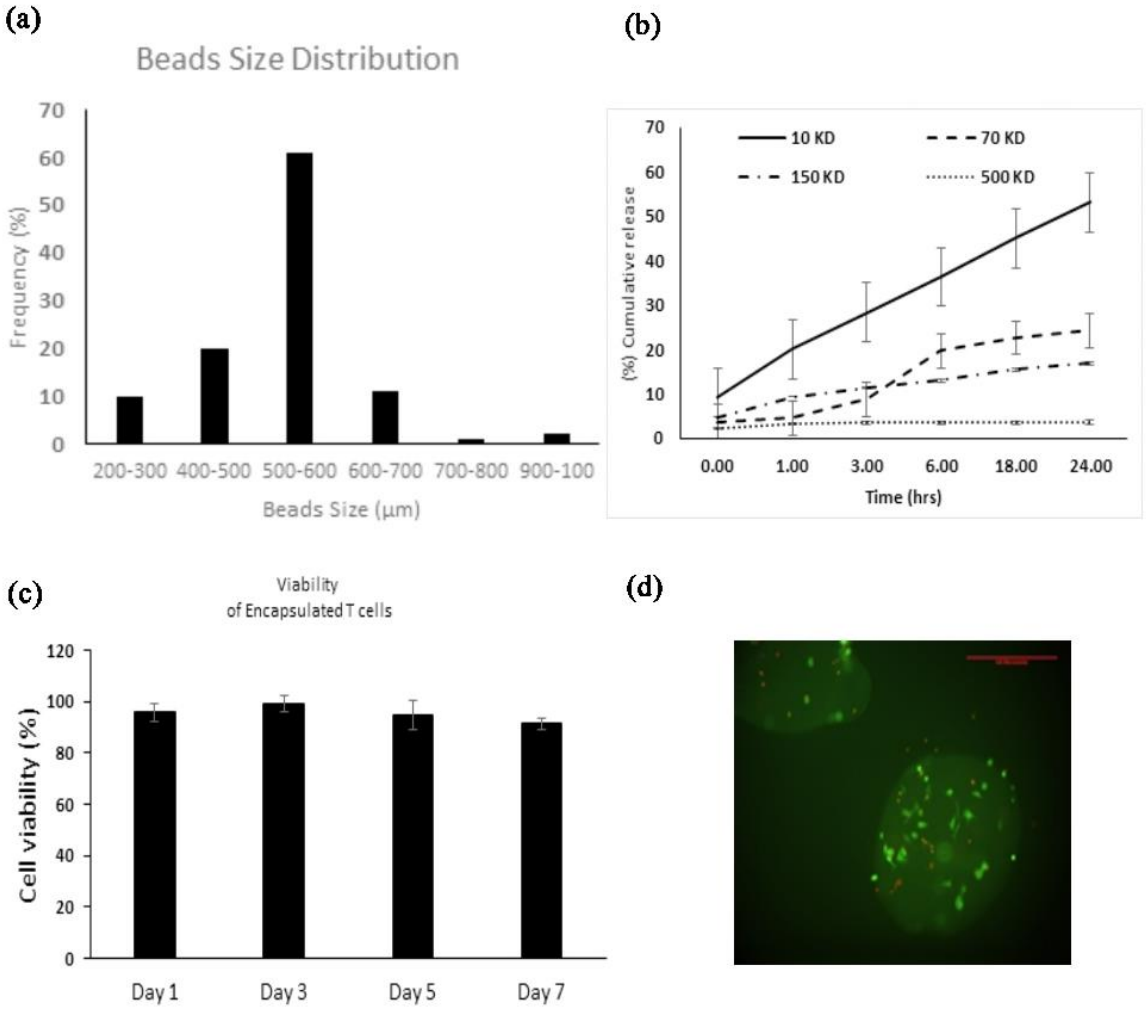

Figure 3-3 Characterization of cell encapsulated alginate beads. Specifically, we determine (a) the bead size distribution, (b) beads' pore size by measuring the release of FITC-labeled dextran with different molecular weight from alginate beads, (c) the viability of the encapsulated cells in alginate beads, and show (d) representative photo of (left) encapsulated T cells and cancer cells in alginate beads stained with LIVE/DEAD Viability/Cytotoxicity (alive (Green), dead (red)).

the beads. Since most of the cancer chemokines, such as human CXCL12 (10 kDa) and CCL21 (15 kDa), are smaller than 70 kDa, the alginate beads should allow the diffusion and release of the biomolecules produced by the encapsulated cells. On the other hand, since most of the host

immunological macromolecules are bigger than 150 kDa, alginate beads can protect the encapsulated T and KD cells from immune reactions as described earlier [138]. The effect of encapsulation on cell survival was also examined. Our results revealed that there was no difference between the cell viability of the T cells in the culture plate and alginate beads after 7 days of culture (**Figure** 3-3 **c**). Also, the fluorescence image of the T and PCa cells encapsulated in alginate beads showed the presence of viable cells sporadically distributed inside the bead with round morphology (**Figure** 3-3 **d**). These results support that the alginate capsules prepared by 1% concentration of sodium alginate and cross-linked in 1% calcium chloride can retain the cell viability for at least 7 days.

3.5.4. The chemotactic property of encapsulated cells in vitro.

The ability of the variously prepared cell encapsulated alginate beads to release cancer chemotactic biomolecules was assessed using a Transwell migration system [86]. The results show that, in agreement with the cell culture results, encapsulation of the T cells and KD cells in the ratio of 1:1 can release products with highest KD cell migration potential among all test groups, including KD cells alone, T cells alone, 1:3 and 3:1 (ratios of T cells:KD cells), and cell-free alginate beads (**Figure** 3-4). This result confirmed that the interaction between T cells and KD cells is essential to cancer chemotactic molecule production. Furthermore, the bioactivity and function (at least chemokine release) of the T cells and KD cell co-culture were not impacted by alginate encapsulation.

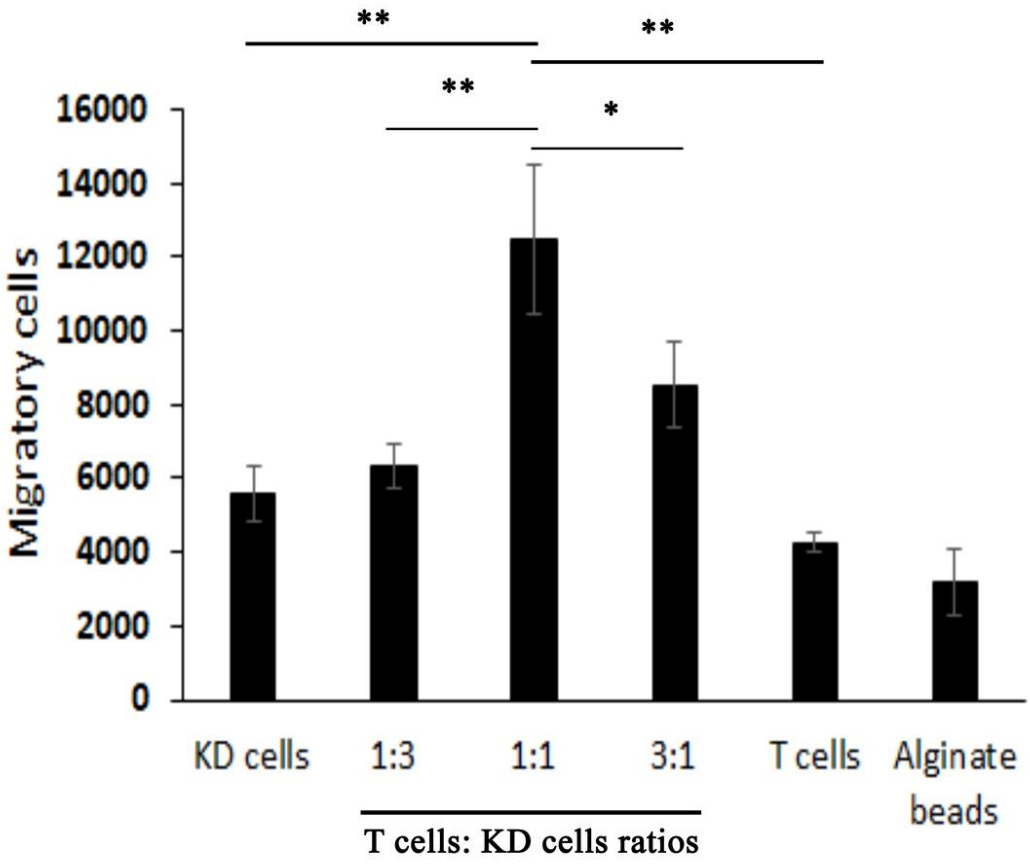

Figure 3-4 The extent of chemotactic agents released by variously prepared alginate beads including alginate beads encapsulated with KD cells alone, with T cells alone, with KD cells:T cells in the different ratio -1:3, 1:1, and 3:1. The beads were cultured in serum-free media for 4 days. The conditioned media was then assessed on their chemotactic potential using a Transwell system. All groups except alginate beads group have the identical cell number which is 65±7 cell/beads. Data are mean ± Std, (*P-value<0.05, ** P-value<0.01).

3.5.5. In vivo chemotactic assessment of metastatic LN mimetic

It is well established that metastatic LNs promote cancer metastasis [139, 140]. It is likely that cell encapsulated alginate beads would promote cancer cell migration *in vivo*. To test this hypothesis, a limited animal study was carried out in which saline (as negative control), alginate beads alone, T-cell encapsulated alginate beads, and T cell + KD cells encapsulated alginate beads were

implanted in the subcutaneous space for 21 hours. DiD-labeled KD cells were then intravenously administered in animals. NIR images were taken at the beads implantation site at different time points (1, 2 and 5 days after beads implantation) and the fluorescent intensities of the implant sites were then calculated to reflect the extent of KD cell recruitment (**Figure** 3-5 **a**). As anticipated, there was a strong fluorescent signal associated with T+KD cells encapsulated beads compared to beads alone or T cells encapsulated beads **(Figure** 3-5 **a**). The fluorescent signal in the implantation site was also increased with time, which supports the active cancer cells recruitment activities of encapsulated T +KD cells (**Figure** 3-5 **b**).

The results from this preliminary study showed that the implantation of T+KD cells encapsulated beads can decrease the biodistribution of cancer cells in the vital organs, such as lung, liver and bone. These results support that T+KD cells encapsulated beads can be used a new platform for studying the mechanism governing metastasized LN responses as well as for reducing cancer metastasis by attracting metastatic cancers to the implant site for local eradication with localized radiation and/or chemotherapy.

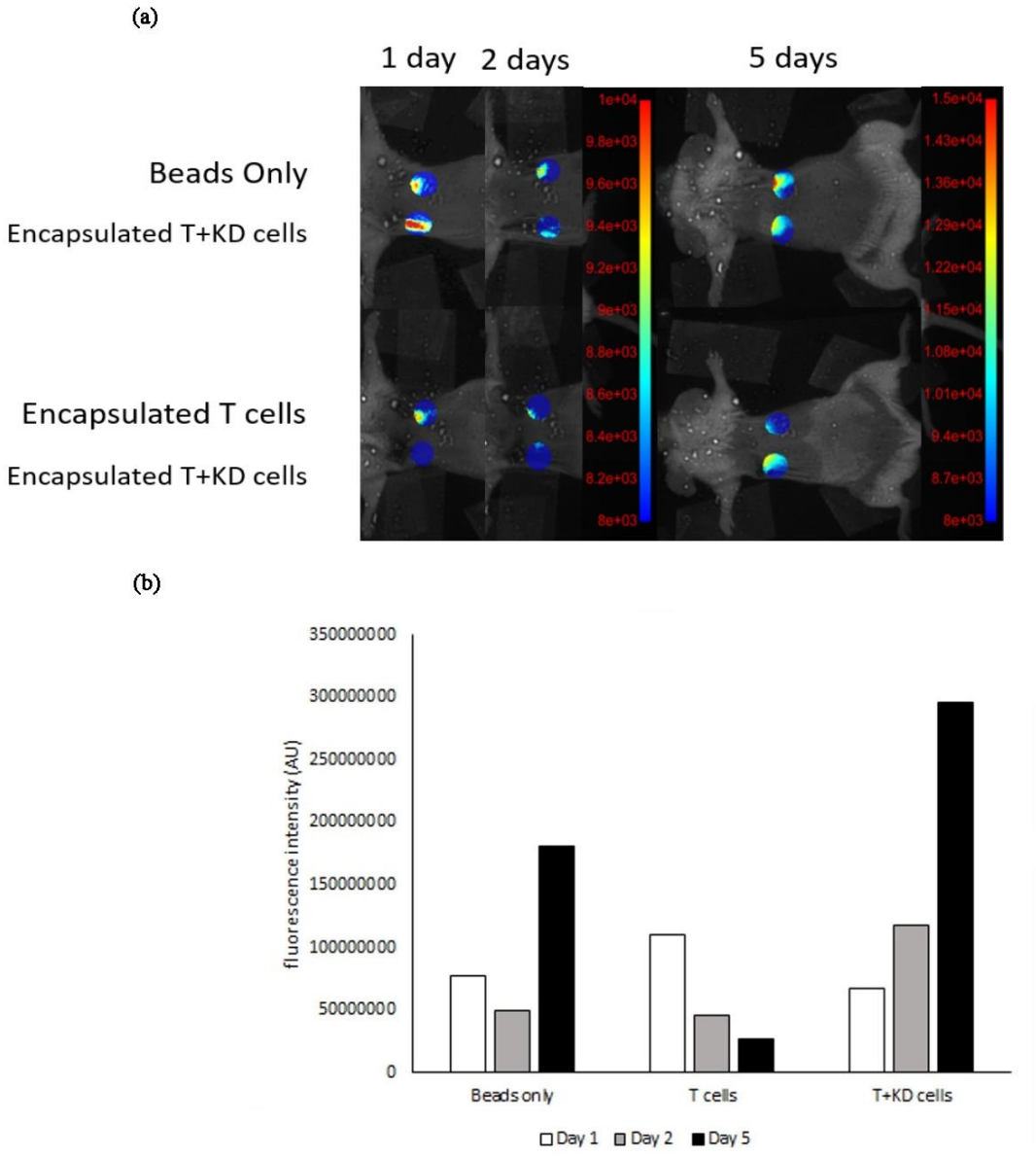

Figure 3-5 The chemotactic potential of various alginate beads was assessed using an animal model. Three groups of samples were tested including alginate beads only (labeled as "beads only", N=1), Encapsulated T cells (labeled as "T cells", N=1) and encapsulated T cells and KD cells with the ratio of 1:1 (labeled as "T+KD cells. N=2). The animals were implanted with test samples on the backs for 21 hrs and then followed with intravenous administration of DiD-labeled KD cells. (a) NIR images were taken on day 1, 2, and 5 after cell transplantation. (b) The fluorescent intensity at the implantation sites was taken to estimate the numbers of DID label PCa cells recruited by the bead implants.

3.6.Conclusion

The results of this study support that the T cells and KD cells encapsulated in alginate beads can be fabricated to simulate metastasized LNs. The LN mimetic devices can be used as an *in vitro* tool to investigate how cancer:LN cells interaction may lead to cancer LN metastasis. By incorporating patients' own cancer cells and lymphocytes, this device allows us to test different blockers on their ability to reduce LN metastasis. Finally, it is possible that such LN mimetic device can be implanted nearby the primary tumor site as a decoy to reduce cancer LN metastasis.

Chapter 4

4.1.RECRUITMENT OF ENDOGENOUS PROGENITOR CELLS BY ERYTHROPOIETIN LOADED PARTICLES FOR IN SITU CARTILAGE REGENERATION

Keywords: Hyaluronic acid microscaffolds, erythropoietin, endogenous progenitor cells, cell recruitment, chondrogenesis, cartilage injury, post-traumatic osteoarthritis

This article has been submitted to Journal of Advanced Healthcare on July 15th 2019.

4.2.Abstract

Cartilage injury affects millions of people throughout the world and at this time there is no cure. While transplantation of stem cells has shown some success in the treatment of injured cartilage, such treatment is limited by the limited cell sources and safety concerns. To overcome these drawbacks, a microscaffolds system was developed capable of targeting, reducing the inflammatory response and recruiting endogenous progenitor cells to cartilage defect. To further investigate this concept, erythropoietin (EPO)-loaded-hyaluronic acid (HA) microscaffolds (HA+EPO) were fabricated and characterized. The average size of the HA-microscaffolds was 4.2 μm with EPO loading capacity of 17.6 μg/mg. HA-microscaffolds have shown good cell-compatibility and can target chondrocytes via CD44 receptors. HA+EPO have been designed to slowly release EPO of the course of 96 hours while recruiting progenitor cell. Finally, the ability of HA+EPO to repair cartilage defects was assessed using a rabbit model of full-thickness cartilage defect. Our results show that the intra-articular administration of EPO, HA, and EPO+HA reduce the number of inflammatory cells inside the synovial-fluid, while EPO+HA had the greatest anti-inflammatory effects. Furthermore, among all groups, EPO+HA achieved the greatest progenitor cell recruitment and subsequent chondrogenesis. The results of this work support that, by targeting and localizing the release of growth-factors, HA+EPO can reduce inflammatory responses and promote progenitor cells responses. This new platform represents an alternative treatment to stem cell transplantation for the treatment of cartilage injury.

4.3.Introduction

Post-traumatic osteoarthritis (PTOA) is a type of osteoarthritis that develops after joint injury and is most prevalent in the ankles, knees and hips [141]. It is estimated that more than 6 million people alone in the US suffer from PTOA, which accounted for annual healthcare expenditures of

approximately 3 billion dollars (US) in 2013 [142]. All indications are that PTOA will pose an even more significant challenge in the coming years as the US and world's population continues to age and people remain active and more likely to injury their joints. An effective, safe, less invasive and cost-effective means of treating PTOA is therefore much needed. The current standard therapy for PTOA includes muscle-strengthening exercise, weight loss, the use of anti-inflammatory drugs, intra-articular injections and in many cases surgical intervention [143]. Unfortunately, none of these options alter the natural history of the disease nor restore the full function of these injured cartilages.

In recent years, substantial progress has been made in the area of stem cells and tissue engineering for regeneration of cartilage tissues. Specifically, it is well established that mesenchymal stem cells (MSCs) can be differentiated into chondrocytes to form cartilage-like tissue in culture [144, 145]. Furthermore, recent studies have indicated that isolation, purification and injection of progenitor cells into the diarthrodial joints may improve cartilage regeneration after the onset of osteoarthritis, by reducing localized inflammatory responses in mice [146, 147]. However, administration of MSCs for cartilage regeneration has limited applications due to the costly and time-consuming processes of isolating, expansion and culture of autologous MSCs. To overcome these limitations, recent studies utilized endogenous synovial progenitor/stem cells for tissue regeneration in cartilage defects by homing resident progenitor cells to the site of injury [148, 149]. In addition, several recent reports have documented the presence of the synovial progenitor/stem cells in the synovial fluid/membrane and the numbers of progenitor cells increased with the severity of OA. Interestingly, chemoattractant releasing scaffolds have been used as a strategy to cue these progenitor cells to the site of the injury for inducing chondrogenesis. For example, acellular cartilage matrix conjugated with a bone marrow homing peptide has been employed to

repair full-thickness cartilage defect in a rabbit model by triggering endogenous progenitor/stem cell recruitment [148]. To elicit sustained endogenous progenitor cell recruitment, micro/nano particles have been used as microscaffolds to support cell growth and differentiation by the localized release of growth factors at the site of injury [150].

Stem cells are characterized as cells endogenous stem cells are tissue-specific progenitor cells within the adult tissue that have the ability to self-renew and differentiate into specific cell types. Endogenous or residential stem cells are normally quiescent and losing homeostasis activate these cells leading to restore tissue function. Self-regeneration of the injured tissues requires a high number of endogenous stem cells. That is why endogenous stem cells are recruited to the site of injury from multiple tissues through extracellular matrix signaling [151]. The recruited stem cells will be differentiated into various types of cells by different signaling factors and play a vital role in tissue regeneration [152].

Hyaluronic acid (HA) based particles are a good microscaffold candidate for cartilage tissue engineering. First, HA, is a naturally occurring polysaccharide, and has been used in many tissue engineering applications [153]. Second, HA is the main component of synovial fluids and cartilage matrix and can be degraded in the presence of hyaluronidase (HAase) existing in synovial fluid [154]. Third, it is well established that HA particles have a high affinity for cells with CD44 receptors [155]. Since the expression of CD44 in articular cartilage tissue is closely correlated with the severity of OA [156, 157], it is likely that HA particles can accumulate on the surface of injured cartilage by targeting its CD44 receptors. Finally, HA microscaffolds have been developed as an effective carrier for targeted delivery of BMP-2 *in vitro* to promote cartilage repair and regeneration [158]. However, to the best of our knowledge, microscaffolds systems have not been explored for their ability to induce endogenous progenitor cell-mediated cartilage repair.

This report summarizes a study which was aimed at developing new technology for triggering intrinsic cartilage regeneration by provoking endogenous progenitor cell responses. Briefly, HA microscaffolds were fabricated to targeted CD44+ chondrocytes. Some of these microscaffolds were loaded with erythropoietin (EPO). EPO is a FDA approved growth factor with the ability to modulate /progenitor/stem cell responses, including proliferation and differentiation [159]. Localized released of EPO has been shown to promote endogenous progenitor cell recruitment and osteogenic differentiation at the site of bone defect *in vivo* [88]. Using both in *vitro and ex vivo* models, we assessed the ability of HA microscaffolds to target activated human chondrocytes and OA cartilage tissues. Finally, using rabbit microfracture defect model [160-163], we investigated the ability of HA microscaffolds, EPO, HA microscaffolds+EPO to promote endogenous progenitor cell responses and chondrogenesis at the site of injured cartilage.

4.4.Results and Discussion

4.4.1. Characterizations of HA microscaffolds and its EPO release property

The spherical morphology of FITC-labeled HA microscaffolds can be seen under a fluorescence microscope (**Figure** 4-1 **a**). The size distribution of HA microscaffolds was determined to be 1-15 µm with an average size of 4.2 µm (**Figure** 4-1 **b**). SEM images further confirmed the spherical shape of HA microscaffolds with a slight reduction in particle sizes (**Figure** 4-1 **c**) due to the sample dehydration during preparation for SEM. Our observations support that HA microscaffolds have good cell compatibility based on the viability of human chondrocytes that was unchanged in the presence of increasing concentrations (up to 2.0 mg/ml) of HA microscaffolds (**Figure** 4-1 **d**). To assess the ability of HA microscaffolds to release EPO, FITC-labeled-EPO was loaded into microscaffolds. The loading capacity was found to be 17.6 µg/mg. The ability of HA microscaffolds to release EPO was then evaluated. The release profile showed a fast release of

EPO (~55%) during the first 4 hours (**Figure** 4-1 **e**). This burst release may help to create a cytokine gradient that is essential for cell recruitment [164]. The EPO release rate slowed after 24 hrs and only 30% of the remaining EPO was released during the following 3 days. The slow release of EPO may help to create EPO gradient that is important for achieving continuous progenitor cell recruitment.

Since EPO is able to trigger the recruitment of MSCs [88], the bioactivity of released EPO was determined based on its ability to promote migration of progenitor cells (**Figure** 4-1 **f**). Our results show that HA microscaffolds by themselves have no MSCs recruitment activities, while released EPO can trigger MSCs recruitment. These results confirmed the bioactivity of released EPO and supported the potential for using EPO-loaded HA microscaffolds to promote eSC recruitment into the site of injured cartilage. In fact, EPO has been shown to trigger the migration and proliferation of bone marrow-derived MSCs and it has also been shown to promote chondrogenesis and chondrocyte proliferation [165].

4.4.2. The ability of HA microscaffolds to target chondrocytes and injured cartilage

The ability of HA microscaffolds to target chondrocytes through CD44 receptor was assessed using human cartilage cells and osteoarthritic tissue explants. We found that HA microscaffolds have good affinity for cartilage cells. In fact, the amount of cell-associated HA microscaffolds and the extent of CD44 expression increased with an increasing number of activated cells (**Figure** 4-2 **a and b**). Further analyses revealed a linear relationship (R^2=0.97) between the amount of HA microscaffolds and the extent of CD44 receptor expression (**Figure** 4-2 **c**). These results confirm that HA microscaffolds target chondrocytes via their CD44 receptors.

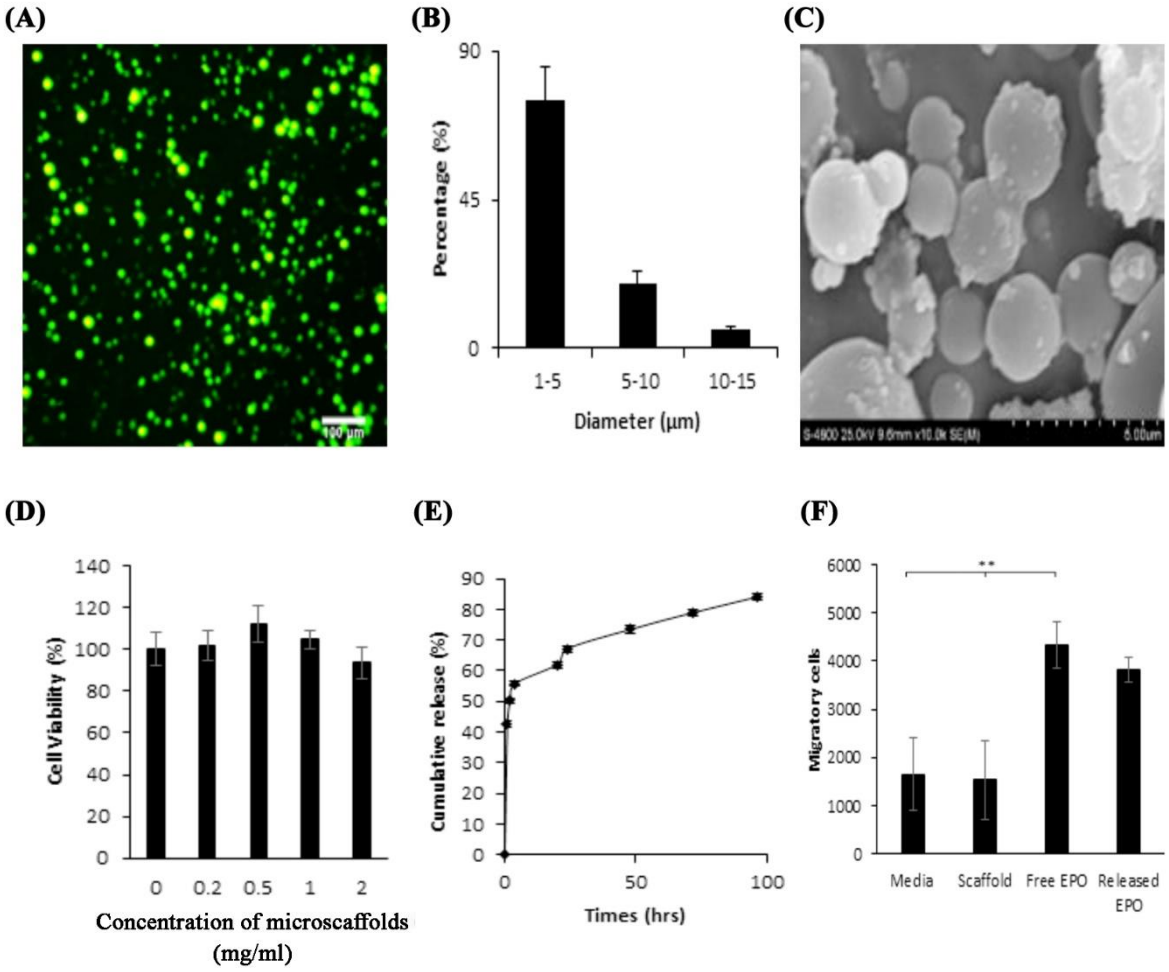

Figure 4-1 Physical and biological characterization of HA microscaffolds loaded with EPO. (a) Fluorescence imaging (100x) of the FITC-conjugated microscaffolds; (b) size distribution calculated using ImageJ. (c) A representative SEM image of the microscaffolds; (d) In vitro cytotoxicity of HA microscaffolds using primary human chondrocytes and Alamar Blue assay. (e) EPO release profile from HA microscaffolds. (f) Recruitment of the human MSCs toward various groups (control, HA microscaffolds [abbreviated as "scaffold"], free EPO, or EPO released from scaffolds [abbreviated as "Released EPO"]) using Transwell migration assay. (Mean ± SD; **$p < 0.01$).

Further study was carried out to evaluate HA microscaffolds' capability of targeting injured human cartilage explants. Specifically, human OA tissues were incubated with different concentrations of HA microscaffolds for different periods of time. The accumulation of HA microscaffolds on different areas of OA tissues was then quantified using the Kodak *in vivo* imaging system. The images revealed that HA microscaffolds accumulation on OA tissues was both time and microscaffolds concentration dependent (**Figure** 4-2 **d**). By quantifying and comparing the tissue associated microscaffolds' fluorescent intensities (previously reported [166]), we found that, even at low concentrations, HA microscaffolds could target and accumulate on the surface of the OA tissue (**Figure** 4-2 **e**). The peak of the targeting efficiency occurred within 90 minutes of incubation and the accumulation of HA microscaffolds on tissue increased with increased concentrations of HA microscaffolds (**Figure** 4-2 **e**).

We then investigated the role of CD44 on the HA microscaffold:OA tissue interaction using CD44 blocking antibody(**Figure** 4-2 **f).** Interestingly, our results show that the blockage of CD44 receptors significantly reduced the accumulation of the HA microscaffolds on OA tissue by a factor of 8. Our results show the importance of CD44 receptor in mediating HA microscaffold-accumulation on injured cartilage tissue, and these findings were confirmed in a previous report [167]. These findings support our hypothesis that HA microscaffolds can be used as a carrier to target and deliver macromolecules to injured cartilage via CD44 receptors.

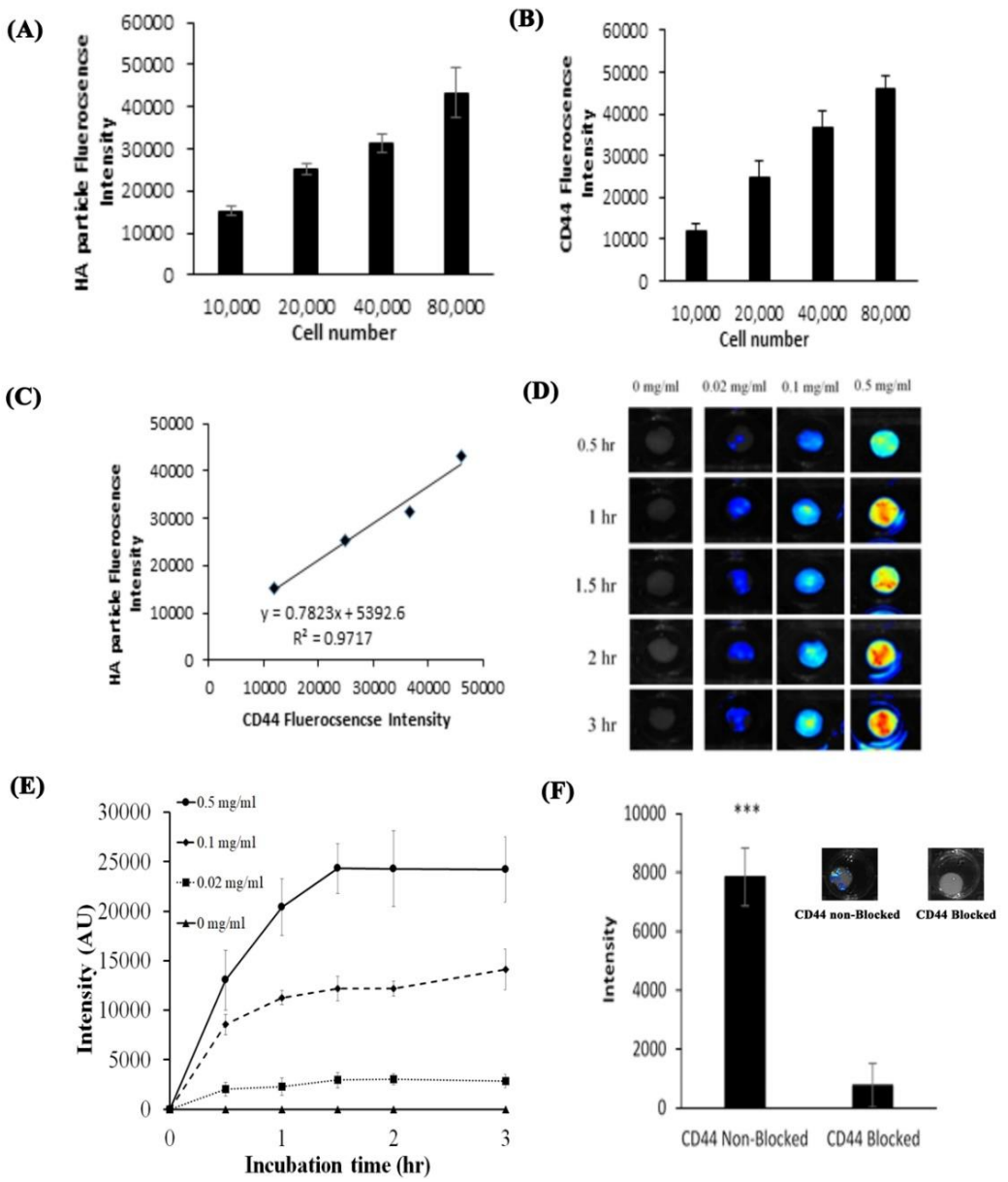

Figure 4-2 *In vitro* characterization of HA microscaffolds. (a) The fluorescent intensity of FITC-conjugated HA microscaffolds associated with different numbers of human chondrocytes. (b) The fluorescent intensity of CD44 receptor associated with different numbers of human chondrocytes. (c) There was a good linear relationship between the amount of HA microscaffolds and the extent of CD44 receptor expression with an R^2 of 0.97. (d) Time and dose-dependent fluorescent images of osteoarthritic human tissue incubated with different concentrations of HA microscaffolds (0.02, 0.1 and 0.5 mg/ml). (e) The fluorescent intensities of all tissue incubated with different concentrations of HA microscaffolds for different periods of time (up to 180 minutes) were calculated and compared. n=4 for all groups. (f) The fluorescent intensity associated to HA microscaffolds incubated with OA human explant tissue pre-treated with CD44 blocking antibody or control. (Mean ± SD; **$p < 0.001$).

4.4.3. Micro-CT analysis

The ability of HA microscaffolds and EPO-loaded HA microscaffolds to promote chondrogenic regeneration was evaluated using an animal model. Injured cartilage specimens were treated with microscaffolds (as control), free EPO, HA microscaffolds (HA) or microscaffolds loaded with EPO (HA+EPO). After implantation for different periods of time, the synovial fluid and cartilage tissue were isolated for different analyses. The 12- and 26-week implants underwent Micro-CT imaging and reconstruction process (**Figure** 4-3). At 12-weeks, the 2D reconstruction images of coronal cutting view and 3D image of rabbit cartilages showed newly formed bony and cartilage-like tissues in HA+EPO group, but not in other groups (**Figure** 4-3 **a**). At week 26, we observed that the cartilage tissues with the EPO, HA and HA+EPO treatment were almost completely filled with homogenous and integrated cartilage tissues in the defect sites while the unrepaired empty zones remained in the saline group. The quantitative data extracted from micro-CT confirmed that, at week 12, there was no significant difference in bone volume fraction (BVF) between the EPO (42.16±13.21 %), HA (31.49±4.14%), and saline (34.52±2.15%) (**Figure** 4-3 **b**). On the other hand, the BVF of the EPO (67.12±13.21 %) and HA (57.76±11.42 %) is significantly higher than

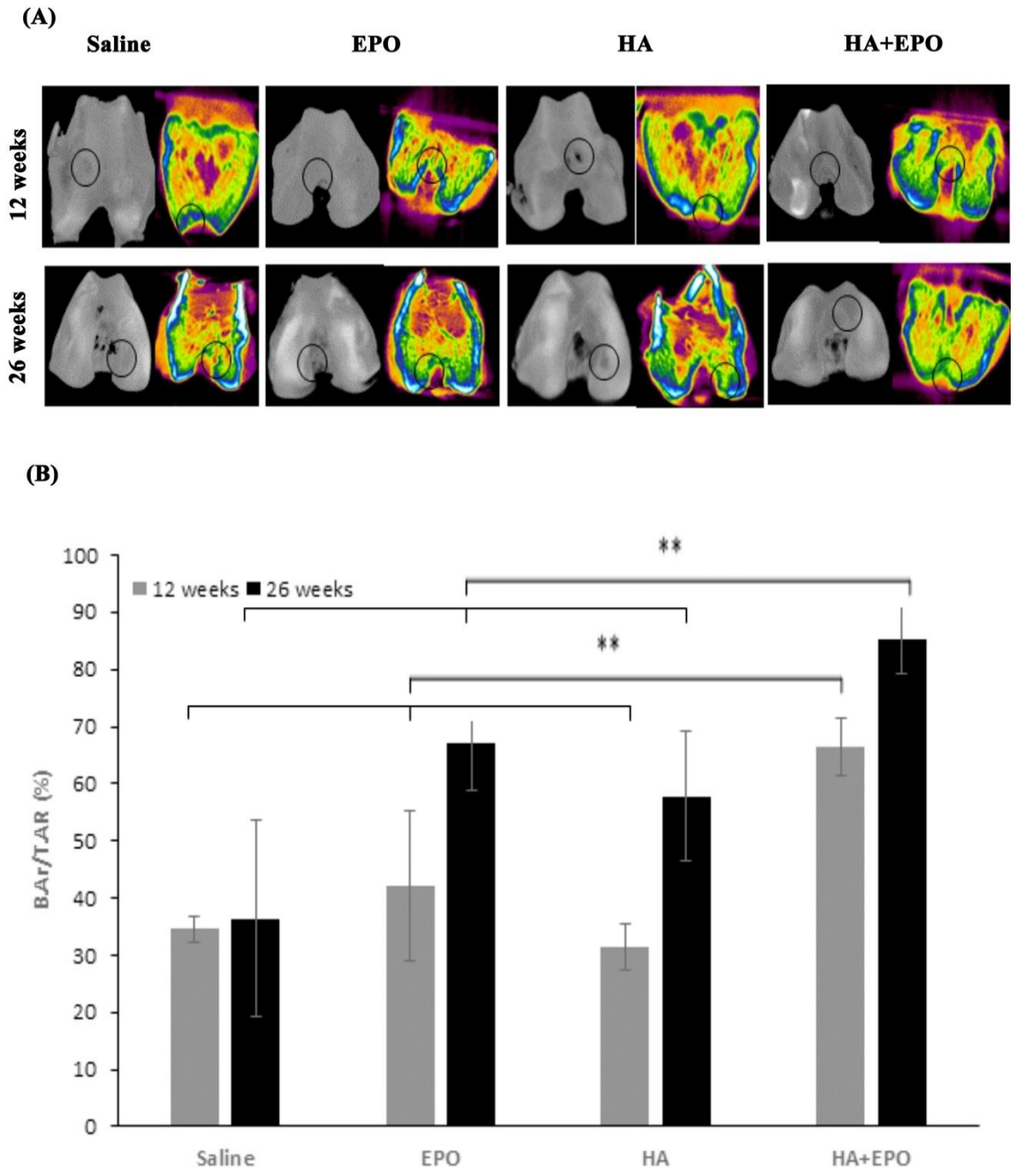

Figure 4-3 Micro-CT image analysis of the rabbit cartilages 12- and 26-weeks post-surgery. (a) 2D coronal view and 3D image of the cartilage (b) bone volume fraction (BVF) data extracted form micro-CT images VOI (n = 4). (Mean ± SD; **p < 0.01).

the saline (36.34±17.16%) 26 weeks post-surgery (**Figure** 4-3 **b**).In addition, The BVF of the HA+EPO is significantly higher compared to all other groups 12 weeks (66.54±5.00 %) and 26 weeks (85.30±6.13 %) post-operatively (*p*-values <0.01). Taken together, the micro-CT results demonstrate that the HA+EPO treatment possesses the ability to stimulate cartilage repair as early as at week 12. However, individually EPO and HA microscaffold treatment groups only showed healing of the injured cartilage at 26 weeks.

4.4.4. Synovial cell analysis

Subsequent analyses were carried out to assess the ability of various treatments on inflammatory responses in synovial fluid. It is well established that the increasing number of inflammatory cells in the synovial fluid is an indicator of early OA [168]. As shown in Figure 2-4, among all treatment groups, HA+EPO treatment group has the lowest numbers of CD11b+ inflammatory cells in the synovial fluid. Specifically, the treatment of EPO, HA, or HA+EPO reduced the inflammatory cell recruitment in synovial fluid for 45.9±28.6, 29.5±8.8, or 6.8±3.7%, respectively (**Figure** 4-4 **b**). The decrease in inflammation found in the sample treated with HA+EPO can be attributed to HA's ability to bind to CD44, the ligand of leukocytes [169]. Blocking the binding site of CD44 may result in the reduction of white blood cells, and therefore, less inflammatory responses in the synovium [170]. It should be noted that EPO has been reported to have an anti-inflammatory effect as well [171].

4.4.5. Progenitor cell recruitment

We have hypothesized that the improved healing effect of EPO-loaded HA microscaffolds is caused by the increasing recruitment of endogenous progenitor cells to the site of cartilage injury and degeneration. To test the hypothesis, we analyzed and compared the presence of progenitor cells at the site of the injured cartilage among different groups, at week 12. Both CD29 and CD90

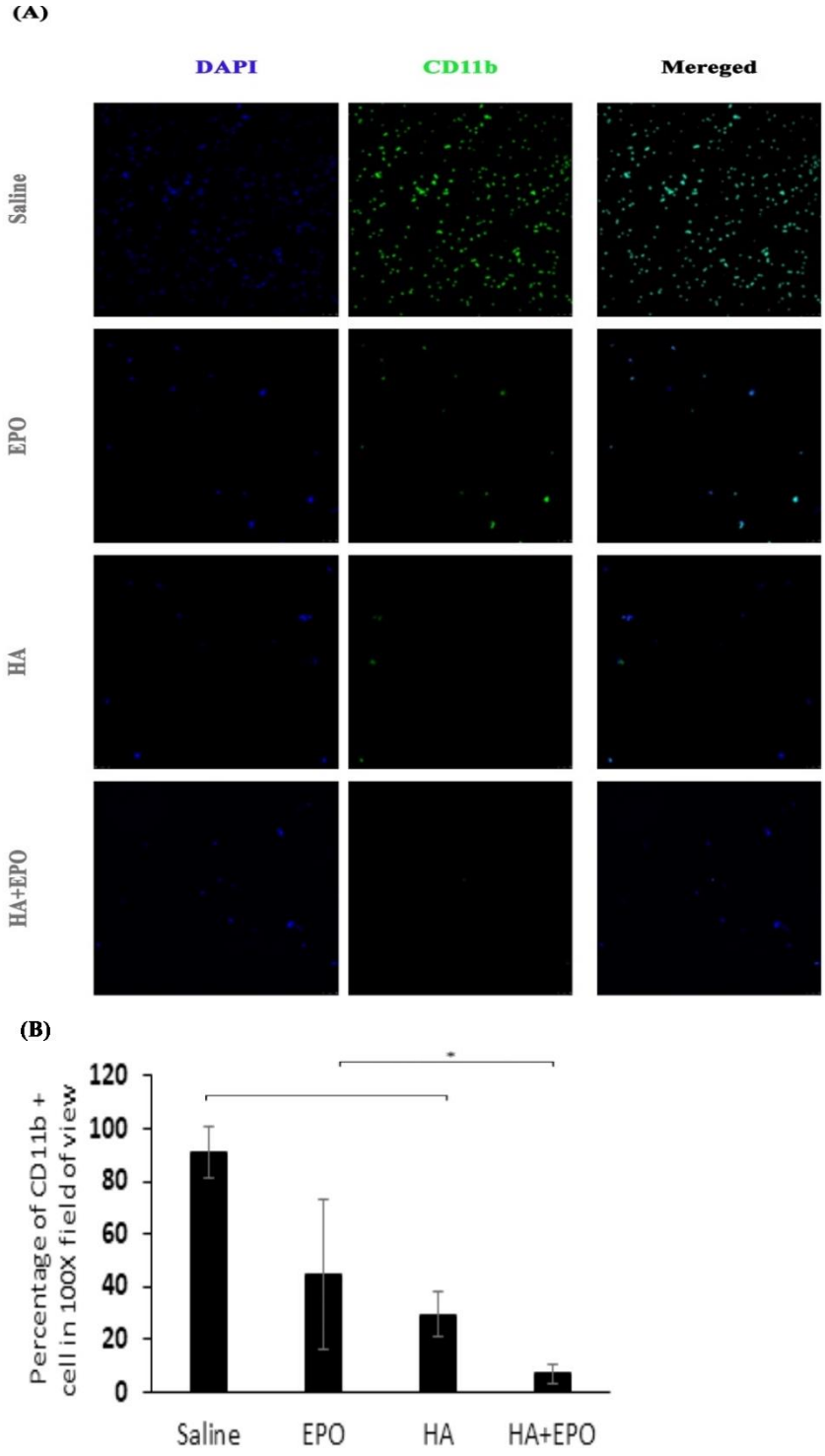

Figure 4-4 The presence of CD11b+ inflammatory cells in the synovial fluid of treated tissues 12-week post-surgery. (a) Inflammatory cells detection migrated to the synovial fluid. (b) Quantification of inflammatory cells present in the synovial fluid (Mean ± SD; **$p < 0.01$).

markers were used to identify the presence of progenitor cells in injured cartilage for primarily two reasons. First, it is well established that CD29, CD44, CD90, and CD105 are positive markers for progenitor/stem cells [172-174]. Second, many studies reported the increased expression of CD29 and CD90 on the MSCs [175, 176]. Our results show that, as expected, there are more (~3.4 fold) CD29+ (green)/CD90 (red) cells (1,156±683 cells/mm^2) at the site of injury than the control group (**Figure** 4-5 **a and b**). On the other hand, the treatments of EPO and HA microscaffold alone did not increase progenitor cell recruitment when compared to the non-treatment control (**Figure** 4-5 **a and b**). These results support our overall assumption that the HA+EPO treatment enhanced progenitor cells recruitment to the site of injury that might promote cartilage regeneration.

4.4.6. Chondrogenesis evaluation

To assess whether the recruited progenitor cells induce chondrogenic differentiation, we investigated the expression of two major chondrogenic biomarkers (proteoglycans and collagen II) on different tissue samples using Toluidine blue and immunohistochemical staining, respectively [177]. Representative tissue images are shown in **Figure** 4-6 **a**. Higher glycosaminoglycan (GAG) deposition (both proteoglycans and collagen II) were seen in HA+EPO than those in controls, EPO and HA at week 12 and 26 (**Figure** 4-6 **b and c**). However, there was no statistically significant difference in both chondrogenic markers among the control group, HA group and EPO group (**Figure** 4-6 **b and c**). The results thus far support that HA+EPO treatment facilitated progenitor cell recruitment to the injury site leading to significantly improved chondrogenesis as reflected by localized increased GAG and collagen II production.

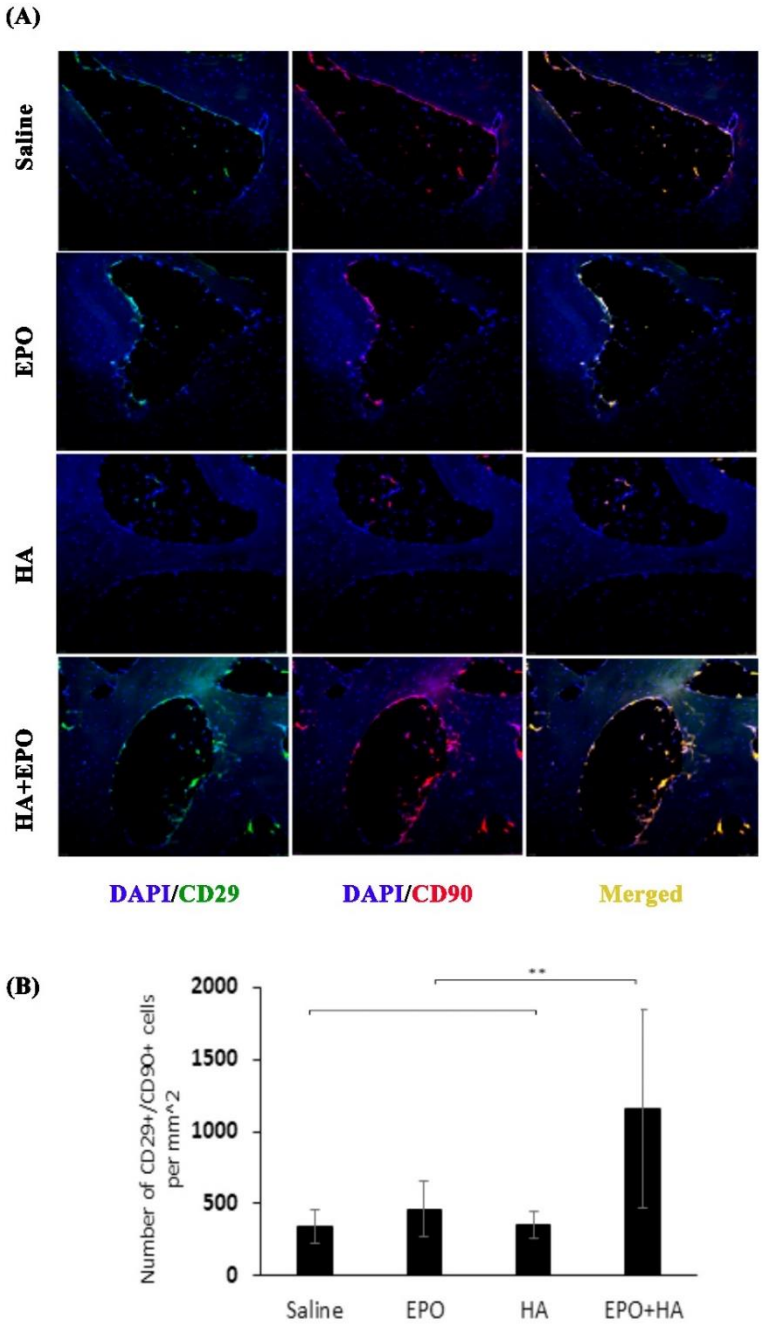

Figure 4-5 Recruitment of CD29+/CD90+ progenitor cells in variously treated tissues 12-week post-surgery. (a) Images of progenitor cells at the injury site. (b) Quantification of progenitor cells recruited to the injured cartilage (Mean ± SD; **p < 0.01).

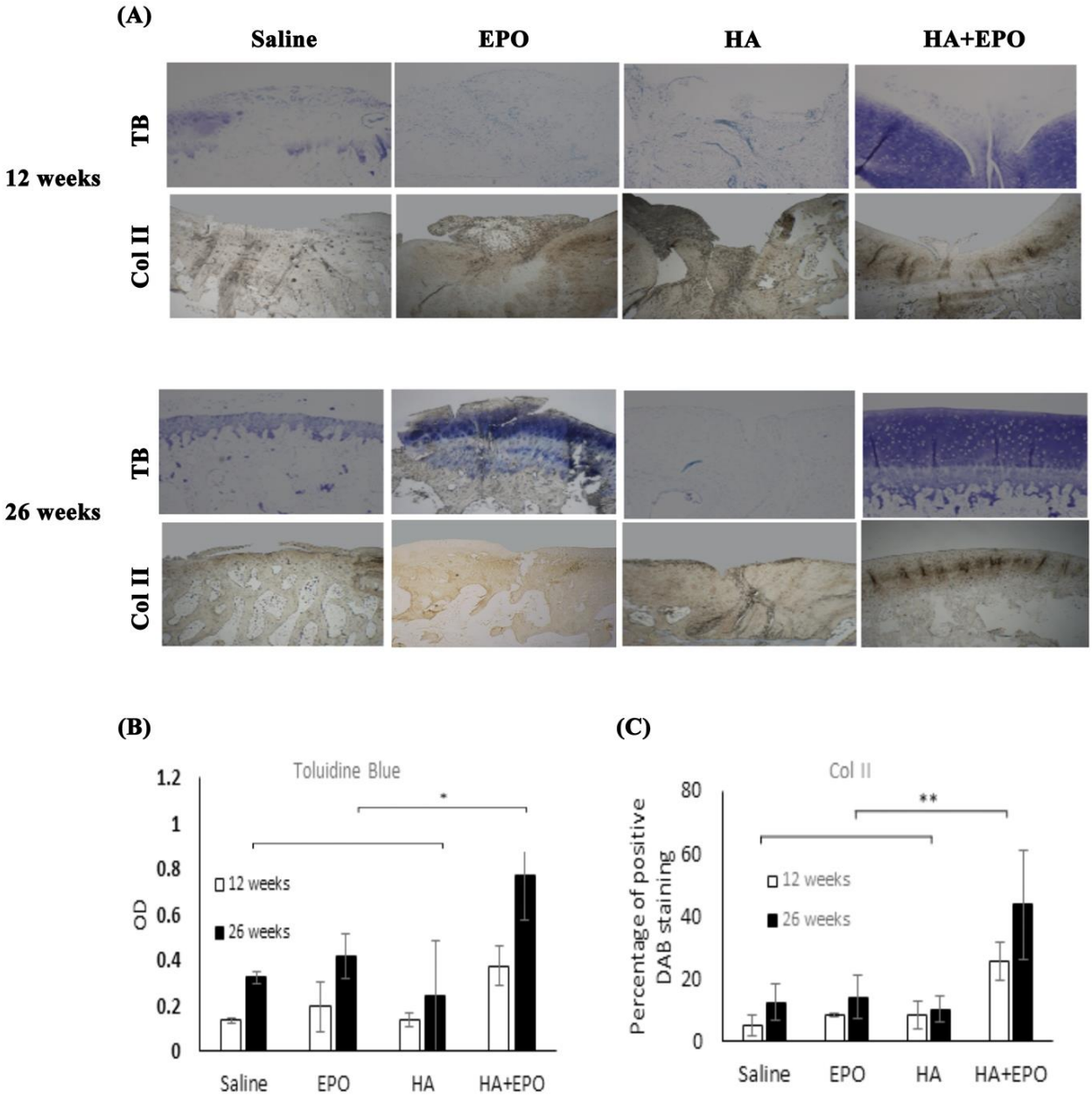

Figure 4-6 Chondrogenesis evaluation of the rabbit cartilage 12- and 26-weeks post-surgery. (a) Images of tissues stained with toluidine blue (labeled as "TB") or collagen II (labeled as "Col II"). Quantification and statistical analyses of (b) toluidine blue and (c) collage II stained tissue (Mean ± SD; *$p < 0.5$, **$p < 0.01$).

4.4.7. Histology assessment of the repaired tissues

To evaluate the ability of HA+EPO to complete repair of the injured cartilage, all the tissues sections were further analyzed using H&E and safranin O staining for morphological and cartilage tissue regeneration (GAG production) (**Figure** 4-7). At week 12, the saline group had the most irregular tissue morphology as compared with other groups. The defect area in EPO and HA groups was filled with unintegrated and loose tissue while HA+EPO treatment had more highly organized tissue filled with chondrocyte-like cells (**Figure** 4-7 **a**). Meanwhile, the tissue section images from 26 weeks post-surgery showed that the saline and EPO treatment still had empty spaces in the place of the injury, surrounded by a poorly organized and disordered tissue. On the other hand, HA and HA+EPO treatment were shown to have regenerated a well-integrated and organized tissue within the defect sites (**Figure** 4-7 **a**). Specifically, HA treatment generated some fibroblast-like tissue in the place of the injury while HA+EPO treatment generated cartilage-like tissue in the defect site, integrating well with the surrounding site and providing a smooth continuous surface. Although the EPO treatment shows high production of GAG, it was not well distributed throughout the entire repair tissue. The repaired cartilage was evaluated according to the Pineda cartilage repair score, on 4 different categories (**Table** 4-1). The overall results show that HA+EPO had the lowest Pineda repair scores among all groups in both time points (**Figure** 4-7 **b**). In summary, the histology data demonstrated that the HA+EPO treatment could significantly increase cartilage regeneration starting at week 12 post-surgery and achieve complete tissue recovery by 26 weeks.

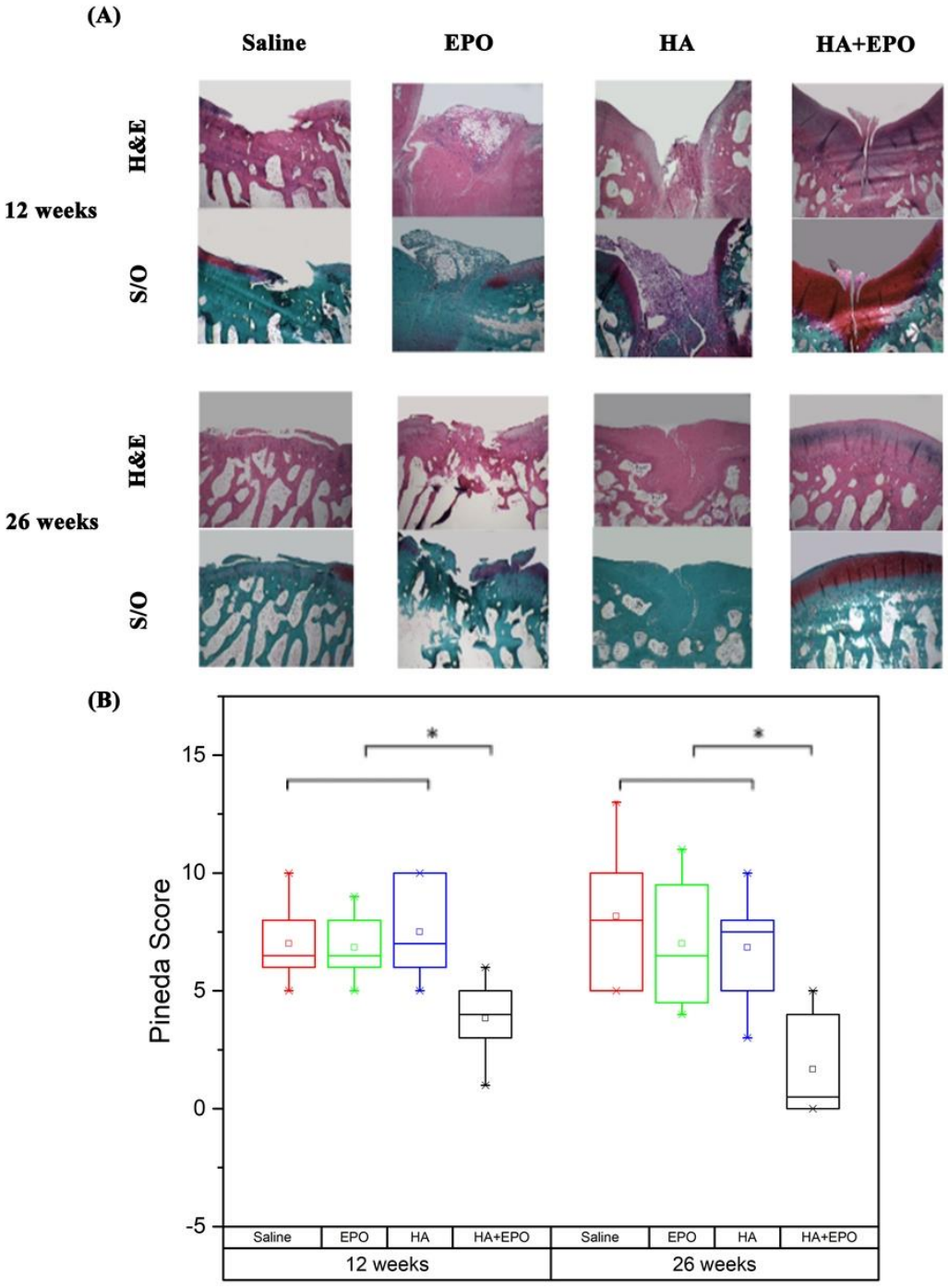

Figure 4-7 Histology analysis of the defect rabbit cartilage 12- and 26-weeks post-surgery. (a) Images of H&E staining & Safranin O staining. (b) Pineda repair scores of the repaired cartilage based on H&E and safranin O staining of the cartilage. The lower Pineda score, the more cartilage regeneration. (Median ± interquartile range; *$p < 0.5$).

Table 4-1 Pineda Cartilage repair score.

Characteristics	Score
Filling of defect	
125%	1
100%	0
75%	1
50%	2
25%	3
0%	4
Reconstruction of osteochondral junction	
Yes	0
Almost	1
Not Close	2
Matrix staining	
Normal	0
Reduced staining	1
Significantly reduced staining	2
Faint staining	3
No stain	4
Cell morphology	
Normal	0
Most hyaline and fibrocartilage	1
Mostly fibrocartilage	2
Some fibrocartilage, but mostly	3
Nonchondrocytic cells	4

4.5.Conclusion

In this study, a new treatment-EPO loaded HA microscaffolds were developed and investigated for their ability to stimulate and support cartilage regeneration in injured cartilage by eliciting endogenous progenitor cell response. Our *in vitro* results determined the released kinetic and bioactivity of released EPO releases from HA microscaffolds for recruiting progenitor cells. On the other hand, HA microscaffolds are found to have a high affinity for human chondrocytes and osteoarthritic tissue by interacting with their CD44 receptor. The chondrogenic property of EPO-loaded HA microscaffolds was evaluated using a rabbit microfracture defect model. The *in vivo* data showed that EPO loaded HA microscaffolds not only reduced the inflammatory cells in

synovial fluid but also enhanced endogenous progenitor cell recruitment and improved the regeneration of cartilage tissue. Overall results support that EPO loaded HA microscaffolds have a great potential to be used as a treatment for regeneration of injured cartilage by inducing endogenous progenitor cell responses.

4.6.Experimental Section

4.6.1. Materials

Hyaluronic acid sodium salt (HA) (700KDa) was purchased from LifeCore Biomedical (Chaska, MN). 1-heptanol (98%) and NaCl were obtained from Sigma-Aldrich (St. Louis, MO). Dioctyl sulfosuccinate sodium salt (AOT, 96%), divinyl sulfone (DVS, 98%) and, 2,2,4-Trimethylpentane (isooctane, 99%) were purchased from Fisher Scientific (Hampton, NH). CF488A and CF647A amine dye were supplied from Biotium, Inc. (Fremont, CA). N-Hydroxysuccinimide (NHS) was purchased from Thermo Scientific (Rockford, IL). Collagenase type 2 was purchased from Worthington Biochemical (Lakewood, NJ). Erythropoietin (EPO) was purchased from Amgen Inc. (Thousand Oak, CA). CD29 (FITC-conjugated anti-human integrinβ1 monoclonal antibody (MAB1951F-100) and CD90 (Alexa Fluor 594-conjugated anti-rat/mouse Thy1.1, Ox-7) were purchased from Millipore (Darmstadt, Germany) and BioLegend (San Diego, CA), respectively.

4.6.2. Cell isolation and culture

Human chondrocyte was isolated from discarded human OA tissues (N=4) during arthroscopic surgery without the patient's identity by following the published procedure [155]. The isolated cells were cultured with a concentration of 10^4 cells/ml in Dulbecco's Modified Eagle's medium (DMEM) (Sigma-Aldrich, St. Louis, MO) supplemented with 10% heat-inactivated fetal bovine serum (FBS) (Atlanta Biologicals, Atlanta, GA) and 1% penicillin/streptomycin (Gibco, Waltham, MA). Human bone marrow-derived mesenchymal stem cells (PCS-500-012) (ATCC, Manassas, VA) were cultured in mesenchymal stem cell basal medium (PCS-500-030) (ATCC, Manassas, VA) supplemented with 7% heat-inactivated FBS, 2.4

mM recombinant insulin-like growth factor-1, 5 ng/ml recombinant fibroblast growth factor-beta, 2.4 mM L-Alanyl-L-Glutamine (all from ATCC, Manassas, VA) and 1% penicillin/streptomycin.

4.6.3. HA microscaffolds production and characterization

HA microscaffolds were prepared as described in a recent publication [178]. To enhance visualization of HA microscaffolds, some HA microscaffolds were labeled with fluorescent dyes (CF488A and CF647A amine dye) as described previously [179]. Morphology and microstructure of the HA microscaffolds were analyzed using Leica DMi8 Fluorescence microscope (Leica, Wetzlar, Germany) and scanning electron microscopy (FE-SEM, S-4800 316 Hitachi, operating at 5 kV). The size of microscaffolds was determined using ImageJ software (US National Institutes of Health). The cytotoxicity of HA microscaffolds was assessed using primary human chondrocytes isolated from normal human articular cartilage (from PromoCell, Heidelberg, Germany) and Alamar Blue assay (Bio-Rad, Hercules, CA, USA), according to the manufacturer's instructions [180].

4.6.4. EPO-loaded microscaffold production and characterization

EPO loaded HA microscaffolds was prepared by mixing dried HA microscaffolds and EPO according to a previous report [158]. To determine loading capacity, EPO was labeled with FITC follow manufacturer's protocol [179]. Then the loading capacity was calculated based on the following equation: $\frac{EPO_{Intial}-EPO_{Supernatant}}{Mass\ of\ dried\ HA\ microscaffold}$ where $EPO_{Initial}$ and $EPO_{Supernatant}$ are mass of initial and not absorbed EPO, respectively, which were measured using the microplate reader and calculated based on the standard curve of FITC-Labeled-EPO. To determine EPO release, FITC-Labeled-EPO loaded HA microscaffolds were suspended in 0.5 ml of PBS (pH=7). At various time points, the supernatants were collected and the released media were replenished with an equal amount of the fresh one. The amounts of released EPO were measured based on the fluorescence

intensity of FITC-Labeled-EPO. The cumulative release was defined as the total amount of released EPO at a predetermined time relative to the initial loading amount. To test the bioactivity of the released EPO, a Transwell migration assay was performed as described earlier [87, 88]. The migration ability of MSCs toward the released EPO from microscaffolds was assessed compared to the standard EPO.

4.6.5. Cell and tissue targetting property of HA microscaffolds

Different numbers of human chondrocytes (1, 2, 4 and 8 × 10^4) were incubated with CF647-HA microscaffolds (final concentration of 0.1mg/mL in complete DMEM) for 15 min. They were centrifuged and then washed with fresh media 3X; the extent of scaffold binding to chondrocytes was assessed by measuring cell-associated fluorescent intensities using a microplate fluorometer. The extent of CD44 expression on different numbers of human chondrocytes was also measured using FITC-conjugated CD44 antibody (HCAM (IM7), sc-18849) Santa Cruz Biotechnology, Inc. (Dallas, Texas) by following manufacturer's instructions.

The ability of HA microscaffolds to target human cartilage tissue was also assessed *ex vivo* using discarded human articular cartilage tissue (N=6) isolated during total knee replacement surgery without any patients' identification. The tissues were first incubated with different concentrations (0.02, 0.1 and 0.5 mg/mL) of CF647 conjugated-HA microscaffolds for varying periods (30, 60, 90, 120 and 180 minutes). After an extensive wash with complete media to remove unbounded microscaffolds, the tissues were then imaged using a Kodak in vivo FX Pro imaging system (Carestream Health Inc., New Haven, CT). Furthermore, to determine the role of CD44 in mediating HA microscaffolds accumulation, OA cartilage tissues were immersed in complete medium with or without CD44 HCAM (IM7) blocking antibody (final concentration 10 μg/ml) for 1 hr. CF647-HA microscaffolds (final concentration of 100 μg/ml) was then added into each well

and incubated at 37 °C for 30 minutes. The ability of HA microscaffolds to target CD44 blocked cartilage and its control was quantified using a Kodak *in vivo* imaging system.

4.6.6. Rabbit microfracture defect model

All animals were treated according to the standard guidelines approved by Animal Care and Use Committee (IACUC) at the University of Texas at Arlington in accordance with the Animal Welfare Act and Guide for the Care and Use of Laboratory Animals. New Zealand White Rabbits 3-6 months old weighing between 1.9 and 2.8 kg were randomly divided into 4 groups -- saline, EPO alone, HA microscaffolds alone (abbreviated as HA) and EPO loaded HA microscaffolds (abbreviated as HA+EPO) (N=4/group/time point) for 2 different time points (12 and 26 weeks). The animals were first undergone microfracture defect procedure [161, 162]. At the end of procedure, 20 microliters of different treatments (saline, EPO, HA, or HA+EPO) were implanted on top of the articular cartilage defects. The animals were allowed to move freely within their cages after surgery. After the predetermined time points, animals were sacrificed. The knee joints and synovial fluids were then recovered for the following analyses.

4.6.7. Analysis of synovial inflammatory cells

To quantify the numbers of inflammatory cells in synovial fluid, synovial fluid of the rabbits was aspirated after injection of 1 ml of normal saline solution into the joint space. The synovial fluid cells were spun down on glass slides using cytospin (Cytospin 2, Thermo Shandon, Cheshire, England). The number of inflammatory cells was then determined using cyto-histochemical technique and CD11b (M1/70; Biolegend, San Diego, CA) as described earlier [181].

4.6.8. Micro-computed tomography assessment

Micro-computed tomography assessment of cartilage/bone microarchitecture was carried out on some of the rabbit joints using a High throughput *in vivo* SkyScan micro-CT scanner (Bruker,

Billerica, MA) with an exposure time of 640 ms/frame and the X-ray power at 39 watts during an 18 min scan. 499 images were obtained at a rotation step of 0.72°. The scans were then reconstructed and analyzed using CTVox and CTAn software (Bruker, Billerica, MA). The bone volume fraction (BVF), which is defined as bone volume divided by tissue volume (BV/TV), was then calculated for all of the samples.

4.6.9. Assessment of chondrogenesis and cartilage regeneration

Some tissue samples were fixed in 4% w/v buffered paraformaldehyde, decalcified, embedded in paraffin wax and then sectioned with an approximate thickness of 6 μm using a manual rotary microtome (Leica, Buffalo Grove, IL) by following published procedures [182, 183]. The sections were subsequently stained with hematoxylin and eosin (H&E), Safranin O and Toluidine blue staining [184], followed by imaging via an inverted light microscope (Leica TCS SP8 SMD, Leica, Buffalo Grove, IL). The extent of cartilage repair was then evaluated using the Pineda scoring system (Table 1 supplementary) [185]. All the samples were presented and examined by two observers in a blinded and random order. Furthermore, Toluidine blue was quantified and reported as the optical density of the images went through deconvolution process in ImageJ [186].

The cartilage samples at 12-weeks were assessed for progenitor cell recruitment to the site of injury utilizing immunohistochemistry. It has been documented that synovial stem cells possess dual markers of CD29 and CD90 [174-176]. Briefly, after antigen retrieval, the tissue sections were blocked with 10% goat serum for 30 mines and then followed by overnight incubation with CD29 (FITC-conjugated anti-human integrinβ1 monoclonal antibody and at 4 °C. All the sections images were taken using a confocal laser scanning microscopy and analyzed by LAS X software (Leica, Buffalo Grove, IL). The number of CD29 and CD90 double-positive cells per mm^2 was determined by ImageJ software.

Collagen II production is well established to be a chondrogenic marker [145, 187]. To detect Collagen II secretion in the cartilage, some of the 12- and 26-weeks tissue sections were stained with antibodies to Collagen II (M2139, sc-52658, Santa Cruz Biotechnology, Dallas, Texas), goat anti-mouse HRP secondary antibody (IgG H&L ab6789, Abcam) and finally Diaminobenzidine was used as a chromogen as described earlier [188]. Collagen II was quantified as the percentage of positively stained areas versus the whole as previously established [189].

4.6.10. Statistical analysis

Scoring of histological staining of cartilage tissues are presented as medians ± interquartile range and analyzed with Mann-Whitney test. All other data are expressed as mean ± standard deviation. An independent student t-test was used for the two independent groups while one-way analysis of variance (ANOVA) was utilized for multi-group comparison. An F test was used to examine the equality of the variance. All statistical analyses were performed using SPSS 16 and XLSTAT. A p-value < 0.01 and 0.05 was considered statistically significant.

Chapter 5

5.1.Conclusion

This dissertation summarizes work on the application of the tissue engineering techniques for cancer metastasis treatment and diagnosis as well as cartilage defect regeneration.

Chapter 2 led to the creation of LN-mimetic device - T cells seeded chitin beads, which can mimic the LN microenvironment. The device can be used to identify metastatic PCa and also serve as a powerful tool to investigate the processes governing LN metastasis of PCa and other cancers.

In Chapter 3, T cells and KD cells were encapsulated in alginate beads to simulate metastasized LNs. The encapsulated system can be used as an *in vitro* tool to investigate how cancer:LN cells interaction in cancer LN metastasis. Finally, it is possible that such LN mimetic device can be implanted nearby the primary tumor site as a decoy to reduce cancer LN metastasis.

In Chapter 4, EPO loaded HA microscaffolds were developed for treating cartilage defect. The *in vitro* results confirmed high cell compatibility and slow release of the bioactive EPO. Based on cell culture and a human cartilage explant model, we found that the HA microscaffolds can target the human chondrocytes and osteoarthritic tissue by interacting with their CD44 receptor. Finally, the rabbit model showed that EPO-loaded HA microscaffolds could reduce inflammatory cells in synovial fluid and trigger the recruitment of endogenous progenitor cell led to the regeneration of cartilage tissue.

5.2.Future direction

Although the results from all these studies are exciting, further investigation and development are required to push these methods to the next level, such as clinical implementation or further research advancement. Future efforts should be devoted to several areas, as are summarized below.

First, for LN mimetic device, future studies should aim to clear the interaction of T cells and cancer cells. Future studies should also incorporate the evaluation of the role of different T cell types in metastasis of cancer cells toward lymph nodes. Additionally, the effect of the interaction of cancer cells and T cells on the activation of the T cells should be assessed.

Secondly, for encapsulation of T cells and KD cells for simulation of metastatic lymph node, the interaction of the cells in alginate beads should be studied. Also, trapped cancer cells should be analyzed for the expression of different cancer cell receptors. Furthermore, biodistribution studies should be performed to check the ability of the trap to reduce cancer cell metastasis to other organs.

Finally, for EPO loaded HA microscaffolds, EPO can be loaded chemically instead of physically for longer drug release. In addition, the molecular and cellular mechanisms underlying endogenous stem cell recruitment to the site of injury are still not precisely understood. Therefore, further studies are needed to clarify these questions clearly.

References

1. Mak, M., et al., *Single-cell migration in complex microenvironments: mechanics and signaling dynamics.* Journal of biomechanical engineering, 2016. **138**(2): p. 021004.
2. Xia, H., et al., *Tissue repair and regeneration with endogenous stem cells.* Nature Reviews Materials, 2018. **3**(7): p. 174.
3. Van Vlierberghe, S., P. Dubruel, and E. Schacht, *Biopolymer-based hydrogels as scaffolds for tissue engineering applications: a review.* Biomacromolecules, 2011. **12**(5): p. 1387-1408.
4. Lee, K., E.A. Silva, and D.J. Mooney, *Growth factor delivery-based tissue engineering: general approaches and a review of recent developments.* Journal of the Royal Society Interface, 2010. **8**(55): p. 153-170.
5. Zhang, J.-M. and J. An, *Cytokines, inflammation and pain.* International anesthesiology clinics, 2007. **45**(2): p. 27.
6. Barrientos, S., et al., *Growth factors and cytokines in wound healing.* Wound repair and regeneration, 2008. **16**(5): p. 585-601.
7. Nair, A., et al., *Biomaterial implants mediate autologous stem cell recruitment in mice.* Acta biomaterialia, 2011. **7**(11): p. 3887-3895.
8. Tysseling, V.M., et al., *SDF1 in the dorsal corticospinal tract promotes CXCR4+ cell migration after spinal cord injury.* Journal of neuroinflammation, 2011. **8**(1): p. 16.
9. Liotta, L.A., P.S. Steeg, and W.G. Stetler-Stevenson, *Cancer metastasis and angiogenesis: an imbalance of positive and negative regulation.* Cell, 1991. **64**(2): p. 327-336.
10. Karnoub, A.E., et al., *Mesenchymal stem cells within tumour stroma promote breast cancer metastasis.* Nature, 2007. **449**(7162): p. 557.
11. Todaro, M., et al., *CD44v6 is a marker of constitutive and reprogrammed cancer stem cells driving colon cancer metastasis.* Cell stem cell, 2014. **14**(3): p. 342-356.
12. Yang, J.D., I. Nakamura, and L.R. Roberts. *The tumor microenvironment in hepatocellular carcinoma: current status and therapeutic targets*. in *Seminars in cancer biology*. 2011. Elsevier.
13. Siegel, R.L., K.D. Miller, and A. Jemal, *Cancer statistics, 2018.* CA: a cancer journal for clinicians, 2018. **68**(1): p. 7-30.
14. Brower, V., *Researchers tackle metastasis, cancer's last frontier.* Journal of the National Cancer Institute, 2007. **99**(2): p. 109-111.
15. Logothetis, C.J. and S.-H. Lin, *Osteoblasts in prostate cancer metastasis to bone.* Nature Reviews Cancer, 2005. **5**(1): p. 21.
16. Gervasi, L.A., et al., *Prognostic significance of lymph nodal metastases in prostate cancer.* The Journal of urology, 1989. **142**(2): p. 332-336.
17. Sleeman, J.P., *The lymph node as a bridgehead in the metastatic dissemination of tumors*, in *Lymphatic Metastasis and Sentinel Lymphonodectomy*. 2000, Springer. p. 55-81.
18. Heidenreich, A., et al., *EAU guidelines on prostate cancer. Part 1: screening, diagnosis, and local treatment with curative intent—update 2013.* European urology, 2014. **65**(1): p. 124-137.
19. Carter, C.L., C. Allen, and D.E. Henson, *Relation of tumor size, lymph node status, and survival in 24,740 breast cancer cases.* Cancer, 1989. **63**(1): p. 181-187.
20. Standring, S., *Gray's Anatomy E-Book: The Anatomical Basis of Clinical Practice*. 2015: Elsevier Health Sciences.

21. Treuting, P.M. and S.M. Dintzis, *Comparative anatomy and histology: a mouse and human atlas (expert consult)*. 2011: Academic Press.
22. Kawada, K. and M.M. Taketo, *Significance and mechanism of lymph node metastasis in cancer progression.* Cancer research, 2011: p. canres. 3277.2010.
23. Dintzis, S. and P. Treuting, *Comparative Anatomy and Histology: A Mouse and Human Atlas*. 2011: Academic.
24. Stacker, S.A., et al., *Lymphangiogenesis and lymphatic vessel remodelling in cancer.* Nature Reviews Cancer, 2014. **14**(3): p. 159.
25. Harrell, M.I., B.M. Iritani, and A. Ruddell, *Tumor-induced sentinel lymph node lymphangiogenesis and increased lymph flow precede melanoma metastasis.* The American journal of pathology, 2007. **170**(2): p. 774-786.
26. Van den Eynden, G., et al., *Angiogenesis and hypoxia in lymph node metastases is predicted by the angiogenesis and hypoxia in the primary tumour in patients with breast cancer*. British journal of cancer, 2005. **93**(10): p. 1128-1136.
27. Chung, M.K., et al., *Lymphatic vessels and high endothelial venules are increased in the sentinel lymph nodes of patients with oral squamous cell carcinoma before the arrival of tumor cells.* Annals of surgical oncology, 2012. **19**(5): p. 1595-1601.
28. Lee, J.H., et al., *Quantitative analysis of melanoma-induced cytokine-mediated immunosuppression in melanoma sentinel nodes.* Clinical Cancer Research, 2005. **11**(1): p. 107-112.
29. Nathanson, S.D., *Insights into the mechanisms of lymph node metastasis.* Cancer, 2003. **98**(2): p. 413-423.
30. Alitalo, K. and P. Carmeliet, *Molecular mechanisms of lymphangiogenesis in health and disease.* Cancer cell, 2002. **1**(3): p. 219-227.
31. Kwon, E.D., et al., *Elimination of residual metastatic prostate cancer after surgery and adjunctive cytotoxic T lymphocyte-associated antigen 4 (CTLA-4) blockade immunotherapy.* Proceedings of the National Academy of Sciences, 1999. **96**(26): p. 15074-15079.
32. Hu, S., et al., *Infiltrating T cells promote prostate cancer metastasis via modulation of FGF11→ miRNA-541→ androgen receptor (AR)→ MMP9 signaling.* Molecular oncology, 2015. **9**(1): p. 44-57.
33. DeNardo, D.G., et al., *CD4+ T cells regulate pulmonary metastasis of mammary carcinomas by enhancing protumor properties of macrophages.* Cancer cell, 2009. **16**(2): p. 91-102.
34. Banchereau, J. and R.M. Steinman, *Dendritic cells and the control of immunity.* Nature, 1998. **392**(6673): p. 245-252.
35. Suematsu, S. and T. Watanabe, *Generation of a synthetic lymphoid tissue–like organoid in mice.* Nature biotechnology, 2004. **22**(12): p. 1539.
36. Okamoto, N., et al., *Artificial lymph nodes induce potent secondary immune responses in naive and immunodeficient mice.* The Journal of clinical investigation, 2007. **117**(4): p. 997-1007.
37. Giese, C., et al., *A human lymph node in vitro—Challenges and progress.* Artificial organs, 2006. **30**(10): p. 803-808.
38. Sardi, M., A. Lubitz, and C. Giese, *Modeling Human Immunity In Vitro: Improving Artificial Lymph Node Physiology by Stromal Cells.* Applied In Vitro Toxicology, 2016. **2**(3): p. 143-150.

39. Tomei, A.A., et al., *Fluid flow regulates stromal cell organization and CCL21 expression in a tissue-engineered lymph node microenvironment.* The Journal of Immunology, 2009. **183**(7): p. 4273-4283.
40. Xie, D., et al., *Role of DAB2IP in modulating epithelial-to-mesenchymal transition and prostate cancer metastasis.* Proceedings of the National Academy of Sciences, 2010. **107**(6): p. 2485-2490.
41. Mokhtar, M., et al. *An artificial lymph node architecture for homeostasis in collective robotic systems*. in *Self-Adaptive and Self-Organizing Systems Workshops, 2008. SASOW 2008. Second IEEE International Conference on*. 2008. IEEE.
42. Kobayashi, Y., K. Kato, and T. Watanabe, *Synthesis of functional artificial lymphoid tissues.* Discovery medicine, 2011. **12**(65): p. 351-362.
43. Okamoto, N., et al., *Artificial lymph nodes induce potent secondary immune responses in naive and immunodeficient mice.* Journal of Clinical Investigation, 2007. **117**(4): p. 997.
44. Yang, M., et al., *Real-time whole-body imaging of an orthotopic metastatic prostate cancer model expressing red fluorescent protein.* The Prostate, 2005. **62**(4): p. 374-379.
45. Ismail, A., et al., *Expression of NF-κB in prostate cancer lymph node metastases.* The Prostate, 2004. **58**(3): p. 308-313.
46. Wong, S.Y., et al., *Tumor-secreted vascular endothelial growth factor-C is necessary for prostate cancer lymphangiogenesis, but lymphangiogenesis is unnecessary for lymph node metastasis.* Cancer research, 2005. **65**(21): p. 9789-9798.
47. Pouliot, N., H.B. Pearson, and A. Burrows, *Investigating metastasis using in vitro platforms*, in *Madame Curie Bioscience Database [Internet]*. 2013, Landes Bioscience.
48. Su, W.-H., et al., *Radiation-induced increase in cell migration and metastatic potential of cervical cancer cells operates via the K-Ras pathway.* The American journal of pathology, 2012. **180**(2): p. 862-871.
49. Hirakawa, S., *From tumor lymphangiogenesis to lymphvascular niche.* Cancer science, 2009. **100**(6): p. 983-989.
50. Mebius, R.E., *Lymphoid organogenesis: educating stroma.* Immunology and cell biology, 2007. **85**(2): p. 79.
51. Coussens, L.M. and Z. Werb, *Inflammation and cancer.* Nature, 2002. **420**(6917): p. 860-867.
52. Yousefieh, N., et al., *Regulated expression of CCL21 in the prostate tumor microenvironment inhibits tumor growth and metastasis in an orthotopic model of prostate cancer.* Cancer Microenvironment, 2009. **2**(1): p. 59-67.
53. Ghadjar, P., et al., *Chemokine receptor CCR6 expression level and aggressiveness of prostate cancer.* Journal of cancer research and clinical oncology, 2008. **134**(11): p. 1181.
54. Müller, A., et al., *Involvement of chemokine receptors in breast cancer metastasis.* nature, 2001. **410**(6824): p. 50.
55. Zhou, Y., et al., *CXCR4 is a major chemokine receptor on glioma cells and mediates their survival.* Journal of Biological Chemistry, 2002. **277**(51): p. 49481-49487.
56. Kakinuma, T. and S.T. Hwang, *Chemokines, chemokine receptors, and cancer metastasis.* Journal of leukocyte biology, 2006. **79**(4): p. 639-651.
57. Singh, S., et al., *CXCL12–CXCR4 interactions modulate prostate cancer cell migration, metalloproteinase expression and invasion.* Laboratory investigation, 2004. **84**(12): p. 1666.

58. Sun, Y.X., et al., *Skeletal localization and neutralization of the SDF-1 (CXCL12)/CXCR4 axis blocks prostate cancer metastasis and growth in osseous sites in vivo.* Journal of Bone and Mineral Research, 2005. **20**(2): p. 318-329.
59. Noy, R. and J.W. Pollard, *Tumor-associated macrophages: from mechanisms to therapy.* Immunity, 2014. **41**(1): p. 49-61.
60. Taichman, R.S., et al., *Use of the stromal cell-derived factor-1/CXCR4 pathway in prostate cancer metastasis to bone.* Cancer research, 2002. **62**(6): p. 1832-1837.
61. Singh, S., et al., *CXCL12–CXCR4 interactions modulate prostate cancer cell migration, metalloproteinase expression and invasion.* Laboratory investigation, 2004. **84**(12): p. 1666-1676.
62. Yousefieh, N., et al., *Regulated expression of CCL21 in the prostate tumor microenvironment inhibits tumor growth and metastasis in an orthotopic model of prostate cancer.* Cancer Microenviron, 2009. **2**(1): p. 59-67.
63. Dwivedi, S., et al., *Diagnostic and prognostic significance of prostate specific antigen and serum interleukin 18 and 10 in patients with locally advanced prostate cancer: a prospective study.* Asian Pac J Cancer Prev, 2011. **12**(7): p. 1843-8.
64. Yuzhalin, A. and A. Kutikhin, *Interleukins in Cancer Biology: Their Heterogeneous Role*. 2014: Academic Press.
65. Dinarello, C.A., *Biologic basis for interleukin-1 in disease.* Blood, 1996. **87**(6): p. 2095-2147.
66. Mizel, S.B., *Interleukin 1 and T-cell activation.* Immunology today, 1987. **8**(11): p. 330-332.
67. Apte, R.N., et al., *The involvement of IL-1 in tumorigenesis, tumor invasiveness, metastasis and tumor-host interactions.* Cancer and Metastasis Reviews, 2006. **25**(3): p. 387-408.
68. Ostrand-Rosenberg, S., *Immune surveillance: a balance between protumor and antitumor immunity.* Current opinion in genetics & development, 2008. **18**(1): p. 11-18.
69. Zou, W., *Regulatory T cells, tumour immunity and immunotherapy.* Nature Reviews Immunology, 2006. **6**(4): p. 295.
70. Dienz, O. and M. Rincon, *The effects of IL-6 on CD4 T cell responses.* Clinical immunology, 2009. **130**(1): p. 27-33.
71. Miyahara, Y., et al., *Generation and regulation of human CD4+ IL-17-producing T cells in ovarian cancer.* Proceedings of the National Academy of Sciences, 2008. **105**(40): p. 15505-15510.
72. Kryczek, I., et al., *Endogenous IL-17 contributes to reduced tumor growth and metastasis.* Blood, 2009. **114**(2): p. 357-359.
73. Baker, B.M. and C.S. Chen, *Deconstructing the third dimension–how 3D culture microenvironments alter cellular cues.* J Cell Sci, 2012. **125**(13): p. 3015-3024.
74. Haycock, J.W., *3D cell culture: a review of current approaches and techniques*, in *3D cell culture*. 2011, Springer. p. 1-15.
75. Fernandes, T.G., et al., *Three-dimensional cell culture microarray for high-throughput studies of stem cell fate.* Biotechnology and bioengineering, 2010. **106**(1): p. 106-118.
76. Van Hemert, P., D. Kilburn, and A. Van Wezel, *Homogeneous cultivation of animal cells for the production of virus and virus products.* Biotechnology and Bioengineering, 1969. **11**(5): p. 875-885.
77. Sundqvist, K. and L. Wanger, *Anchorage and lymphocyte function. Contact-induced augmentation of T-cell activation.* Immunology, 1980. **41**(4): p. 883.

78. Sundqvist, K. and L. Wanger, *Anchorage and lymphocyte function II. Contact with non-cellular surfaces, cell density and T-cell activation.* Immunology, 1981. **43**(3): p. 573.
79. Meli, L., et al., *Influence of a three-dimensional, microarray environment on human cell culture in drug screening systems.* Biomaterials, 2012. **33**(35): p. 9087-9096.
80. Giard, D.J., et al., *Virus production with a newly developed microcarrier system.* Applied and environmental microbiology, 1977. **34**(6): p. 668-672.
81. Flaim, C.J., S. Chien, and S.N. Bhatia, *An extracellular matrix microarray for probing cellular differentiation.* Nature methods, 2005. **2**(2): p. 119.
82. Pörtner, R. and C. Giese, *An overview on bioreactor design, prototyping and process control for reproducible three-dimensional tissue culture.* Drug testing in vitro. WILEY-VCH Verlag, Weinheim, 2007.
83. Wu, K., et al., *The mechanism of DAB2IP in chemoresistance of prostate cancer cells.* Clinical Cancer Research, 2013. **19**(17): p. 4740-4749.
84. Kosaka, N., et al., *Near infrared fluorescence-guided real-time endoscopic detection of peritoneal ovarian cancer nodules using intravenously injected indocyanine green.* International journal of cancer, 2011. **129**(7): p. 1671-1677.
85. Nizri, E., et al., *Analysis of histological and immunological parameters of metastatic lymph nodes from colon cancer patients reveals that T-helper 1 type immune response is associated with improved overall survival.* Medicine, 2016. **95**(45).
86. Ko, C.-Y., et al., *The use of chemokine-releasing tissue engineering scaffolds in a model of inflammatory response-mediated melanoma cancer metastasis.* Biomaterials, 2012. **33**(3): p. 876-885.
87. Thevenot, P.T., et al., *The effect of incorporation of SDF-1α into PLGA scaffolds on stem cell recruitment and the inflammatory response.* Biomaterials, 2010. **31**(14): p. 3997-4008.
88. Nair, A.M., et al., *The effect of erythropoietin on autologous stem cell-mediated bone regeneration.* Biomaterials, 2013. **34**(30): p. 7364-7371.
89. Thompson-Snipes, L., et al., *Interleukin 10: a novel stimulatory factor for mast cells and their progenitors.* Journal of Experimental Medicine, 1991. **173**(2): p. 507-510.
90. system, R.D., *Mouse IL-10 Antibody*.
91. Cochran, A.J., et al., *Tumour–induced immune modulation of sentinel lymph nodes.* Nature Reviews Immunology, 2006. **6**(9): p. 659.
92. Karaman, S. and M. Detmar, *Mechanisms of lymphatic metastasis.* The Journal of clinical investigation, 2014. **124**(3): p. 922-928.
93. Gotoda, T., et al., *Incidence of lymph node metastasis from early gastric cancer: estimation with a large number of cases at two large centers.* Gastric cancer, 2000. **3**(4): p. 219-225.
94. Ran, S., et al., *Lymphangiogenesis and lymphatic metastasis in breast cancer.* Pathophysiology, 2010. **17**(4): p. 229-251.
95. White, R.R., et al., *Long-term survival in 2,505 patients with melanoma with regional lymph node metastasis.* Annals of surgery, 2002. **235**(6): p. 879.
96. Elisei, R., et al., *Are the clinical and pathological features of differentiated thyroid carcinoma really changed over the last 35 years? Study on 4187 patients from a single Italian institution to answer this question.* The Journal of Clinical Endocrinology & Metabolism, 2010. **95**(4): p. 1516-1527.
97. Yu, X.-M., et al., *Follicular variant of papillary thyroid carcinoma is a unique clinical entity: a population-based study of 10,740 cases.* Thyroid, 2013. **23**(10): p. 1263-1268.

98. Wada, N., et al., *Lymph node metastasis from 259 papillary thyroid microcarcinomas: frequency, pattern of occurrence and recurrence, and optimal strategy for neck dissection.* Annals of surgery, 2003. **237**(3): p. 399.
99. Sleeman, J., A. Schmid, and W. Thiele. *Tumor lymphatics*. in *Seminars in cancer biology*. 2009. Elsevier.
100. Datta, K., et al., *Mechanism of lymph node metastasis in prostate cancer.* Future oncology, 2010. **6**(5): p. 823-836.
101. Heidenreich, A., et al., *EAU guidelines on prostate cancer. Part 1: screening, diagnosis, and local treatment with curative intentâ€"update 2013.* European urology, 2014. **65**(1): p. 124-137.
102. Sleeman, J.P. and W. Thiele, *Tumor metastasis and the lymphatic vasculature.* International Journal of Cancer, 2009. **125**(12): p. 2747-2756.
103. Alitalo, K., T. Tammela, and T.V. Petrova, *Lymphangiogenesis in development and human disease.* Nature, 2005. **438**(7070): p. 946.
104. Bolenz, C., et al., *The role of lymphangiogenesis in lymphatic tumour spread of urological cancers.* BJU international, 2009. **104**(5): p. 592-597.
105. Karkkainen, M.J., T. Mäkinen, and K. Alitalo, *Lymphatic endothelium: a new frontier of metastasis research.* Nature cell biology, 2002. **4**(1): p. E2.
106. Hirakawa, S., et al., *VEGF-A induces tumor and sentinel lymph node lymphangiogenesis and promotes lymphatic metastasis.* Journal of Experimental Medicine, 2005. **201**(7): p. 1089-1099.
107. Hirakawa, S., et al., *VEGF-C–induced lymphangiogenesis in sentinel lymph nodes promotes tumor metastasis to distant sites.* Blood, 2007. **109**(3): p. 1010-1017.
108. Ruffell, B., et al., *Lymphocytes in cancer development: polarization towards pro-tumor immunity.* Cytokine & growth factor reviews, 2010. **21**(1): p. 3-10.
109. Ostroumov, D., et al., *CD4 and CD8 T lymphocyte interplay in controlling tumor growth.* Cellular and molecular life sciences, 2018. **75**(4): p. 689-713.
110. Björndahl, M.A., et al., *Vascular endothelial growth factor-a promotes peritumoral lymphangiogenesis and lymphatic metastasis.* Cancer research, 2005. **65**(20): p. 9261-9268.
111. Takeuchi, H., et al., *CCL21 chemokine regulates chemokine receptor CCR7 bearing malignant melanoma cells.* Clinical cancer research, 2004. **10**(7): p. 2351-2358.
112. Ding, Y., et al., *Association of CC chemokine receptor 7 with lymph node metastasis of esophageal squamous cell carcinoma.* Clinical cancer research, 2003. **9**(9): p. 3406-3412.
113. Oliveira-Neto, H.H., et al., *Involvement of CXCL12 and CXCR4 in lymph node metastases and development of oral squamous cell carcinomas.* Tumor Biology, 2008. **29**(4): p. 262-271.
114. Hennessy, B.T., et al., *Outcome after pathologic complete eradication of cytologically proven breast cancer axillary node metastases following primary chemotherapy.* J Clin Oncol, 2005. **23**(36): p. 9304-9311.
115. Giuliano, A.E., et al., *Locoregional recurrence after sentinel lymph node dissection with or without axillary dissection in patients with sentinel lymph node metastases: long-term follow-up from the American College of Surgeons Oncology Group (Alliance) ACOSOG Z0011 randomized trial.* Annals of surgery, 2016. **264**(3): p. 413.
116. Hakamivala, A., et al., *Development of 3D Lymph Node Mimetic for Studying Prostate Cancer Metastasis.* Advanced Biosystems, 2019. **3**(7).

117. Heile, A. and T. Brinker, *Clinical translation of stem cell therapy in traumatic brain injury: the potential of encapsulated mesenchymal cell biodelivery of glucagon-like peptide-1.* Dialogues in clinical neuroscience, 2011. **13**(3): p. 279–286.
118. Shah, K., *Encapsulated stem cells for cancer therapy.* Biomatter, 2013. **3**(1): p. 1-7.
119. Laham, R.J., et al., *Local perivascular delivery of basic fibroblast growth factor in patients undergoing coronary bypass surgery results of a phase I randomized, double-blind, placebo-controlled trial.* Circulation, 1999. **100**(18): p. 1865-1871.
120. Siegel, R.L., K.D. Miller, and A. Jemal, *Cancer statistics, 2019.* CA: a cancer journal for clinicians, 2019. **69**(1): p. 7-34.
121. Chambers, A.F., A.C. Groom, and I.C. MacDonald, *Metastasis: dissemination and growth of cancer cells in metastatic sites.* Nature Reviews Cancer, 2002. **2**(8): p. 563.
122. Wan, F., et al., *Oxidized low-density lipoprotein is associated with advanced-stage prostate cancer.* Tumor Biology, 2015. **36**(5): p. 3573-3582.
123. Chan, E.-S., et al., *Prediction models for shape and size of ca-alginate macrobeads produced through extrusion–dripping method.* Journal of colloid and interface science, 2009. **338**(1): p. 63-72.
124. Apostol, B.L., et al., *A cell-based assay for aggregation inhibitors as therapeutics of polyglutamine-repeat disease and validation in Drosophila.* Proceedings of the National Academy of Sciences, 2003. **100**(10): p. 5950-5955.
125. Gåserød, O., A. Sannes, and G. Skjåk-Bræk, *Microcapsules of alginate–chitosan. II. A study of capsule stability and permeability.* Biomaterials, 1999. **20**(8): p. 773-783.
126. Asthana, A., et al., *Facile single step fabrication of microchannels with varying size.* Lab on a Chip, 2009. **9**(8): p. 1138-1142.
127. Vandenbossche, G.M., P. Van Oostveldt, and J.P. Remon, *A fluorescence method for the determination of the molecular weight cut-off of alginate-polylysine microcapsules.* Journal of pharmacy and pharmacology, 1991. **43**(4): p. 275-277.
128. Das, S., et al., *Tumor cell entry into the lymph node is controlled by CCL1 chemokine expressed by lymph node lymphatic sinuses.* Journal of Experimental Medicine, 2013. **210**(8): p. 1509-1528.
129. Issa, A., et al., *Vascular endothelial growth factor-C and CC chemokine receptor 7 in tumor cell–lymphatic cross-talk promote invasive phenotype.* Cancer research, 2009. **69**(1): p. 349-357.
130. Khang, M.K., et al., *Correction: Preparation of a novel injectable in situ-gelling nanoparticle with applications in controlled protein release and cancer cell entrapment.* RSC advances, 2018. **8**(72): p. 41376-41376.
131. Hakamivala, A., S. Moghassemi, and K. Omidfar, *Modeling and optimization of the niosome nanovesicles using response surface methodology for delivery of insulin.* Biomedical Physics & Engineering Express, 2019.
132. Alitalo, A. and M. Detmar, *Interaction of tumor cells and lymphatic vessels in cancer progression.* Oncogene, 2012. **31**(42): p. 4499.
133. Vose, B., F. Vanky, and E. Klein, *Human tumour—lymphocyte interaction in vitro. V. Comparison of the reactivity of tumour-infiltrating, blood and lymph-node lymphocytes with autologous tumour cells.* International journal of cancer, 1977. **20**(6): p. 895-902.
134. Kang, A., et al., *Cell encapsulation via microtechnologies.* Biomaterials, 2014. **35**(9): p. 2651-2663.

135. Lotfipour, F., S. Mirzaeei, and M. Maghsoodi, *Evaluation of the effect of CaCl2 and alginate concentrations and hardening time on the characteristics of Lactobacillus acidophilus loaded alginate beads using response surface analysis.* Advanced pharmaceutical bulletin, 2012. **2**(1): p. 71.
136. Cao, N., X. Chen, and D. Schreyer, *Influence of calcium ions on cell survival and proliferation in the context of an alginate hydrogel.* ISRN Chemical Engineering, 2012. **2012**.
137. Dvorak, M.M., et al., *Physiological changes in extracellular calcium concentration directly control osteoblast function in the absence of calciotropic hormones.* Proceedings of the National Academy of Sciences, 2004. **101**(14): p. 5140-5145.
138. de Vos, P., et al., *Alginate-based microcapsules for immunoisolation of pancreatic islets.* Biomaterials, 2006. **27**(32): p. 5603-5617.
139. Kryczek, I., et al., *CXCL12 and vascular endothelial growth factor synergistically induce neoangiogenesis in human ovarian cancers.* Cancer research, 2005. **65**(2): p. 465-472.
140. Ji, R.-C., *Lymph nodes and cancer metastasis: new perspectives on the role of intranodal lymphatic sinuses.* International journal of molecular sciences, 2016. **18**(1): p. 51.
141. Favero, M., et al., *Early knee osteoarthritis.* RMD open, 2015. **1**(Suppl 1): p. e000062.
142. Rivera, J.C., et al., *Post-traumatic OA: Unique implications for the military.* 2013.
143. Cho, H., et al., *Study of osteoarthritis treatment with anti-inflammatory drugs: Cyclooxygenase-2 inhibitor and steroids.* BioMed research international, 2015.
144. Sekiya, I., et al., *In vitro cartilage formation by human adult stem cells from bone marrow stroma defines the sequence of cellular and molecular events during chondrogenesis.* Proceedings of the National Academy of Sciences, 2002. **99**(7): p. 4397-4402.
145. Bosnakovski, D., et al., *Chondrogenic differentiation of bovine bone marrow mesenchymal stem cells (MSCs) in different hydrogels: influence of collagen type II extracellular matrix on MSC chondrogenesis.* Biotechnology and bioengineering, 2006. **93**(6): p. 1152-1163.
146. Leijs, M.J., et al., *Effect of arthritic synovial fluids on the expression of immunomodulatory factors by mesenchymal stem cells: an explorative in vitro study.* Frontiers in immunology, 2012. **3**: p. 231.
147. Suzuki, S., et al., *Properties and usefulness of aggregates of synovial mesenchymal stem cells as a source for cartilage regeneration.* Arthritis research & therapy, 2012. **14**(3): p. R136.
148. Lu, J., et al., *Increased recruitment of endogenous stem cells and chondrogenic differentiation by a composite scaffold containing bone marrow homing peptide for cartilage regeneration.* Theranostics, 2018. **8**(18): p. 5039.
149. Chen, F.-M., et al., *Homing of endogenous stem/progenitor cells for in situ tissue regeneration: promises, strategies, and translational perspectives.* Biomaterials, 2011. **32**(12): p. 3189-3209.
150. Oliveira, M.B. and J.F. Mano, *Polymer-based microparticles in tissue engineering and regenerative medicine.* Biotechnology progress, 2011. **27**(4): p. 897-912.
151. Barile, L., et al., *Endogenous cardiac stem cells.* Progress in cardiovascular diseases, 2007. **50**(1): p. 31-48.
152. Xin, Z.-C., et al., *Recruiting endogenous stem cells: a novel therapeutic approach for erectile dysfunction.* Asian journal of andrology, 2016. **18**(1): p. 10.
153. Xu, X., et al., *Hyaluronic acid-based hydrogels: from a natural polysaccharide to complex networks.* Soft matter, 2012. **8**(12): p. 3280-3294.

154. Litwiniuk, M., et al., *Hyaluronic acid in inflammation and tissue regeneration.* Wounds, 2016. **28**(3): p. 78-88.
155. Hayward, S.L., C.L. Wilson, and S. Kidambi, *Hyaluronic acid-conjugated liposome nanoparticles for targeted delivery to CD44 overexpressing glioblastoma cells.* Oncotarget, 2016. **7**(23): p. 34158.
156. Zhang, F.-J., et al., *Expression of CD44 in articular cartilage is associated with disease severity in knee osteoarthritis.* Modern rheumatology, 2013. **23**(6): p. 1186-1191.
157. Deng, R.-H., B. Qiu, and P.-H. Zhou, *Chitosan/hyaluronic acid/plasmid-DNA nanoparticles encoding interleukin-1 receptor antagonist attenuate inflammation in synoviocytes induced by interleukin-1 beta.* Journal of Materials Science: Materials in Medicine, 2018. **29**(10): p. 155.
158. Xu, X., et al., *Heparin-decorated, hyaluronic acid-based hydrogel particles for the controlled release of bone morphogenetic protein 2.* Acta biomaterialia, 2011. **7**(8): p. 3050-3059.
159. Liu, N., et al., *Effect of erythropoietin on mesenchymal stem cell differentiation and secretion in vitro in an acute kidney injury microenvironment.* Genet Mol Res, 2013. **12**: p. 6477-6487.
160. Hidaka, C., et al., *Acceleration of cartilage repair by genetically modified chondrocytes over expressing bone morphogenetic protein-7.* Journal of Orthopaedic Research, 2003. **21**(4): p. 573-583.
161. Kang, S.-W., et al., *Articular cartilage regeneration with microfracture and hyaluronic acid.* Biotechnology letters, 2008. **30**(3): p. 435-439.
162. Strauss, E., et al., *The efficacy of intra-articular hyaluronan injection after the microfracture technique for the treatment of articular cartilage lesions.* The American journal of sports medicine, 2009. **37**(4): p. 720-726.
163. Strauss, E.J., et al., *Biochemical and biomechanical properties of lesion and adjacent articular cartilage after chondral defect repair in an equine model.* The American journal of sports medicine, 2005. **33**(11): p. 1647-1653.
164. Khang, M.K., et al., *Preparation of a novel injectable in situ-gelling nanoparticle with applications in controlled protein release and cancer cell entrapment.* RSC Advances, 2018. **8**(60): p. 34625-34633.
165. Wan, L., et al., *EPO promotes bone repair through enhanced cartilaginous callus formation and angiogenesis.* PLoS One, 2014. **9**(7): p. e102010.
166. Peng, Z., et al., *Design of a portable imager for near-infrared visualization of cutaneous wounds.* Journal of biomedical optics, 2017. **22**(1): p. 016010.
167. Knudson, C.B. and W. Knudson, *Hyaluronan and CD44: modulators of chondrocyte metabolism.* Clinical Orthopaedics and Related Research®, 2004. **427**: p. S152-S162.
168. Benito, M.J., et al., *Synovial tissue inflammation in early and late osteoarthritis.* Annals of the rheumatic diseases, 2005. **64**(9): p. 1263-1267.
169. Katayama, Y., et al., *CD44 is a physiological E-selectin ligand on neutrophils.* Journal of experimental medicine, 2005. **201**(8): p. 1183-1189.
170. Puré, E. and C.A. Cuff, *A crucial role for CD44 in inflammation.* Trends in molecular medicine, 2001. **7**(5): p. 213-221.
171. Feng, Q., *Beyond erythropoiesis: the anti-inflammatory effects of erythropoietin*. 2006.

172. Kolf, C.M., E. Cho, and R.S. Tuan, *Mesenchymal stromal cells: biology of adult mesenchymal stem cells: regulation of niche, self-renewal and differentiation.* Arthritis research & therapy, 2007. **9**(1): p. 204.
173. Kern, S., et al., *Comparative analysis of mesenchymal stem cells from bone marrow, umbilical cord blood, or adipose tissue.* Stem cells, 2006. **24**(5): p. 1294-1301.
174. Deng, J., et al., *A silk fibroin/chitosan scaffold in combination with bone marrow-derived mesenchymal stem cells to repair cartilage defects in the rabbit knee.* Journal of Materials Science: Materials in Medicine, 2013. **24**(8): p. 2037-2046.
175. Tan, S.L., et al., *Isolation, characterization and the multi-lineage differentiation potential of rabbit bone marrow-derived mesenchymal stem cells.* Journal of anatomy, 2013. **222**(4): p. 437-450.
176. Yang, J., et al., *Regulation of the secretion of immunoregulatory factors of mesenchymal stem cells (MSCs) by collagen-based scaffolds during chondrogenesis.* Materials Science and Engineering: C, 2017. **70**: p. 983-991.
177. Cancedda, R., *Cartilage and bone extracellular matrix.* Current pharmaceutical design, 2009. **15**(12): p. 1334-1348.
178. Li, S., et al., *Hyaluronic Acid-Based Optical Probe for the Diagnosis of Human Osteoarthritic Cartilage.* Nanotheranostics, 2018. **2**(4): p. 347.
179. Yoon, H.Y., et al., *Tumor-targeting hyaluronic acid nanoparticles for photodynamic imaging and therapy.* Biomaterials, 2012. **33**(15): p. 3980-3989.
180. Hirata, K., et al., *Chemical synthesis and cytotoxicity of neo-glycolipids; rare sugar-glycerol-lipid compounds.* Heliyon, 2018. **4**(10): p. e00861.
181. Clatworthy, M.R. and K.G. Smith, *FcγRIIb balances efficient pathogen clearance and the cytokine-mediated consequences of sepsis.* Journal of Experimental Medicine, 2004. **199**(5): p. 717-723.
182. Shao, X.X., et al., *Evaluation of a hybrid scaffold/cell construct in repair of high-load-bearing osteochondral defects in rabbits.* Biomaterials, 2006. **27**(7): p. 1071-1080.
183. Grigolo, B., et al., *Osteoarthritis treated with mesenchymal stem cells on hyaluronan-based scaffold in rabbit.* Tissue Engineering Part C: Methods, 2009. **15**(4): p. 647-658.
184. Schmitz, N., et al., *Basic methods in histopathology of joint tissues.* Osteoarthritis and cartilage, 2010. **18**: p. S113-S116.
185. Shi, J., et al., *Nanopolymers delivery of the bone morphogenetic protein-4 plasmid to mesenchymal stem cells promotes articular cartilage repair in vitro and in vivo.* Journal of Nanomaterials, 2012. **2012**: p. 2.
186. Varghese, F., et al., *IHC Profiler: an open source plugin for the quantitative evaluation and automated scoring of immunohistochemistry images of human tissue samples.* PloS one, 2014. **9**(5): p. e96801.
187. Lee, H.J., et al., *Changes in surface markers of human mesenchymal stem cells during the chondrogenic differentiation and dedifferentiation processes in vitro.* Arthritis & Rheumatism: Official Journal of the American College of Rheumatology, 2009. **60**(8): p. 2325-2332.
188. Yang, W., et al., *Targeted delivery of FGF2 to subchondral bone enhanced the repair of articular cartilage defect.* Acta biomaterialia, 2018. **69**: p. 170-182.
189. Park, D.Y., et al., *The degeneration of meniscus roots is accompanied by fibrocartilage formation, which may precede meniscus root tears in osteoarthritic knees.* The American journal of sports medicine, 2015. **43**(12): p. 3034-3044.

List of Publications

Scientific Articles

1. **A. Hakamivala,** Y. Huang, Y. Chang, Z. Pan, A. Nair, J-T. Hsieh, L. Tang. "*Development of 3D Lymph Node Mimetic for Studying Prostate Cancer Metastasis*", Advanced Biosystem, **3**(7). 2019.

2. **A. Hakamivala**, S li, K Robinson, Y Huang, S Yu, B Yuan, J Borrelli Jr, L Tang "*Recruitment of endogenous progenitor cells by erythropoietin loaded particles for situ cartilage regeneration*", Bioactive Materials, 2019. (submitted)

3. **A. Hakamivala**, S. Moghassemi, K. Omidfar. "*Modeling and optimization of the niosome nanovesicles using response surface methodology fro delivery of insulin"* Biomedical physics and engineering express, **6**(4). 2019.

4. **A. Hakamivala**, A. Nojoomi, A. Farzadi, A. Aminian, N. Azuan Abu. *"Parametric process optimization to improve the accuracy and mechanical properties of 3D printed parts"*MRS advances, **4**(24): p. 1383-1392. 2019.

5. Y. Huang, **A. Hakamivala,** S. Li, A. Nair, R Saxena, J-T. Hsieh, L. Tang *"Trapping circulating prostate cancer cells using chemokine releasing microparticles"* Sientific reports, 2019. (submitted)

6. H. Vu, J. Zhou, Y. Huang, **A. Hakamivala**, M. Khang, L. Tang "*Development of a dual-wavelength fluorescent nanoprobe for in vivo and in vitro cell tracking consecutively*", Bioorganic & Medicinal Chemistry, **27**(9): p. 1855-1862. 2019.

7. N. Pandey, A. Urias, V. Jones, S. Yaman, **A. Hakamivala**, B. Rodionov, J. Liao, P. Zimmern, K. Nguyen, Y. Hong "*Optimizing the nanoparticle enhanced adhesion of mussel inspired hydrogels for tissue interfacing*", The Journal of Urology, **201**(Supplement 4): p. e19. 2019.

8. MK. Khang, J. Zhou, Y. Huang, **A. Hakamivala**, L. Tang "*Preparation of a novel injectable in situ-gelling nanoparticle with applications in controlled protein release and cancer cell entrapment"* RSC Advances, **8**: p. 34625-34633. 2018.

9. S. Li, W. Cong, **A. Hakamivala**, Y. Huang, J. Borrelli, L. Tang "*Hyaluronic Acid-Based Optical Probe for the Diagnosis of Human Osteoarthritic Cartilage",* Nanotheranostics, **2**(4): p. 347-359. 2018.

10. N. Pandey, **A. Hakamivala**, C. Xu, P. Hariharan, B. Radionov, Z. Huang, J. Liaom, L. Tang, P. Zimmern, K.T. Nguyen, Y. Hong "*Biodegradable nanoparticles enhanced adhesiveness of mussel-like hydrogels at tissue interface*" Advanced healthcare materials, **7**(7): p. 1701069. 2018.

11. Y. Huang, J. Zhou, **A. Hakamivala**, J. Wu, Y. Hong, J. Borrelli, L. Tang, *"An optical probe for detecting chondrocyte apoptosis in response to mechanical injury***",** Scientific Reports, **7**(1): p. 10906. 2017.

12. E. Yazdi, S. Moghassemi, Z. Maharat, **A. Hakamivala**, S. Kashanian, K. Omidfar, "*Effect of Silibinin Loaded Nano-Niosomal Coated with Trimethyl Chitosan on miRNAs Expression in 2D and 3D Models of t47D Breast Cancer Cell Line*", Artificial Cells, Nanomedicine, and Biotechnology, **46**(3): p. 524-535. 2017.

13. S. Moghassemi, A. Hadjizadeh, **A. Hakamivala**, K. Omidfar, "*Growth Factor-Loaded nano-niosomal Gell Formulation and Characterization*", AAPS PharmSciTech, **18**(1): p. 34-41. 2017.

14. S. Moghassemi, E. Parnian, **A. Hakamivala**, M. Darzianiazizi, M. Mowlavi, B. Larijani, K. Omidfar "*Uptake and transport of insulin across intestinal membrane model using trimethyl chitosan coated insulin niosomes*", Materials Science and Engineering: C, **46**(1): p. 333-340. 2015.

Abstracts

1. **A. Hakamivala**, J. Hsieh, L.Tang "*Fabrication of 3D lymph node mimetic and its potential for cancer diagnosis*". Society For Biomaterials Annual Meeting & Exposition, Seattle, Washington, USA. 2019.

2. M. Khang, J. Zhou, **A. Hakamivala**, L. Tang "*An Avidin-Biotin Nanoparticle System for Detecting and Treating Inflammatory Diseases*". Society For Biomaterials Annual Meeting & Exposition, Seattle, Washington, USA. 2019.

3. M. Khang, J. Zhou, Y. Huang, **A. Hakamivala**, S. Li, L. Tang "*Preparation of Injectable Thermogelling Nanoparticles for chemokine release and Cancer Cell Entrapment*". Society For Biomaterials Annual Meeting & Exposition, Seattle, Washington, USA. 2019.

4. S Li, J Zhou, **A. Hakamivala**, Y Huang, W Cong, J Borrelli, L Tang "*Treatment of Osteoarthritis Using Macrophage-Targeting Hyaluronic Acid Microscaffolds*". Society for Biomaterials Anuual Meeting & Exposition. Atlanta, Georgia, USA. 2018.

5. **A. Hakamivala**, Y. Huang, L. Tang. "*Metastatic Lymph Node Microenvironment and its Application for Investigation of Cancer Metastasis*", 4th annual iC3 life science summit, Arlington, Texas, USA. 2018.

6. **A. Hakamivala**, Y. Huang, L. Tang. "*Characterization of Metastatic LymphNode Microenvironment andits Application for Investigation of Cancer Metastasis* ". Innovation day, Arlington, Texas, USA. 2018.

7. M Khang, J Zhou, **A Hakamivala**, L Tang. *"*A Novel Injectable, in situ-gelling Nanoparticle and its Application in Cancer Cell Trapper in vivo". Innovation day, Arlington, Texas, USA. 2018..

8. Y Huang, **A Hakamivala**, S Li , L. Tang. "*A Diagnostic Device for Capturing Metastatic Esophageal Cancer"* Innovation day, Innovation day, Arlington, Texas, USA. 2018.

9. **A. Hakamivala**, A. Nair, J.T. Hsieh, L. Tang "*Lymph Node Mimetic for Investigating Cancer Metastasis*" BMES Annual Meeting, Phoenix, Arizona, USA. 2017.

10. Y. Huang, **A. Hakamivala**, A. Nair, J.T. Hsieh, L. Tang *"CCL-21 Releasing Cancer Trap for Capturing Metastatic Prostate Cancer"* BMES Annual Meeting, Phoenix, Arizona, USA. 2017.

11. S. Li, J. Zhou, **A. Hakamivala**, R. Saxena, J. Borrelli, L. Tang. "*Stem cell therapy of PTOA using erythropoietin-incorporated HA microscaffolds***",** Military Health System Research Symposium (MHSRS), Kissimmee, Florida, USA. 2017.

12. **A. Hakamivala**, C. Chicas, J. Castro, C. Wallace, A. Nair, L.Tang **"***Development of Lymph Node Construct for Investigating Prostate Cancer Metastasis",* BMES Annual Meeting, Minneapolis, Minnesota, USA. 2016.

13. N. Pandey, **A. Hakamivala**, P. Hariharan, B. Rodionov, Z. Huang, P. Zimmern, K. Nguyen, L. Tang, Y. Hong, **"***Nanoparticle enhanced adhesion of mussel inspired hydrogels for tissue interfacing",* BMES Annual Meeting, Minneapolis, Minnesota, USA. 2016.

14. Y. Huang, **A. Hakamivala**, A. Nair, J. Hsieh, L. Tang **"***Cancer Trap for Capturing Metastatic Prostate Cancer",* BMES Annual Meeting, Minneapolis, Minnesota, USA. 2016.

15. **A. Hakamivala,** A. Nair, Y. Huang, Q. Yang, L. Tang, **"***Artificial Lymph Node Construct for Cancer Diagnosis and Therapy.",* The 12th Annual celebration of Excellence by students, Arlington, Texas, USA. 2016.

Awards and Honors

- ✓ Awarded Dissertation Fellowship summer 2019, sponsored by the college of engineering, the University of Texas at Arlington, April 2019.

- ✓ Selected as the second place of graduate projects of innovation day 2018, Sponsored by Dean of Engineering, the University of Texas at Arlington, April 2018.

- ✓ Selected as Outstanding Bioengineering Students to receive Alfred & Janet Potvin Excellence in Biomedical Engineering Award, Department of Bioengineering, the University of Texas at Arlington, March 2018.

- ✓ Selected as highly qualified candidates to receive a Graduate Teaching Fellowship and Enhanced Graduate Teaching Assistantship of Bioengineering Department of University of Texas at Arlington, September 2014.

Biographical Information

Amirhossein Hakamivala was born in Tehran, Iran to an engineer father and a teacher mother who inculcated in him an aptitude, desire and motivation towards education. He pursued his bachelor's in biomaterials and tissue engineering in the prestigious Amirkabir University of Technology in Tehran.

During his undergraduate studies, he worked on a few projects in a nano-biomaterial's lab. The most important ones were the evaluation of bisphosphonate release from the nano-hydroxyapatite/gelatin scaffolds for osteoporosis treatment and development of technical knowledge for the production of an artificial hydroxyapatite eyeball sample as a replacement for an eviscerated eye. Also, he came across the concept of neural network modeling. He worked with his advisor, Dr. Mehran Solati, on a research project fixated on the optimization of conditions for calcium phosphate synthesis.

He graduated from his bachelor's program with honors and was one of the top 10 students. Hence, he was granted a direct master's program without having to apply. During his master's, his proposal about the properties of gelatin-chitosan/BCP composite scaffolds was approved by the Nanotechnology initiative council (NIC) in Tehran. Also, he got funding for one of his projects titled "Niosome Coated Chitosan Nanoparticle as insulin delivery system" from the Biosensor Research Center at the University of Medical Science where he met Dr. Omidfar. He completed his master's after 3 consecutive terms and ranked first among 63 candidates.

His high GPA during his master gave him the privilege to get into a Ph.D. program without having to apply. Also, he was offered a full scholarship by the bioengineering department of the University of Texas at Arlington. He came to the United States of America to pursue a Ph.D. degree in biomedical engineering and joined Dr. Liping Tang's research group. During his Ph.D. studies, he

has participated in several research endeavors. His main focus was on the application of tissue engineering techniques for cartilage regeneration and cancer metastasis diagnosis.

In addition to being Dr. Tang's doctoral student, Amir also currently is an intern in the R&D materials group of Surgical IOL in Alcon. Apart from a full-time research workload, Amir enjoys soccer, tennis, ping pong, bowling, and swimming.